



**THEORETICAL COMPARISON OF THE EXCITED ELECTRONIC  
STATES OF THE URANYL ( $\text{UO}_2^{2+}$ ) AND URANATE ( $\text{UO}_4^{2-}$ ) IONS USING  
RELATIVISTIC COMPUTATIONAL METHODS**

THESIS

Eric V. Beck, Captain, USAF

AFIT/GNE/ENP/03-01

**DEPARTMENT OF THE AIR FORCE  
AIR UNIVERSITY**

**AIR FORCE INSTITUTE OF TECHNOLOGY**

---

---

**Wright-Patterson Air Force Base, Ohio**

APPROVED FOR PUBLIC RELEASE; DISTRIBUTION UNLIMITED.

The views expressed in this thesis are those of the author and do not reflect the official policy or position of the United States Air Force, Department of Defense, or the United States Government.

AFIT/GNE/ENP/03-01

THEORETICAL COMPARISON OF THE EXCITED ELECTRONIC STATES OF THE  
LINEAR URANYL ( $\text{UO}_2^{2+}$ ) AND TETRAHEDRAL URANATE ( $\text{UO}_4^{2-}$ ) IONS USING  
RELATIVISTIC COMPUTATIONAL METHODS

THESIS

Presented to the Faculty

Department of Engineering Physics

Graduate School of Engineering and Management

Air Force Institute of Technology

Air University

Air Education and Training Command

In Partial Fulfillment of the Requirements for the

Degree of Master of Science (Nuclear Science)

Eric V. Beck, BS

Captain, USAF

March 2003

APPROVED FOR PUBLIC RELEASE; DISTRIBUTION UNLIMITED.


THEORETICAL COMPARISON OF THE EXCITED ELECTRONIC STATES OF  
THE LINEAR URANYL ( $\text{UO}_2^{2+}$ ) AND TETRAHEDRAL URANATE ( $\text{UO}_4^{2-}$ ) IONS  
USING RELATIVISTIC COMPUTATIONAL METHODS

Eric V. Beck, BS  
Captain, USAF

Approved:

  
Larry W. Burggraf (Chairman)

7 Mar 2003  
date

  
Jean-Philippe Blaudeau (Member)

7 MAR 2003  
date

  
David E. Weeks (Member)

10 Mar 03  
date

## Acknowledgments

There are many people I'd like to thank for their help and contributions to this research. First and foremost, I'd like to thank my advisors, Dr. Larry Burggraf, Dr. Jean-Phillipe Blaudeau, and Dr. David Weeks. Dr. Burggraf, for having the faith in my ability to undertake such a daunting project despite my doubts, and for his gentle guidance and support for this work. Dr. Blaudeau for the countless hours he spent teaching me literally everything I know about relativistic quantum mechanics. Without him, this project would have surely failed. And last, but not least, Dr. Weeks, for his probing comments and suggestions that forced me to be precise in my language and develop a true understanding of many of the theoretical concepts.

In addition to my advisors, I'd like to thank Dave Doaks and Jim Gray. They have assembled a powerful, and unfortunately, under-utilized 96 processor parallel computing cluster at AFIT, where I performed most of my calculations. I hope that the abuse I put the cluster through will lead to a more capable system for future students. Dave and Jim have done a tremendous job. I can't give them enough praise.

I also have to thank Dr. Frank Duan at the MSRC for compiling and installing NWChem on their Compaq ES 40/45s for my use, as well as providing several useful suggestions during my geometry optimizations.

Last, but definitely not least, I have to thank my wife and my two children,. They graciously accepted the demands AFIT placed on my time, and their support and love is unconditional. I am truly blessed to have them.

Eric V. Beck

## Table of Contents

Acknowledgments.....	iv
List of Figures.....	vii
List of Tables.....	viii
Abstract.....	x
I. Introduction.....	1
II. Theory.....	4
Relativistic Effects in Chemistry.....	5
The Dirac Equation.....	12
Relativistic Many-Electron Hamiltonians.....	20
Dirac Hartree-Fock Theory.....	24
Relativistic Effective Core Potentials.....	32
Electron Correlation Models.....	35
Summary.....	45
III. Resources and Methodology.....	46
Hardware Resources.....	46
Software Resources.....	47
Geometry Optimizations.....	49
Overview of COLUMBUS Calculations.....	50
COLUMBUS Calculations on Uranyl ( $\text{UO}_2^{2+}$ ).....	51
COLUMBUS Calculations on Uranate ( $\text{UO}_4^{2-}$ ).....	55
IV. Results and Discussion.....	59
Uranyl Geometry Optimization Results.....	59
Large-core Uranyl ( $\text{UO}_2^{2+}$ ) Results.....	63
Small-core Uranyl ( $\text{UO}_2^{2+}$ ) Results.....	72
Small-core Uranate ( $\text{UO}_4^{2-}$ ) Results.....	80
V. Conclusions and Recommendations.....	86
Appendix A: Symmetry Considerations for the Linear Uranyl Ion.....	89
Appendix B: Symmetry Considerations of the Tetrahedral Uranate Ion.....	94

Appendix C: State Assignments Using MR-CISD Wave Functions .....	99
Uranyl MR-CISD State Assignment .....	99
Uranate MR-CISD State Assignment.....	101
List of Abbreviations .....	103
Bibliography .....	105
Vita.....	115

## List of Figures

Figure 1. Schematic Representation of the Assumptions in Russell-Sanders and j-j Spin-Orbit Coupling Schemes (Gerloch, 1986: 61).....	9
Figure 2. Correlation Diagram of the Various States Arising From a $d^2$ Electronic Configuration Using Both Russell-Sanders and j-j Spin-Orbit Coupling (Gerloch, 1986: 78).....	10
Figure 3. Electronic Ground State for Uranyl Using Both Non-relativistic HF and Four-component, Fully Relativistic DHF Methods (de Jong, 1999: 45) .....	31
Figure 4. Large-core Uranyl SCF Potential Energy Surface .....	64
Figure 5. Large-core Uranyl MCSCF Potential Energy Surface .....	65
Figure 6. Large-core MR-CISD Uranyl Electronic States from Molecular Orbitals.....	67
Figure 7. Large-core MR-CISD Uranyl Electronic States from Natural Orbitals.....	68
Figure 8. Small-core Uranyl SCF Potential Energy Surface .....	72
Figure 9. Small-core Uranyl MCSCF Potential Energy Surface .....	73
Figure 10. Small-core Uranyl MR-CISD Electronic States From Molecular Orbitals.....	74
Figure 11. Small-core Uranyl MR-CISD Electronic States From Natural Orbitals .....	75
Figure 12. Uranate SCF Potential Energy Surface .....	81



## List of Tables

Table 1. Uranyl Geometry Optimization Results .....	61
Table 2. COLUMBUS Large-Core Uranyl Ground-State Calculation Results.....	62
Table 3. COLUMBUS Small-Core Uranyl Ground-State Calculation Results.....	62
Table 4. Uranate NWChem 4.0.1 Geometry Optimization Results.....	63
Table 5. Large-core Uranyl SCF Symmetric Stretch Vibrational Frequencies .....	64
Table 6. Large-core Uranyl MCSCF Symmetric Stretch Vibrational Frequencies.....	66
Table 7. Large-core Uranyl MR-CISD Symmetric Stretch Vibrational Frequencies .....	69
Table 8. Large-core Uranyl Wave Function Compositions.....	70
Table 9. Electronic Transition Energies from Large-core MR-CISD Results.....	71
Table 10. Large-core Uranyl Results from Zhang et al (Zhang, 1999: 6884) .....	71
Table 11. Small-core Uranyl SCF Equilibrium Bond Length and Symmetric Stretch Vibrational Frequency .....	73
Table 12. Small-core Uranyl MCSCF Symmetric Stretch Vibrational Frequencies.....	74
Table 13. Small-core Uranyl MR-CISD Symmetric Stretch Vibrational Frequencies .....	76
Table 14. Small- and Large-core Uranyl Wave Function Compositions .....	77
Table 15. Electronic Transition Energies from Small-core MR-CISD Results.....	78
Table 16. Comparison Between Theoretical and Experimental Uranyl Fluorescent Electronic Spectra and Symmetric Stretch Vibrational Frequencies (Rabinowitch et al, 1964: 48) .....	79
Table 17. Small-core Uranate SCF Symmetric Stretch Vibrational Frequencies.....	82

Table 18. Small-core Uranate MR-CISD Double Group Terms Of A Symmetry in $D_2$ and Their GS Compositions .....	84
Table 19. Small-core Uranate MR-CISD Double Group Terms Of $B_1$ Symmetry in $D_2$ and Their GS Compositions .....	84
Table 20. Small-core Uranate MR-CISD Low-Lying Vertical Electronic Transition Energies at 1.9253 Å.....	85
Table 21. Correlation Between $D_{\infty h}$ and $D_{2h}$ Symmetry Point-Groups (Cotton, 1971: 359-362).....	89
Table 22. Uranium Atomic Orbitals in $D_{\infty h}$ and $D_{2h}$ Symmetry Point Groups .....	90
Table 23. Two Oxygen Atomic Orbitals Along z-axis in $D_{\infty h}$ and $D_{2h}$ .....	91
Table 24. Uranyl Possible States from CISD References in both AS and $\omega\omega$ Coupling Schemes.....	92
Table 25. Total Wave Function Symmetry in $D_{2h}$ From Reference Electronic Configurations.....	93
Table 26. Correlation Table Between $T_d$ and $D_2$ Symmetry Point-Groups (Cotton, 1971: 356-363).....	95
Table 27. Linear Combination of Uranium Atomic Orbitals in $T_d$ and $D_2$ Symmetry Point Groups.....	96
Table 28. Combination of Four Tetrahedral Oxygen Atomic s-Orbitals in $T_d$ and $D_2$ .....	97
Table 29. Uranate Total Wave Function Symmetry in $D_2$ From Reference Electronic Configurations .....	98

## Abstract

This thesis examines the ground and excited electronic states of the uranyl ( $\text{UO}_2^{2+}$ ) and uranate ( $\text{UO}_4^{2-}$ ) ions using Hartree-Fock self-consistent field (HF SCF), multi-configuration self-consistent field (MCSCF), and multi-reference single and double excitation configuration interaction (MR-CISD) methods. The MR-CISD calculation included spin-orbit operators. Molecular geometries were obtained from self-consistent field (SCF), second-order perturbation theory (MP2), and density functional theory (DFT) geometry optimizations using the NWChem 4.01 massively parallel *ab initio* software package. COLUMBUS version 5.8.1 was used to perform in-depth analysis on the HF SCF, MCSCF, and MR-CISD potential energy surfaces.

Excited state calculations for the uranyl ion were performed using both a large- and small core relativistic effective core potential (RECP) in order to calibrate the method. This calibration included comparison to previous theoretical and experimental work on the uranyl ion. Uranate excited states were performed using the small-core RECP as well as the methodology developed using the uranyl ion.

THEORETICAL COMPARISON OF THE EXCITED ELECTRONIC STATES OF THE  
LINEAR URANYL ( $\text{UO}_2^{2+}$ ) AND TETRAHEDRAL URANATE ( $\text{UO}_4^{2-}$ ) IONS USING  
RELATIVISTIC COMPUTATIONAL METHODS

## I. Introduction

The chemical properties of uranium and plutonium oxides are critically important to nuclear applications. Of particular importance in the chemistry of these actinide compounds is the oxidation state. Uranium, like all the actinides, can possess a wide range of oxidation states, ranging from +3 to +6, due to chemical activation of the uranium 5f orbitals via relativistic effects. As a result, the oxidation state of uranium can be influenced by its local chemical environment, which in turn influences the geometry of the uranium oxide compounds. Uranium oxidation state plays a very important role throughout the nuclear fuel cycle, and it plays a critical role in the mobility of uranium in the environment. This oxidation state can be inferred through spectroscopic measurements, providing a simple and inexpensive tool for use in such areas as nuclear forensics and environmental monitoring.

Additionally, the stockpile stewardship<sup>1</sup> program demands a thorough understanding of the processes by which uranium and plutonium components age, as well as the effect this aging has on the reliability and performance of nuclear weapons. A cornerstone of the stockpile stewardship program is theoretical modeling and simulation

---

<sup>1</sup> Stockpile stewardship refers to the substantial effort undertaken by the U.S. Department of Energy to maintain and certify the U.S. nuclear weapon arsenal without resorting to underground nuclear testing--<http://www.doe.gov>.

of the basic physics and chemistry involved in the design, manufacture, maintenance, and operation of a nuclear weapon. Again, non-invasive electronic spectroscopic methods can be used to diagnose the extent of nuclear weapon component aging, based on the relationship between uranium oxidation state and its local chemical environment.

Uranium oxidation is of particular interest. Oxygen and uranium readily react, forming a wide range of complex oxides over a range of temperatures and pressures (Wanner, 1992). The uranyl ion,  $\text{UO}_2^{2+}$ , is an unusually stable oxide of uranium, and it is present in a majority of complex uranium(VI) oxides (Pyykkö, 1998: 3787-3788; Zhang 1999:6880).

While there is a large amount of experimental data on the various properties of uranium and plutonium (Katz et al, 1986; Wanner, 1992), theoretical understanding of the spectra of these elements has progressed slowly. *Ab initio*<sup>2</sup> quantum mechanical theoretical techniques have made great strides in understanding of molecules consisting of lighter elements, and computational methods have been quite successful in predicting thermodynamic and spectroscopic properties of these compounds. Unfortunately, such progress in the actinide compounds has progressed more slowly, for two main reasons.

The first difficulty is the sheer number of electrons to deal with in actinide compounds. Common uranium oxide compounds such as  $\text{UO}_2$  have 108 electrons, while more complex oxides such as  $\text{U}_3\text{O}_8$  have over 300 electrons. Accurately treating such large numbers of electrons becomes computationally intensive, and it has only been in the last decade that such molecules can be treated with the accuracy necessary to compare theoretical and experimental electronic spectra. A second difficulty is the fact that relativistic effects must be accounted, not as perturbations to, but on an equal footing with electron correlation in these heavy molecular systems for even moderate accuracy. This is in stark contrast to lighter molecules where relativistic effects can be neglected in

---

<sup>2</sup> Latin for "from the beginning", Merriam-Webster's Collegiate Dictionary, 2002, <http://www.webster.com>

all but high-precision theoretical calculations (Pyykkö, 1998: 563-594; Balasubramanian, 1997: 1-27).

With the development of faster computers, especially massively parallel computer systems, as well as quantum chemistry software codes designed to take advantage of these computer architectures, there has been an increasing number of theoretical investigations of actinide compounds. However, the theoretical calculation of excited electronic states for actinide compounds is a difficult problem, and there are relatively few in-depth studies of the excited states of uranium oxides necessary for understanding the electronic spectra.

This research focuses on two uranium oxide ions in particular: uranyl ( $\text{UO}_2^{2+}$ ) and uranate ( $\text{UO}_4^{2-}$ ) ions. Starting from optimized, theoretical, gas-phase molecular geometries, electronic spectra calculations from single and double excitations with spin-orbit coupling included were computed and compared with experimental and other theoretical results. The calculations involving uranyl were used to calibrate and validate the method, while those involving  $\text{UO}_4^{2-}$  were an attempt to begin understanding the influence of the local oxygen coordination on the electronic spectra of uranium oxides. Particular interest was paid to the first excited states of both.

The theory relevant to calculations of the electronic spectra of uranium oxides is laid out in chapter two. Next, the hardware and software resources used in this research, as well as the methodology behind the study of uranyl and uranate electronic spectra is described in chapter three. Results and discussion of the results is included in chapter four, followed by conclusions drawn from this research and recommendations for further research in chapter five.

## II. Theory

*Ab initio* quantum mechanical theoretical techniques have been applied to molecules containing light elements with increasing success in the past several decades. Application of these theoretical techniques to light-atom molecules, especially organic molecules, has yielded vast insight into the properties of these molecules such as molecular geometries for ground and transition states, electron affinities, ionization potentials and more. Advances in computing power, coupled with quantum chemistry software designed specifically to take maximum advantage of these computers has increased the applicability to larger molecules. Such calculations have become an indispensable tool to theoreticians and experimentalists alike.

Complications arise when applying theory to molecules containing heavy elements, especially actinide molecules. The two most difficult complications to the theoretical treatment of heavy-element molecules are increased electron correlation and relativistic effects.

First, these heavy-element molecules contain a large number of electrons whose motions are coupled through electrostatic and quantum mechanical interactions. Electron correlation effects can contribute roughly 1 eV (23 kcal/mol) to the total electronic energy per electron pair (Raghavachari, 1996: 12960). Using this rule of thumb, electron correlation accounts for 46 eV of the total electronic energy in the uranium

atom. An accurate treatment of electronic correlation is critical in order to perform meaningful comparisons between theoretical and experimental spectra.

A second complicating factor in the theoretical treatment of heavy-element molecules is the increasing importance relativistic effects play in the accurate description of ground and excited electronic states with increasing atomic number,  $Z$ . Several reviews examine relevant chemical effects due to relativistic quantum mechanical treatments (Pyykkö, 1988: 563-594; Pepper et al, 1991: 719-741; Kaltsoyannis, 1997: 1-11).

### **Relativistic Effects in Chemistry**

There are three main relativistic effects in atomic and molecular chemistry, all of which are roughly the same magnitude, and they approximately scale as  $Z^4$  (Pyykkö, 1988, 564). The first main relativistic effect is considered a direct relativistic effect, and it consists of a radial contraction of atomic orbitals, along with a lowering of the energy level of the electronic state. This effect is due primarily to the relativistic mass increase as electron velocities become appreciable fractions of the speed of light. Simple replacement of the relativistic mass expression for the electron in the Bohr radius formula yields

$$a_0 = \frac{4\pi\epsilon_0\hbar^2\sqrt{1-\left(\frac{v}{c}\right)^2}}{m_0e^2}. \quad (1)$$

Here,  $\hbar$  is Planck's constant divided by  $2\pi$ ,  $\epsilon_0$  is the permittivity of free space,  $e$  is the electron charge, and  $m_0$  is the electron mass. As electron speeds,  $v$ , approach the



speed of light,  $c$ , the Bohr radius,  $a_0$ , shrinks. Electron orbitals with high densities near the nucleus experience the largest contractions, where electron speeds are largest. For electrons in the hydrogenic 1s shell, the average fraction of the speed of light is given by  $\frac{Z}{137}$  (Pyykkö, 1988: 563). For uranium, this is  $0.67c$ , yielding a 1s orbital radial contraction of roughly 26%. All atomic orbitals have some density near the nucleus, therefore, all atomic orbitals experience some contraction. However, the inner s- and p-orbitals nearest the nucleus experience the most contraction (Pyykkö, 1988: 563). In light-element molecules, this orbital contraction is small and negligible in all but the highest precision calculations, but the effect becomes dramatic in actinide elements such as uranium.

The second relativistic effect is considered to be an indirect effect, and it consists of a radial expansion and increase in the electronic energy levels of outer atomic orbitals. This is due to more effective nuclear charge screening by the inner, contracted electrons, reducing the effective nuclear charge experienced by the outer electrons. Additionally, relativistic contraction of the inner s- and p- electron shells increase the electron density near the nucleus, crowding out the outer d- and f- electron shells. This is due to the fact that there is a decrease in electron density near the nucleus for orbitals with increasing orbital angular momentum. Thus, the direct orbital contraction competes with the indirect orbital expansion. In general, the result of this interplay between relativistic effects is to contract and stabilize s- and p- atomic orbitals, while d- and f- orbitals expand and destabilize in energy. The orbital expansion and contraction can affect bond lengths (Pyykkö, 1988: 571) and force constants (Pyykkö, 1988: 580), which in turn

affect molecular vibrational frequencies. These relativistic effects obviously affect the observed spectra of heavy-element molecules, but not as much as the splitting of states caused by the third major relativistic effect, spin-orbit coupling.

Intrinsic electron spin is a natural result of a Lorentz-covariant description of the quantum mechanically wave equation (Balasubramanian, 1997: 76-78). This spin angular momentum couples with the electron orbital angular momentum, lifting degeneracy in atomic orbitals with angular momentum. Thus, the three degenerate p-orbitals in non-relativistic theory split into one  $p_{\frac{1}{2}}$  orbital and two degenerate  $p_{\frac{3}{2}}$  orbitals. Of the three effects, spin-orbit coupling has the largest impact in atomic and molecular spectra, even for low-Z atoms and molecules. For light atoms, a perturbative treatment of spin-orbit coupling known as Russell-Sanders coupling or L-S coupling often yields sufficient accuracy for electronic transition energies. This coupling scheme treats magnetic spin-orbit coupling as a small perturbation to the electron-electron electrostatic interaction. Orbital angular momentum and spin angular momentum are still “nearly” good quantum numbers in this coupling scheme, and both L and S commute with the Hamiltonian in Russell-Sanders coupling scheme. Atomic states are described by term symbols

$$\begin{aligned}
 & {}^{2S+1}L_J \\
 & S = 0, 1, 2, \dots \\
 & L = S, P, D, F, \dots \\
 & J = L + S
 \end{aligned}$$

with S equal to the total spin multiplicity, and L is the total orbital angular momentum (0, 1, 2, ..). Traditional spectroscopic notation is used for the total orbital angular

momentum, with S representing zero total orbital angular momentum, P representing one unit of orbital angular momentum and so on. J is the total angular momentum of the electron, given by the sum of orbital and spin angular momenta. Examples of Russell-Sanders term symbols include  $^3P_2$ ,  $^1S_0$ , and  $^3D_4$  (Gerloch, 1986: 69-74).

On the other end of the perturbation spectrum, more appropriate for very heavy atoms, the electron-electron electrostatic interaction is treated as a perturbation to the magnetic spin-orbit coupling. This coupling scheme is known as j-j coupling. In this coupling scheme, neither L nor S commute with the Hamiltonian. However, the total angular momentum, J, still commutes with the atomic Hamiltonian, and hence, is a good quantum number. The term symbol for j-j coupling is given by the J value for the state (Gerloch, 1986: 74-76).

Figure 1 contains a schematic representation of the two spin-orbit coupling extremes (Gerloch, 1986: 61). The horizontal springs represent electrostatic coupling between the electrons, while the vertical springs represent magnetic coupling between the electron intrinsic magnetic moments. In Russell-Sanders coupling, the electron orbital angular momenta couple strongly, as do each electron's spin angular momenta. These total orbital and spin angular momenta then couple weakly. The opposite is true of j-j coupling. In j-j coupling, each electron's orbital and spin angular momenta couple strongly, and this individual total angular momentum couples weakly with the other electrons total angular momenta.

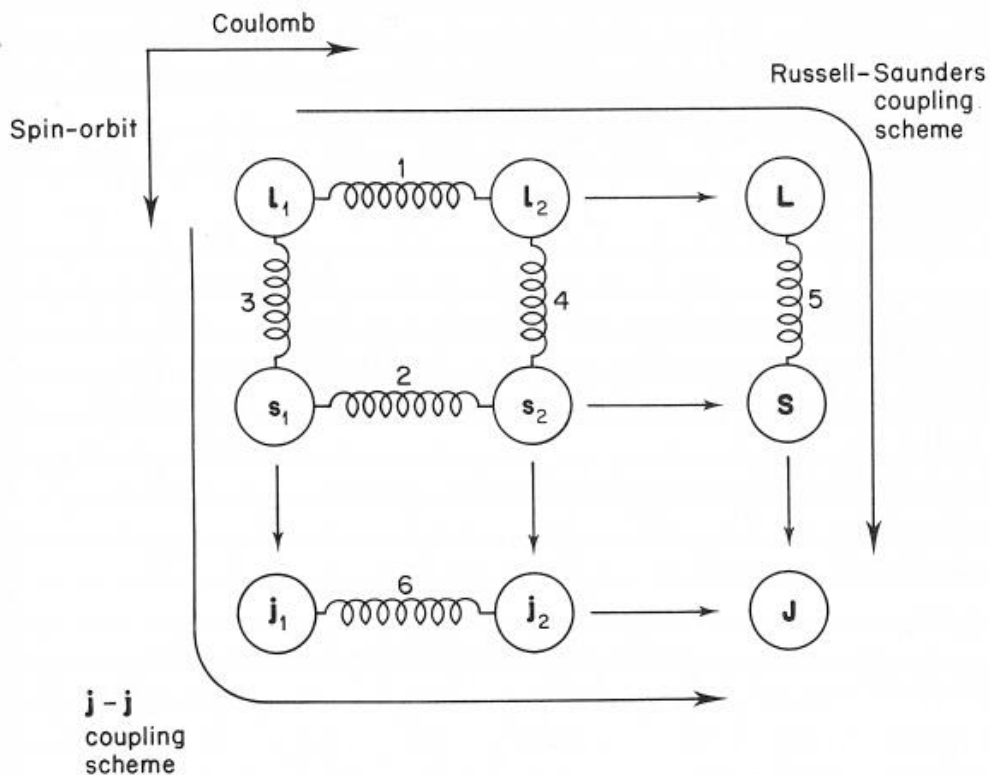


Figure 1. Schematic Representation of the Assumptions in Russell-Sanders and j-j Spin-Orbit Coupling Schemes (Gerloch, 1986: 61)

Most elements on the periodic table fall between these two perturbation extremes, and so intermediate coupling is more appropriate than either perturbative treatment. Intermediate coupling is not a separate coupling scheme, but occurs as deviations from the separate perturbative treatments given by L-S and j-j coupling (Gerloch, 1986: 77). Figure 2 illustrates the effect of Russell-Sanders, intermediate, and j-j spin-orbit coupling on a  $d^2$  electronic configuration. Figure 2 shows the effect of spin-orbit coupling on an atomic electronic state with two electrons in the d-shell. The left-hand side shows the term symbols that arise due to Russell-Sanders coupling, while the right-hand side shows

the effect of j-j coupling on the same electronic configuration. Here, the importance of spin-orbit coupling to electronic spectroscopy is evident. Without taking into account spin-orbit coupling, both the number of states and their relative ordering will be incorrect.

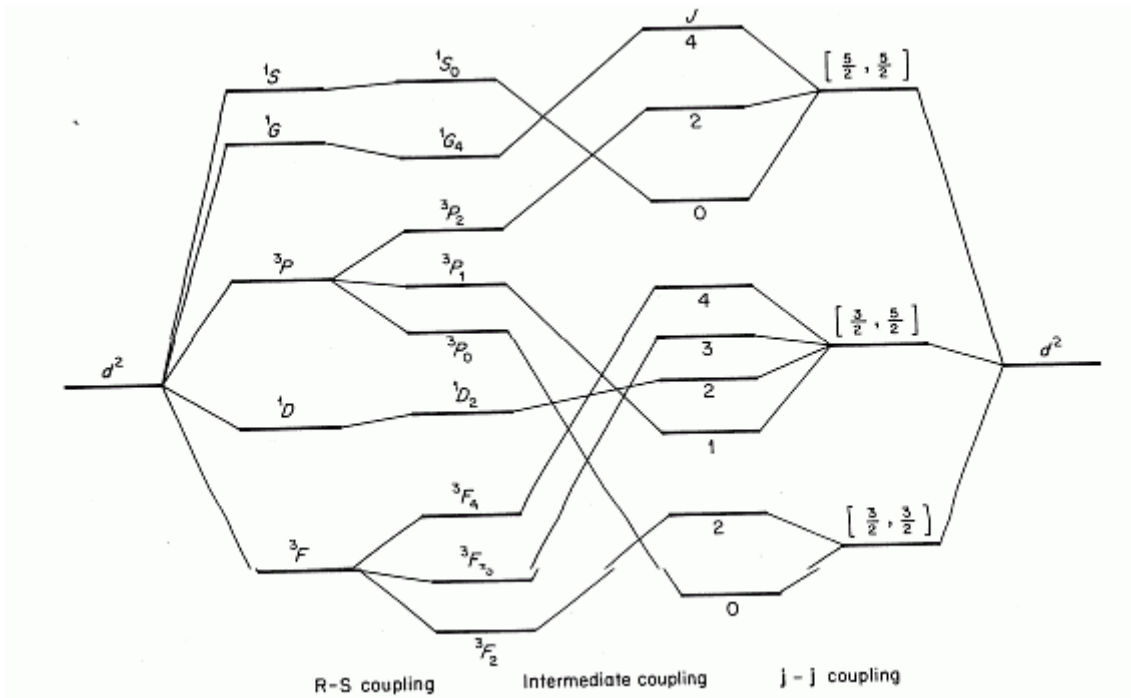


Figure 2. Correlation Diagram of the Various States Arising From a  $d^2$  Electronic Configuration Using Both Russell-Sanders and j-j Spin-Orbit Coupling (Gerloch, 1986:

78)

Relativity also affects the symmetry of molecules, because of electron spin. Under the assumption that the total electronic wave function can be separated (the product of a spatial and spin wave functions), each wave function may possess separate symmetry, and the total, observable state symmetry is given by the product of the spatial

and spin symmetries. For example, singlet spin states are completely symmetric, while triplet spin states transform like the components of the angular momentum operator. Thus, a completely symmetric spatial wave function multiplied by a triplet spin wave function will not be totally symmetric. For systems with a spin-orbit Hamiltonian, the symmetry point groups can have twice the number of symmetry operations, and are called double point groups. This doubling of the order of the symmetry point groups is due to the introduction of  $\frac{1}{2}$ -integral angular momentum values. Systems possessing an even number of electrons obey Bose-Einstein (bosons) statistics, and the total wave function of bosonic systems is symmetric with respect to rotations by  $2\pi$ . Systems possessing an odd number of electrons obey Fermi-Dirac statistics (fermions), and fermionic wave functions change sign up the exchange of two particles. This exchange is equivalent to a rotation by  $2\pi$ , and so a rotation of  $4\pi$  returns a fermionic system to its original state. While bosonic systems transform according to the irreducible representations of the single point groups, the rotation by  $2\pi$  is a new symmetry operation for fermionic systems, doubling the order of the symmetry point group. For example, rotations of a closed-shell molecule, such as uranyl ( $\text{UO}_2^{2+}$ ) transforms according to the normal irreducible representations of the  $D_{\infty h}$  point group. Rotating the molecule by  $2\pi$  leaves the molecule (wave function) unchanged. However, for an open-shell molecule, such as  $\text{UO}_2$ , such is not the case. Such molecules transform according to the extra irreducible representations generated by a rotation of  $2\pi$ . Rotating the  $\text{UO}_2$  molecule by  $2\pi$  introduces a phase factor into the total electronic wave function. A rotation by  $4\pi$  in this case returns the molecule (wave function) to its original configuration.

These three main effects, orbital contraction and energy stabilization, orbital expansion and energy destabilization, and spin-orbit coupling, along with the consequential double group symmetry constitute the chemically relevant relativistic effects in atoms and molecules. The most important, from a spectroscopic standpoint is spin-orbit coupling, even in the spectra of the lightest elements. A quantum mechanical treatment of the electron must account for the intrinsic magnetic moment of the electron, and the Dirac equation accomplishes this quite elegantly.

### The Dirac Equation

Relativity has played a role in quantum mechanical systems since the inception of the theory. Attempts at finding a Lorentz invariant form for Schrödinger's equation led to two Lorentz-covariant equations: the Klein-Gordon equation, and the Dirac equation. Schrödinger's equation, a non-relativistic quantum mechanical wave equation, is given by

$$H\Psi = E\Psi, \quad (2)$$

where the Hamiltonian, H, and energy, E, operators are given by

$$H(\vec{r}, t) = \frac{p^2(\vec{r}, t)}{2m} + V(\vec{r}, t), \quad (3)$$

and

$$E(t) = -\frac{\hbar}{i} \frac{\partial}{\partial t}. \quad (4)$$

The momentum operator, p, is defined by

$$p(\vec{r}, t) = \frac{\hbar}{i} \nabla. \quad (5)$$

Here,  $m$  is the electron mass,  $i$  is the imaginary number,  $\hbar$  is Planck's constant divided by  $2\pi$ ,  $V(\vec{r}, t)$  is the potential energy operator, and  $p(\vec{r}, t)$  is the electron momentum.

$\Psi$  is the electronic wave function.

This equation, because of the non-equivalent treatment of the spatial and temporal variables, is not Lorentz invariant, and therefore is limited to non-relativistic phenomena. Early attempts at making a Lorentz-covariant equation began by quantizing the Lorentz-covariant relativistic energy expression

$$E^2 = p^2 c^2 + m_0^2 c^4. \quad (6)$$

Again,  $p$  is the electron momentum,  $c$  is the speed of light, and  $m_0$  is the electron rest-mass, and  $E$  is the electron energy.

Replacing the energy and momentum expressions with their quantized counterparts leads to the Klein-Gordon wave equation for a free particle (Balasubramanian, 1997: 99-101; Messiah, 1999: 884-888; Bjorken and Drell, 1964: 4-6, 198-206)

$$-\hbar^2 \frac{\partial^2 \Psi}{\partial t^2} = -\hbar^2 c^2 \nabla^2 \Psi + m_0^2 c^4 \Psi. \quad (7)$$

While this scalar wave function is Lorentz-covariant, it has several undesirable properties, making it unacceptable as a wave function for the electron. First, the probability density associated with it is not positive definite, resulting in possible negative probability densities. Additionally, both positive and negative energy solutions to this equation exist, complicating early interpretation of the wave function. The fact that the probability density is not positive definite makes this equation a poor choice for an electronic wave function; however, the Klein-Gordon turns out to be a valid



relativistic wave equation for spin-free fields, such as pi mesons (Messiah, 1999: 888; Balasubramanian, 1997: 108).

Dirac took a different approach in formulating a Lorentz-covariant equation for a free electron (Dirac, 1928: 610-624; Dirac, 1928: 351-361; Balasubramanian, 1997: 110-119). He began with the same Lorentz-covariant expression for the energy of a free particle as the Klein-Gordon equation,

$$E^2 = p^2 c^2 + m_0^2 c^4 . \quad (8)$$

Taking the square root yields the Dirac Hamiltonian,

$$H_{Dirac} = \pm \sqrt{p^2 c^2 + m_0^2 c^4} . \quad (9)$$

Quantizing this expression by the usual substitutions for the energy and momentum operators yields a Hamilton that involves a first-order time derivative. However, the square root in the operator makes application problematic and hopelessly complicated. Dirac circumvented this problem by introducing a new degree of freedom into the relativistic Hamiltonian, effectively completing the square. This yielded a more tractable Hamiltonian operator

$$H_{Dirac} = c(\vec{\alpha}_1 \cdot \vec{p}_1 + \vec{\alpha}_2 \cdot \vec{p}_2 + \vec{\alpha}_3 \cdot \vec{p}_3) + \vec{\beta} m_0 c^2 . \quad (10)$$

The Dirac equation,

$$\frac{i\hbar}{c} \frac{\partial \Psi}{\partial t} = c(\vec{\alpha}_1 \cdot \vec{p}_1 + \vec{\alpha}_2 \cdot \vec{p}_2 + \vec{\alpha}_3 \cdot \vec{p}_3) \Psi + \vec{\beta} m_0 c^2 \Psi , \quad (11)$$

results from this Hamiltonian (Kellogg, 1997: 4-6).

Requiring solutions to this equation to simultaneously satisfy the Klein-Gordon equation places restrictions on the components of the  $\vec{\alpha}_i$  and  $\beta$  matrices:

$$\alpha_i \alpha_j + \alpha_j \alpha_i = 2\delta_{ij}, \quad (12)$$

$$\beta^2 = 1, \quad (13)$$

and

$$\alpha_k \beta + \beta \alpha_k = 0. \quad (14)$$

In order to satisfy these restrictions both  $\tilde{\alpha}_i$  and  $\beta$  must be at least four-by-four matrices, which operate on a four-component vector wave function. The  $\tilde{\alpha}_i$  and  $\beta$  matrices are defined as

$$\tilde{\alpha}_1 = \begin{pmatrix} 0 & 0 & 0 & 1 \\ 0 & 0 & 1 & 0 \\ 0 & 1 & 0 & 0 \\ 1 & 0 & 0 & 0 \end{pmatrix}, \quad (15)$$

$$\tilde{\alpha}_2 = \begin{pmatrix} 0 & 0 & 0 & -i \\ 0 & 0 & i & 0 \\ 0 & -i & 0 & 0 \\ i & 0 & 0 & 0 \end{pmatrix}, \quad (16)$$

$$\tilde{\alpha}_3 = \begin{pmatrix} 0 & 0 & 1 & 0 \\ 0 & 0 & 0 & -1 \\ 1 & 0 & 0 & 0 \\ 0 & -1 & 0 & 0 \end{pmatrix}, \quad (17)$$

and

$$\tilde{\beta} = \begin{pmatrix} 1 & 0 & 0 & 0 \\ 0 & 1 & 0 & 0 \\ 0 & 0 & -1 & 0 \\ 0 & 0 & 0 & -1 \end{pmatrix}. \quad (18)$$

The Dirac equation is then a set of four, coupled, first order partial differential equations in space and time. The four-component wave function solution to this equation corresponds to two positive energy components and two negative energy components, each with a spin-up and spin-down component (Messiah, 1999: 888-892, 920-924). The  $\vec{\alpha}_i$  operators are velocity operators, while  $\beta$  is an parity operator. Observable quantities associated with this new internal degree of freedom are the energy, relativistic mass, current density, total angular momentum, spin, and parity. The operators associated with these observables are (Messiah, 1999: 921)

energy:

$$H = e\phi + \vec{\alpha} \cdot \left(\vec{p} - \frac{e\vec{A}}{c}\right) + \beta m_0 c^2, \quad (19)$$

where H is the Dirac Hamiltonian,  $\phi$  and  $\vec{A}$  are external electric and magnetic potentials, respectively. The relativistic mass is given by

$$M = H - e\phi. \quad (20)$$

Current density is found using

$$j(\vec{r}) = \vec{\alpha} \cdot \delta(\vec{r} - \vec{r}_0), \quad (21)$$

where  $\delta(\vec{r} - \vec{r}_0)$  is the Dirac delta function. Electron spin is given by

$$S_i = \frac{1}{2} \vec{\sigma}_i, \quad (22)$$

where  $\vec{\sigma}_i$  is the  $i^{\text{th}}$  Pauli spin matrix. Finally, the parity of the wave function is given by

$$P = \beta P_0, \quad (23)$$

where  $P_0$  is the initial parity. These Pauli spin matrices can be expressed in terms of the  $\vec{\alpha}_i$  matrices (Messiah, 1999: 891):

$$\vec{\sigma}_z = -i\vec{\alpha}_x\vec{\alpha}_y, \quad (24)$$

$$\vec{\sigma}_x = -i\vec{\alpha}_y\vec{\alpha}_z, \quad (25)$$

and

$$\vec{\sigma}_y = -i\vec{\alpha}_z\vec{\alpha}_x. \quad (26)$$

In the presence of an external field, the Dirac Hamiltonian,  $H_D$ , becomes

$$H_D = e\phi + c\vec{\alpha} \cdot \left(\vec{p} - \frac{e\vec{A}}{c}\right) + \beta m_0 c^2. \quad (27)$$

For the hydrogen atom, in the absence of an external magnetic field, this equation reduces to

$$E\Psi = [c(\vec{\alpha} \cdot \vec{p}) + \beta m_0 c^2 + e\phi]\Psi. \quad (28)$$

While it is possible to construct an exact solution to this equation in terms of spherical harmonics for the angular coordinates and hypergeometric functions for the radial coordinate, such a construction does not shed much light on the nature of the bound energy states. The details of the solution can be found in various sources (Messiah, 1999: 930-933; Balasubramanian, 1997: 159-175; Bethe et al, 1957: 63-71). The electronic energy levels for the Dirac hydrogen atom are given by (Bethe et al, 1956: 67-68)

$$E_{nj} = \frac{m_0 c^2}{\sqrt{1 + \left( \frac{Z\alpha}{n - j + \frac{1}{2} + \sqrt{(j + \frac{1}{2})^2 - Z^2 \alpha^2}} \right)^2}}. \quad (29)$$

Here,  $\alpha$  is the fine structure constant, defined as

$$\alpha = \frac{e^2}{4\pi\epsilon_0\hbar c}, \quad (30)$$

and the total angular momentum quantum number,  $j$ , takes on the values

$$j = l + \frac{1}{2}, |l - \frac{1}{2}|. \quad (31)$$

The binding energy of the hydrogen atom is given by  $E_{nj} - E_0$ , where  $E_0 = m_0c^2$ .

Expanding  $E_{nj} - E_0$  in powers of  $(Z\alpha)^2$ , where  $\alpha$  is the fine structure constant given above, and assuming  $Z\alpha \ll 1$ , yields (Bethe et al, 1956: 84)

$$E_{nj} = -\frac{(Z\alpha)^2}{2n^2} + \frac{(3 + 6j - 8n)(Z\alpha)^4}{8(1 + 2j)n^4} - \dots \quad (32)$$

The first term is the non-relativistic energy for the bound electronic states of the hydrogen atom. Higher order corrections involve both the principle quantum number  $n$ , as well as the total angular momentum quantum number  $j$ . This illustrates the importance of a relativistic picture of the atom. Corrections to the non-relativistic energy increase roughly as  $Z^4$ . Note that this Taylor series expansion in powers of  $(Z\alpha)^2$  is appropriate for  $Z\alpha \ll 1$ . This expansion leads to the Russell-Sanders spin-orbit coupling scheme.

Such an approximation is not valid for uranium, where  $Z\alpha = 0.6$ . In this case,

$\frac{1}{Z} \ll (Z\alpha)^2$ , and the electrostatic electron-electron interaction can be treated as a

perturbation to the magnetic interaction between the electron and the field of the nucleus.

This approximation leads to the j-j spin-orbit coupling scheme, which is more appropriate for very heavy elements.

Detailed examination of the negative energy component solutions to the Dirac equation for the free electron shows in the non-relativistic limit where  $E - m_0c^2 \ll m_0c^2$ , are much larger than the negative energy components, especially in the valence region (Balasubramanian, 1997: 143-144). Thus, the four-component Dirac wave function naturally separates into two large and two small components. Rewriting the Dirac equation in terms of two, coupled differential equations with two, two-component wave functions yields the Pauli approximation to the Dirac Hamiltonian in the absence of an external magnetic field (Balasubramanian, 1997: 145-147)

$$H_{Pauli} = E + e\phi + \frac{1}{2m_0}\nabla^2 + \frac{1}{2m_0c^2}(E + e\phi)^2 + i\frac{\mu_0}{2m_0c}\vec{E} \cdot \vec{p} - \frac{\mu_0}{2m_0c}[\vec{\sigma} \cdot (\vec{E} \times \vec{p}) - \mu_0(\vec{\sigma} \cdot \vec{H})] \quad (33)$$

where  $\vec{H}$  is the magnetic field,  $\vec{E}$  is the electric field, and  $\mu_0$  is the Bohr magneton, defined by

$$\mu_0 = \frac{e\hbar}{2m_0c}. \quad (34)$$

While somewhat cumbersome, the separate terms have simple interpretations. The first three terms are the non-relativistic Schrödinger Hamiltonian. The next term is the mass-velocity correction that accounts for the variation in electron mass with speed. The fifth term is known as the Darwin term, and is a result of “zitterbewegung”, or trembling motion. It is a result of the Heisenberg uncertainty principle. Non-relativistically, the uncertainty in the location of an electron can be measured to any accuracy using higher and higher energy photons. Relativistically, there is a limit to this

photon energy used to locate the electron, because at photon energies above  $2m_0c^2$ , pair production can occur. This results in an effective smearing of the charge of the electron (Balasubramanian, 1997: 186). The final two terms account for the spin-orbit coupling between the intrinsic electron magnetic moment and the orbital angular momentum. The successes of the Dirac equation is the prediction of electron spin as an observable property in the non-relativistic limit, as well as accounting for the correct value for the electron magnetic moment. Thus, the inclusion of electronic spin in the non-relativistic theory as an additional assumption is validated and explained in the non-relativistic limit of the Dirac equation.

### **Relativistic Many-Electron Hamiltonians**

Now that a Lorentz-covariant electronic wave function is available for the hydrogen atom, the next logical step is to try to extend this approach to larger atoms and molecules.

A relativistic wave function for a many-electron atom can be constructed as the sum of the one-electron Dirac Hamiltonians along with an electron-electron interaction term

$$H = \sum_i h_d^i + \sum_{i<j} B_{ij} , \quad (35)$$

where the  $i^{\text{th}}$  one-electron Dirac Hamiltonian,  $h_d^i$  is given by

$$h_d^i = e\phi + c\vec{\alpha} \cdot \left( \vec{p}_i - \frac{e\vec{A}}{c} \right) + \vec{\beta}m_0c^2 , \quad (36)$$

while  $B_{ij}$  represents a general electron-electron interaction term.

This approach is analogous with the non-relativistic approximation to the many-electron Hamiltonian based upon the one-electron Schrödinger equation for the hydrogen atom.

Next, a Lorentz-covariant description of electron-electron interactions,  $B_{ij}$ , is required. Unfortunately, the electron-electron interaction requires the more detailed treatment afforded by quantum electrodynamics, where vacuum interactions, virtual photon exchanges, and electron self-interactions are treated perturbatively. Even then, there is no closed form for a Lorentz-covariant electron-electron interaction. Such interactions must be treated approximately (Balasubramanian, 1997: 180; Messiah, 1999: 955-956; Bethe et al, 1956: 170). The first such approximation, widely used, is the approximation that relativistic corrections to the electron-electron interaction are small and negligible, and that the Coulomb interaction is an appropriate description, correct to zeroth order. This leads to the Dirac-Coulomb Hamiltonian (Kellogg, 1997: 15)

$$H_{DC} = \sum_i h_d^i + \sum_{i<j} \frac{e^2}{4\pi\epsilon_0 r_{ij}}. \quad (37)$$

Here,  $r_{ij}$  is the interelectron distance. This Hamiltonian is not Lorentz-covariant; however, corrections to the Coulombic interaction are small for large electron separation, and the Dirac-Coulomb Hamiltonian is quite successful. Another approach to determining the electron-electron interaction is to perturbatively expand the quantum electrodynamics interaction term in powers of the fine structure constant, and retain those terms of order  $\alpha^2$ . This yields the Dirac-Coulomb-Breit Hamiltonian (Bethe et al, 1956: 170; Balasubramanian, 1997: 180; Jackson, 1975: 593-595; Breit, 1932: 616-624)



$$H_{DCB} = \sum_i h_d^i + \sum_{i<j} \frac{e^2}{4\pi\epsilon_0} \left( \frac{1}{r_{ij}} - \frac{\vec{\alpha}_i \cdot \vec{\alpha}_j}{2r_{ij}} - \frac{(\vec{\alpha}_i \cdot \vec{r}_{ij})(\vec{\alpha}_j \cdot \vec{r}_{ij})}{2r_{ij}^3} \right). \quad (38)$$

This approximate Hamiltonian is still not Lorentz-covariant; however, it accounts for most of the chemically relevant electron-electron interaction effects. The first term is the electrostatic Coulomb interaction between two electrons, the second term accounts for first order magnetic interactions between the intrinsic magnetic moments of the electron. The last term accounts for the retardation of the propagation of the electromagnetic field of the electron due to the finite speed of light.

Another method, based on perturbative expansion of the Dirac-Coulomb-Breit Hamiltonian in powers of  $\alpha^2$  yields the Breit-Pauli Hamiltonian, given by (Balasubramanian, 1997: 193-194)

$$H_{BP} = H_{nr} + H_{mv} + H_{retardation} + H_{Darwin} + H_{SO} + H_{SS} + H_{external}, \quad (39)$$

where

$$H_{nr} = \sum_i \frac{p_i^2}{2m_0} - \frac{Ze^2}{4\pi\epsilon_0 r_i} + \sum_{i<j} \frac{e^2}{4\pi\epsilon_0 r_{ij}}, \quad (40)$$

$$H_{mv} = \sum_i \frac{p_i^4}{8m^3 c^2}, \quad (41)$$

$$H_{retardation} = -\frac{Ze^2}{8\pi\epsilon_0 m^2 c^2} \sum_{i<j} \left( \frac{\vec{p}_i \cdot \vec{p}_j}{r_{ij}} + \frac{(\vec{r}_{ij} \cdot \vec{p}_i)(\vec{r}_{ij} \cdot \vec{p}_j)}{r_{ij}^3} \right), \quad (42)$$

$$H_{Darwin} = \frac{ie\hbar}{(2m_0 c)^2} \sum_i \vec{p}_i \cdot \vec{E}_i, \quad (43)$$

$$H_{SO} = \frac{\mu}{m_0 c} \sum_i \vec{s}_i \cdot \left( \vec{E}_i \times \vec{p}_i + \sum_{i<j} \frac{2e}{r_{ij}^3} [\vec{r}_{ij} \times \vec{p}_j] \right), \quad (44)$$

$$H_{SS} = \left( \frac{e\hbar}{m_0c} \right)^2 \sum_{i<j} \left[ \frac{\vec{s}_i \cdot \vec{s}_j}{r_{ij}^3} - 3 \frac{(\vec{s}_i \cdot \vec{r}_{ij})(\vec{s}_j \cdot \vec{r}_{ij})}{r_{ij}^5} - \frac{8\pi}{3} (\vec{s}_i \cdot \vec{s}_j) \delta^3(\vec{r}_{ij}) \right], \quad (45)$$

and

$$H_{external} = \frac{e\hbar}{m_0c} \sum_i \vec{H}_i \cdot \vec{s}_i + \frac{e}{m_0c} \sum_i \vec{A}_i \cdot \vec{p}_i. \quad (46)$$

Here,  $\mu$  is the electron magnetic moment, and  $\vec{s}_i$  is the spin angular momentum of the  $i^{\text{th}}$  electron. The first term,  $H_{nr}$ , is the non-relativistic many-electron Hamiltonian. The second term,  $H_{mv}$ , is the mass-velocity term, which corrects for the relativistic variation in electron mass near the speed of light. The third term,  $H_{retardation}$ , corrects for the finite propagation speed of the electromagnetic field of the electron. The fourth term,  $H_{Darwin}$ , is the Darwin correction, described earlier. These four terms comprise scalar relativistic effects, and do not require a two-component wave function to implement. The fifth term,  $H_{SO}$ , is the spin-orbit coupling between the intrinsic spin angular momentum of the electron and the orbital angular momenta of all the electrons. The next term,  $H_{SS}$ , is the spin-spin coupling between the intrinsic spin-angular momenta of multiple electrons. In order to incorporate these terms, a two-component wave function is required. The last term,  $H_{external}$ , involves the interaction with an external electric and magnetic field. While only a perturbative treatment, valid for light atoms and molecules, the Breit-Pauli Hamiltonian sheds some light on the expected effects present in relativistic many-electron Hamiltonians.

With a well defined, albeit approximate, many-electron Hamiltonian, the next step in constructing relativistic wave functions is based on the Hartree-Fock mean field

theory. This provides the first theoretical method to many-electron systems; however, electron correlation is not explicitly included.

### Dirac Hartree-Fock Theory

The Hartree-Fock (HF) self-consistent field (SCF) method provides the theoretical framework to determine, non-relativistically, the properly antisymmetrized many-electron single-determinant wave function for atoms and molecules (Szabo et al, 1989: 108-152; Levine, 2000: 305-312). It also provides the basis for correlation calculations through multi-configuration and perturbation methods.

The non-relativistic many-electron Hamiltonian is given by (Levine, 2000: 305)

$$H = -\frac{\hbar^2}{2m_e} \sum_i \nabla^2 - \sum_i \frac{Ze^2}{4\pi\epsilon_0 r_i} + \sum_{i=1}^{n-1} \sum_{j=i+1}^n \frac{e^2}{4\pi\epsilon_0 r_{ij}}. \quad (47)$$

The goal of the HF approximation is to find a set of spin-orbitals, which minimize the ground state electronic energy. It is a variational theory, in that the exact ground state energy of an atom or molecule is a lower bound to the HF energy. Additionally, HF theory is a single determinant theory. This means that the ground state wave function obtained from the variationally optimized set of spin orbitals contains only a single electron configuration. The optimized set of spin-orbitals satisfy the equations (Szabo et al, 1989: 111-112)

$$E_0 = \langle \Psi_0 | H | \Psi_0 \rangle = \frac{-\hbar^2}{2m_e} \sum_a \langle \chi_a | \nabla^2 | \chi_a \rangle - \sum_k \frac{Z_k e^2}{4\pi\epsilon_0} \sum_a \langle \chi_a | \frac{1}{r_{ak}} | \chi_a \rangle + \frac{e^2}{4\pi\epsilon_0} \sum_{a<b} \langle \chi_a \chi_b | \frac{1}{r_{ab}} | \chi_a \chi_b \rangle, \quad (48)$$

where  $\chi_a$  is the spatial wave function of the  $a^{\text{th}}$  electron. The total wave function is the product of individual electron spatial functions,

$$\Psi_0 = |\chi_1 \chi_2 \dots \chi_a \chi_b \dots \chi_N\rangle. \quad (49)$$

The first two terms are one-electron operators, and correspond to the expectation values of the kinetic energy and potential energy of the  $a^{\text{th}}$  electron in the field of the  $k^{\text{th}}$  nucleus. The last term is the expectation value of the Coulomb interaction between the two electrons. It can be expanded into two terms

$$\begin{aligned} & \frac{e^2}{4\pi\epsilon_0} \sum_{a<b} \langle \chi_a \chi_b | \frac{1}{r_{ab}} | \chi_a \chi_b \rangle = \\ & \int d\bar{x}_a \left( \chi_a^*(1) \frac{e^2}{4\pi\epsilon_0} \sum_{a<b} \left( \int d\bar{x}_b |\chi_b(2)|^2 \frac{1}{r_{12}} \right) \chi_a(1) - \frac{e^2}{4\pi\epsilon_0} \chi_a^*(1) \sum_{a<b} \left( \int d\bar{x}_b \chi_b^*(2) \chi_a(2) \frac{1}{r_{12}} \right) \chi_b(1) \right) \end{aligned} \quad (50)$$

Writing equation 50 in operator form yields

$$\iint d\bar{x}_a d\bar{x}_b \chi_a^*(1) \left( \frac{e^2}{4\pi\epsilon_0} \sum_{a \neq b} J_b(1) - K_b(1) \right) \chi_a(1). \quad (51)$$

This final term results in two, one-electron operators, J and K. The first operator is the Coulomb operator and represents the average electric field due to electron two experienced by electron one. This is the origin of the mean-field concept. Each electron experiences an average potential due to all the other electrons. The second term is an exchange potential arising from the Pauli Exclusion Principle. Because the total wave function must be antisymmetric with respect to the exchange of two electrons, the motion between electrons with parallel spins is correlated in the HF theory. As a result, electrons experience an exchange potential, quantum mechanical in nature, which repels electrons with parallel spins and prevents them from occupying the same orbital (Szabo et al, 1989: 111-115). In its eigenvalue form, the HF equations are

$$\left( h + \sum_{a \neq b} J_b - \sum_{a \neq b} K_b \right) \chi_a = \varepsilon_a \chi_a, \quad (52)$$

where  $\varepsilon_a$  is the energy of the  $a^{\text{th}}$  electron. The one-electron operators are defined by

$$h = \frac{-\hbar^2}{2m_e} \sum_a \langle \chi_a | \nabla^2 | \chi_a \rangle - \sum_k \frac{Z_k e^2}{4\pi\epsilon_0} \sum_a \langle \chi_a | \frac{1}{r_{ak}} | \chi_a \rangle, \quad (53)$$

$$J_b \chi_a(1) = \frac{e^2}{4\pi\epsilon_0} \sum_{a < b} \left( \int d\bar{x}_b |\chi_b(2)|^2 \frac{1}{r_{12}} \right) \chi_a(1), \quad (54)$$

and

$$K_b \chi_a(1) = \frac{e^2}{4\pi\epsilon_0} \sum_{a < b} \left( \int d\bar{x}_b \chi_b^*(2) \chi_a(2) \frac{1}{r_{12}} \right) \chi_a(1). \quad (55)$$

The term in parentheses of the first equation is the Fock operator,  $f(\vec{r}_1)$ . In operator form, this equation is

$$f(\vec{r}_1) \psi_i(\vec{r}_1) = \varepsilon_a \psi_i(\vec{r}_1). \quad (56)$$

Expanding the unknown molecular orbitals,  $\psi_i(\vec{r})$ , in terms of a finite set of known basis functions,  $\phi_k$ , yields

$$\psi_i(\vec{r}_1) = \sum_{k=1}^K c_{ki} \phi_k. \quad (57)$$

Here, the  $c_{ki}$  are molecular orbital coefficients. This reduces the HF integro-differential equation to a set of algebraic equations: the Roothan equations (Szabo et al, 1989: 136-138)

$$\sum_{\nu} F_{\mu\nu} c_{\nu i} = \varepsilon_i \sum_{\nu} S_{\mu\nu} c_{\nu i}, \quad (58)$$

where  $F_{\mu\nu}$  is the Fock matrix, defined by

$$F_{\mu\nu} = \int d\vec{r}_1 \phi_\mu^*(1) f(1) \phi_\nu(1), \quad (59)$$

and  $S_{\mu\nu}$  is the overlap matrix, defined by

$$S_{\mu\nu} = \int d\vec{r}_1 \phi_\mu^*(1) \phi_\nu(1). \quad (60)$$

Thus, finding the optimal orbitals that minimize the Hartree-Fock energy consists of solving the Roothan equations in a self-consistent manner.

The non-relativistic HF theory and relativistic Dirac-Hartree-Fock (DHF) theory are analogous. In DHF theory (Saue et al, 1997: 937-948; Oreg , 1975: 830-841; Aoyama et al, 1980: 1329-1332; Matsuoka et al, 1980: 1320-1328; Kim, 1967: 154-39; Lee et al: 1977: 5861-5876; Dyall et al, 1991: 2583-2585), the non-relativistic Hamiltonian is replaced with the Dirac-Coulomb Hamiltonian, and the spin-orbitals have four components instead of one. These spinors can be complex, unlike the non-relativistic case, where the spin-orbitals were real. This four-component wave function is also expanded in a real basis, as was done in the non-relativistic case, where (Saue, 1997: 939)

$$\psi_k = \begin{pmatrix} \chi^L & 0 & 0 & 0 \\ 0 & \chi^S & 0 & 0 \\ 0 & 0 & \chi^L & 0 \\ 0 & 0 & 0 & \chi^S \end{pmatrix} \begin{pmatrix} c_k^\alpha \\ c_k^\beta \\ c_k^\alpha \\ c_k^\beta \end{pmatrix}. \quad (61)$$

Here,  $L$  and  $S$  represent the large and small components, respectively. There are two sets of expansion coefficients now,  $c_k^\alpha$  and  $c_k^\beta$  for the spin-up and spin-down components, respectively. In a manner analogous to the non-relativistic theory, these four-spinors are varied until the total electronic energy is minimized. This leads to a

matrix equation similar to the Hartree-Fock theory, except that the Fock matrix and expansion coefficients are now complex. The Fock matrix splits into two parts, a one-electron matrix (Saue, 1997: 940)

$$F_1 = \begin{pmatrix} V^{LL} & -icd_z^{LS} & 0 & -icd_-^{LS} \\ -icd_z^{SL} & W^{SS} & -icd_-^{SL} & 0 \\ 0 & -icd_+^{SL} & V^{LL} & icd_z^{LS} \\ -icd_+^{SL} & 0 & icd_z^{SL} & W^{SS} \end{pmatrix}, \quad (63)$$

where

$$V_{\mu\nu}^{XY} = \langle \chi_\mu^X | V | \chi_\nu^X \rangle, \quad (64)$$

$$d_{z,\mu\nu}^{XY} = \langle \chi_\mu^X | \frac{\partial}{\partial z} | \chi_\nu^X \rangle, \quad (65)$$

$$d_{\pm,\mu\nu}^{XY} = \langle \chi_\mu^X | \frac{\partial}{\partial x} \pm i \frac{\partial}{\partial y} | \chi_\nu^X \rangle, \quad (66)$$

and

$$W_{\mu\nu}^{XY} = \langle \chi_\mu^X | V - 2c^2 | \chi_\nu^X \rangle. \quad (67)$$

As in the non-relativistic case,  $V$  represents the potential energy of the electron. Atomic units are used here, where  $\hbar = e = m_0 = 1$ , in order to simplify the expressions.

The two-electron Fock matrix, is given by (Saue, 1997: 940):

$$F_2 = \begin{pmatrix} J^{L\alpha} - K^{LaL\alpha} & -K^{LaS\alpha} & -K^{LaL\beta} & -K^{LaS\beta} \\ -K^{SaL\alpha} & J^{S\alpha} - K^{SaS\alpha} & -K^{SaL\beta} & -K^{SaS\beta} \\ -K^{L\beta L\alpha} & -K^{L\beta S\alpha} & J^{L\beta} - K^{L\beta L\beta} & -K^{L\alpha L\beta} \\ -K^{S\beta L\alpha} & -K^{S\beta S\alpha} & -K^{S\beta L\beta} & J^{S\beta} - K^{S\beta S\beta} \end{pmatrix}. \quad (68)$$

Here,  $J^{L\alpha}, J^{L\beta}$  represents the Coulomb operator of the spin-up ( $\alpha$ ) and spin-down ( $\beta$ ) electrons respectively, while  $J^{S\alpha}, J^{S\beta}$  represents the mean-field due to positrons with

spin-up and spin-down, respectively. The exchange operator,  $K$ , becomes more complicated, reflecting the possibility of exchange between electronic ( $L$ ) components and positronic ( $S$ ) components with various spins.

One important difference exists between the non-relativistic Hartree-Fock and its relativistic counterpart. In the non-relativistic theory, the energy eigenvalue corresponding to the Fock operator was guaranteed to be greater than or equal to the exact energy by the variational principle. In the relativistic case, the existence of positronic negative energy solutions means that the DHF energy is not bounded from below. In the non-relativistic case, there were no negative energy solutions. In the relativistic case, electronic solutions look like excited positronic states, and unless care is taken during the solution of the relativistic Roothan equations, variational collapse can occur. This occurs because of the fact that a bound electronic-positronic state is degenerate with an unbound electronic-positronic state in the relativistic theory. Thus, instead of variationally optimizing the orbitals as in the non-relativistic case, the orbitals are minimized with respect to electronic states and simultaneously maximized with respect to positronic states. Another complication with the relativistic DHF theory is that the basis sets for the large and small components are related via a “kinetic balance” requirement (Dyall, 1991: 2585)

$$\chi^S = \vec{\sigma} \cdot \nabla \chi^L. \quad (69)$$

Here, the small component (positronic) wave functions are related to the 2x2 Pauli spin-matrix,  $\vec{\sigma}$ , operating on the gradient of the large component (electronic) wave function.



DHF methods suffer several computational difficulties (Saue, 1997: 937-938). First, spin and spatial wave functions are coupled, resulting in complex total wave functions in general. Thus, spatial and spin symmetry can not be handled separately, which has resulted in substantial computational savings for non-relativistic computations. Another computational difficulty lies in the fact the DHF basis sizes are generally much larger than their non-relativistic counterparts. Both the large and small components are expanded in separate, but coupled basis sets. The small basis set size can be generally twice the size of the large component basis. Computationally, the Hartree-Fock method scales minimally as  $N^4$ , where  $N$  is the number of basis functions. Thus, Dirac-Hartree-Fock calculations typically involve an order of magnitude or more increase in computational complexity over non-relativistic Hartree-Fock computations. These difficulties currently limit DHF methods to atoms and some small molecules. A recent DHF calculation (de Jong, et al, 1999: 45) for  $\text{UO}_2^{2+}$  compares the non-relativistic and relativistic results for the ground electronic states. Electron correlation was included in this calculation via coupled cluster singles and doubles with some triples (CCSD(T)) (Raghavachari, 1996: 12964-12965), and this calculation represents perhaps the all-electron computational state-of-the-art on the ground state of uranyl (de Jong, 1999: 41-52). Figure 3 reproduces the electronic states from the paper.

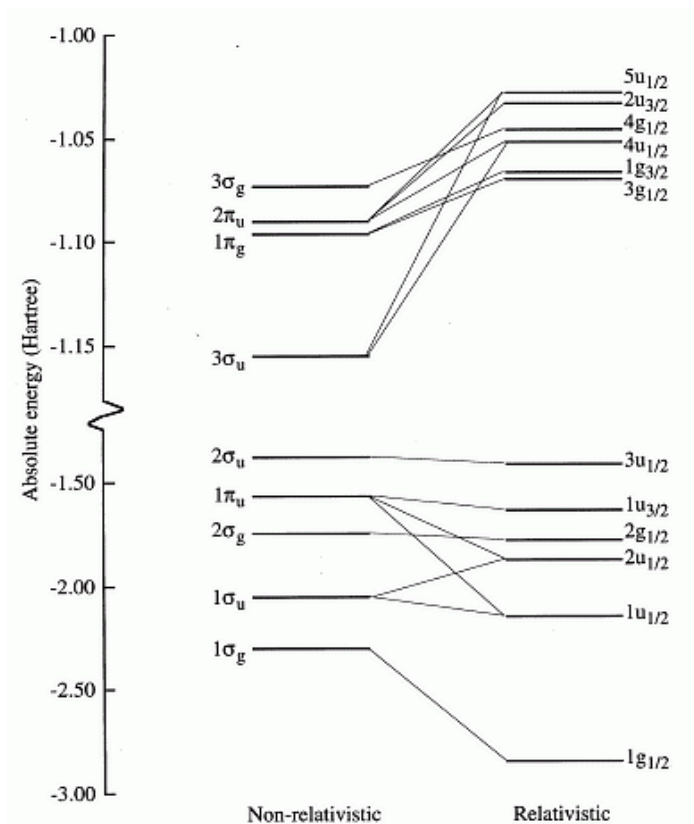


Figure 3. Electronic Ground State for Uranyl Using Both Non-relativistic HF and Four-component, Fully Relativistic DHF Methods (de Jong, 1999: 45)

Dirac-Hartree-Fock theory can result in fairly accurate, fully-relativistic calculations of molecular electronic ground states. Like the non-relativistic counterpart, DHF provides the best, single-determinant wave function, ignoring electronic correlation effects. As such, HF and DHF can describe only the electronic ground state. In order to describe the excited electronic states, electronic correlation needs to be incorporated, and the wave function must be expanded in a series of determinants. As was evident in the DHF equations, the fully relativistic treatment can become quite complicated and computationally intensive. What is needed is a method that is a compromise between the non-relativistic and fully-relativistic methods that also provides computational savings

when computing electron correlation energies using multi-configuration methods.

Relativistic effective core potentials prove to be just such a compromise.

### **Relativistic Effective Core Potentials**

The DHF method provides a basis for constructing the approximate relativistic wave function for atoms and molecules. It is an all-electron method, and the number of electrons that must be treated explicitly for actinide elements and molecules is large. Given the requirements for kinetic balance between the basis sets for the large and small components, the number of basis functions required for accurate treatment of heavy atoms and molecules can easily become formidable for interesting actinide molecules. Thus, a method for accurately treating relativity and only explicitly including those electrons that are relevant chemically is attractive. The relativistic effective core potential (RECP) method accomplishes both of these goals.

Several different types of RECPs exist. Among them include potentials by Küchle, Dolg, Stoll, and Preuss (Küchle et al, 1994: 7535-7542), Hay and Wadt (Hay, 1993: 5469), and Christiansen style RECPs (Ermler et al, 1988: 139-182), among others. The Christiansen style RECPs were selected for this work for their spin-orbit operator.

The RECP method (Pacios, 1985: 2664-2671; Lee et al, 1977: 5861-5876; Ermler et al, 1991: 829-846; Ermler et al, 1988: 139-182) is based upon the assumption that atomic or molecular electrons can be separated into an inert core region and a chemically-active valence region. The RECPs are generated from the large component

valence electron solutions to numerical DHF calculations of the form (Pacios et al, 1985: 2664)

$$\left( \frac{-\nabla^2}{2} - \frac{Z_v}{r} + U_{lj}^{RECP}(r) + J_{lj} - K_{lj} \right) X_{lj} = \varepsilon_{lj} X_{lj}. \quad (70)$$

Here,  $Z_v$  is the number of valence electrons, while  $J_{lj}$  and  $K_{lj}$  represent the Coulomb and exchange terms. Atomic units are used here. This equation is inverted in order to recover the core potential term for a particular value of  $l$  and  $j$ . The radial dependence of the pseudospinor,  $X_{lj}$ , is determined from

$$X_{lj}(r) = \psi_{lj}(r) + F_{lj}(r) \quad (71)$$

$X_{lj}$  is referred to as a pseudospinor, because it approximates the two-component, electronic portion of the fully-relativistic four-component spinor.

The wave functions,  $\psi_{lj}$ , are determined from the large component DHF solutions, while the second term,  $F_{lj}(r)$  is selected to cancel radial oscillations in the core region and eliminate nodes in the pseudospinor. It is critical to generate a nodeless pseudospinor in order to invert equation 70 and recover the core potential (Pacios, 1985: 2664). The core potentials generated are of the form (Ermler et al, 1991: 829-830)

$$U^{RECP} = U_{LJ}^{RECP}(r) + \sum_{l=0}^{L-1} \sum_{j=|l-\frac{1}{2}|}^{|l+\frac{1}{2}|} \sum_{m_j=-j}^j (U_{lj}^{RECP}(r) - U_{LJ}^{RECP}(r)) \cdot |l j m_j\rangle \langle l j m_j| \quad (72)$$

Here,  $|l j m_j\rangle$  and  $\langle l j m_j|$  are projection operators, ensuring the core potentials interact with those parts of the wave function with the corresponding orbital angular momentum,  $l$ , total angular momentum,  $j$ , and z-component of total angular

momentum,  $m_j$ . While the sum over  $l$  is infinite in principle, truncation of the sum at an orbital angular momentum one greater than the largest  $l$  quantum number of the core electrons introduces negligible error (Ermler et al, 1991: 830). A weighted average relativistic effective core potential is then generated by (Ermler et al, 1991: 830; Ermler et al, 1999: 152-153)

$$U^{ARECP} = U_L^{ARECP}(r) + \sum_{l=0}^{L-1} \sum_{m_l=-l}^l (U_l^{ARECP}(r) - U_L^{ARECP}(r)) \cdot |lm_l\rangle\langle lm_l|, \quad (73)$$

and

$$U_l^{ARECP}(r) = \frac{1}{2l+1} \left( l \cdot U_{l,l-\frac{1}{2}}^{RECP}(r) + (l+1) \cdot U_{l,l+\frac{1}{2}}^{RECP}(r) \right). \quad (74)$$

The purpose for generating the average relativistic effective core potential is to separate the scalar relativistic effects (mass-velocity, Darwin terms) from the spin-orbit effects. Scalar relativistic effects can be incorporated into spin-free wave functions. Spin-orbit effects require the introduction of electron spin, and consequently, require a two-component wave function. An effective spin-orbit Hamiltonian is generated by (Ermler et al, 1991: 830; Ermler et al, 1988: 152)

$$H_{SO} = \vec{S} \cdot \sum_{l=1}^L \frac{2}{2l+1} \Delta U_l^{RECP}(r) \sum_{m_l=-l}^l |lm_l\rangle\langle lm_l| \vec{L} |lm_l\rangle\langle lm_l|, \quad (75)$$

where

$$\Delta U_l^{RECP}(r) = U_{l,l-\frac{1}{2}}^{RECP}(r) - (l+1) \cdot U_{l,l+\frac{1}{2}}^{RECP}(r). \quad (76)$$

This spin-orbit Hamiltonian can be written in the form (Ermler et al, 1988: 153)

$$H_{SO} = \sum_l \zeta(r) \left( \vec{L} \cdot \vec{S} \right) \sum_{m_l} |lm_l\rangle\langle lm_l|. \quad (77)$$

The function  $\zeta(r)$  is a constant that depends on the radial quantum number of the orbitals involved. The projection operators  $|l m_l\rangle\langle l m_l|$  in all forms of the effective core potentials ensure that orbitals with the correct angular momentum interact with the correct core potential term. The spin-orbit potential formed this wave acts as a one-electron operator. As such, it is only approximately valid for the Dirac-Coulomb Hamiltonian. Higher-order electron-electron interactions represented by the Dirac-Coulomb-Breit Hamiltonian are not effectively modeled using this spin-orbit operator.

Once the core potential and spin-orbit potentials are obtained, they are approximated by Gaussian function fits of the form

$$U_l^{ARECP}(r) = \frac{1}{r^2} \sum_{i=1}^M C_{li} r^{n_{li}} e^{-\alpha_{li} r^2}, \quad (78)$$

with expansion coefficients  $C_{li}$  and exponents  $\alpha_{li}$ , facilitating their use in standard *ab initio* computational packages.

The benefit of RECPs is that they can be used to incorporate scalar relativistic effects in normally non-relativistic theoretical methods such as HF, MCSCF, or Density Functional Theory (DFT). In addition, RECPs offer a way to substantially reduce the number of explicitly treated electrons. RECPs are currently the most commonly used method for theoretical studies of heavy element molecules.

## Electron Correlation Models

The development of accurate relativistic core and spin-orbit potentials enables the inclusion of relativistic effects in non-relativistic theoretical methods. This allows the successful application of powerful theoretical methods developed for use in light

molecule calculations to be applied to heavy element molecules at a reasonable computational cost. While this section will discuss electron correlation techniques from a non-relativistic standpoint, all have either been applied to relativistic calculations directly, as with MP2 and MCSCF, or indirectly, via RECPs incorporated into the non-relativistic technique.

Electronic correlation effects are not directly observable, according to Raghavachari (Raghavachari, 1996: 12960). Electronic correlation is a measure of that energy that is not accurately modeled by the Hartree-Fock theory. In fact, correlation energy is defined as the difference between the exact non-relativistic energy and the Hartree-Fock energy. This inaccuracy, inherent in the Hartree-Fock model, incorrectly models the dissociation of molecules into constituent atoms. Improvements to HF that model this energy accurately can predict the correct dissociation energies for molecules, among other properties.

Since the HF single determinant wave function frequently accounts for a large fraction of the total electronic energy, one popular and efficient technique for determining electron correlation energies is through perturbation theory. The electron correlation is treated as a small perturbation to the HF wave function, and corrections to the HF wave function and energy are computed via a perturbation expansion. The most frequently used is second order perturbation theory, also known as Møller-Plesset second order perturbation theory (MP2). In MP2, the Fock operator is the zeroth-order Hamiltonian, and both the HF wave function and HF energy are expanded in a power series of the perturbation (Raghavachari et al, 1996: 12962; Szabo et al, 1989: 350-353). Using this perturbative technique, one can show that the HF energy is correct to first

order, and corrections to this energy occur at second order and beyond. Higher order perturbation corrections are possible; however, MP2 is the most frequently used. The perturbed Hamiltonian,  $H'$ , is given by

$$H' = H_0 + V . \quad (79)$$

The zeroth-order Hamiltonian is the Fock operator,

$$H_0 = \sum_i h_i + \sum_{i<j} J_{ij} - K_{ij} , \quad (80)$$

while the perturbation is given by

$$V = \sum_{i<j} \frac{1}{r_{ij}} - J_{ij} + K_{ij} . \quad (81)$$

The sum of the zeroth and first-order energies correspond to the HF energy. The second order correction to the energy is given by (Szabo et al, 1989: 351).

$$E_0^{(2)} = \sum_{i,n \neq i} \frac{|\langle \chi_i | V | \chi_n \rangle|^2}{E_i^{(0)} - E_n^{(0)}} . \quad (82)$$

Here, the unperturbed N electron wave function is written as the product of N spatial wave functions,

$$\Psi_0 = \chi_0 \chi_1 \chi_2 \dots \chi_n \dots \chi_N \quad (83)$$

and  $E_i^{(0)}$  represents the Hartree-Fock energy of the  $i^{\text{th}}$  spatial function. The result of this second-order perturbation expansion of the Hartree-Fock wave function is to introduce some single and double excited state energies into the ground state energy. Singly excited wave functions do not couple directly with the HF wave function. They do; however, couple to the doubly excited wave functions, which in turn are coupled to the HF wave function. This is proven in Brillouin's Theorem (Szabo et al, 1989: 128-129).



MP2 theory scales computationally as the number of basis functions ( $K$ ) to the fifth power ( $K^5$ ) (Raghavachari et al, 1996: 12962), making it attractive compared to HF alone, which scales as  $K^4$ . Higher order perturbations scale as the sixth, seventh, and eighth power for third, fourth, and fifth order perturbations respectively, making perturbations beyond fourth order computationally demanding and seldom used.

Another common technique for modeling electron correlation energy is through a multi-configurational approach, which involves expanding the wave function in a linear combination of excited electronic configurations (Raghavachari et al, 1996: 12962). Various expansion terms then represent exciting electrons from the reference configuration into a number of excited configurations. Then all that is necessary is to determine the expansion coefficients. If all possible configuration state functions were used, the expansion would be exact; however, in practice, this expansion must be truncated. As with the finite basis set expansion for the single determinant wave function, this truncation introduces error into the correlated wave function. This multi-configurational technique is necessary to accurately describe excited electronic states. The reason for this is that excited electronic states with the same term symbols mix with the ground state. The Hartree-Fock neglects this mixing by writing the wave function as a single Slater determinant, however, the actual ground state wave function contains contributions with excited states with the same term symbol. A more accurate wave function expansion requires multiple Slater determinants, where each determinant represents a particular state (ground and excited).

One method for improving upon the HF wave function is to include a relatively small number of additional configurations (Raghavachari et al, 1996: 12967). This

technique is the multi-configuration self-consistent field method (MCSCF). In the MCSCF approach, the wave function is expanded in a small set of configuration wave functions (Szabo et al, 1989: 258).

$$\Psi_{MCSCF} = c_0 \Psi_0 + c_1 \Psi_1 + \dots + c_n \Psi_n, \quad (84)$$

where the  $c_i$  are CI coefficients. Then, both the CI and molecular orbital coefficients are variationally optimized. The MCSCF method is identical to the HF method if only one expansion wave function is used. Reference configurations can be chosen to include chemically relevant states, or states that may be nearly degenerate with the HF ground state. However, this approach can introduce bias into the calculation (Raghavachari et al, 1996: 12967). A way to avoid this bias is to identify a set of active orbitals, typically the highest occupied molecular orbitals (HOMO), and include all possible excited configurations arising from this active space. This is a complete active space (CAS) approach. It is beneficial to use a CAS approach when the excited states of a molecule may not be well-known; however, the number of configurations included in a CAS MCSCF can quickly become enormous if the active space is large, or there are a large number of virtual orbitals.

Another benefit to the MCSCF method is that it provides an improved wave function for use in the more general configuration interaction (CI) approach. The CI wave function is written as

$$\Psi = c_0 \Psi_0 + \sum_a c_1^a \Psi_a^r + \sum_{a,b} c_2^{ab} \Psi_{ab}^{rs} + \sum_{a,b,c} c_3^{abc} \Psi_{abc}^{rst} + \dots \quad (85)$$

Where the first term is the HF wave function, the second term is a sum over all singly excited states from the HF ground state, the third term consists of a sum over all doubly

excitations, etc. Including all possible determinants is a full CI expansion, which provides the correlation exactly; however, such an expansion is almost never possible except for very small systems using minimal basis sets. In practice, this CI expansion must be truncated at some point. It can be shown (Szabo et al, 1989: 128-131) that there is no direct mixing between the HF ground state and the singly excited states. However, the HF ground state does mix with the doubly excited states, which in turn couples to the singly excited states. Thus, the first logical place to truncate the CI expansion in order to obtain an improvement over the HF wave function is to include single and double excitations (CISD). The CISD wave function is given by

$$\Psi_{CISD} = c_0 \Psi_0 + \sum_a c_1^a \Psi_a^r + \sum_{a,b} c_2^{ab} \Psi_{ab}^{rs}, \quad (86)$$

where the expansion coefficients are variationally optimized. The CISD method, while conceptually simple, is very demanding computationally. In an N-electron system using K basis functions, the number of all possible double excitations is given by (Szabo et al, 1989: 234)

$$\binom{N}{2} \binom{2K-N}{2}. \quad (87)$$

Thus, the CISD method scales roughly as  $(2K)^2 N^2$ . Truncating the expansion at the quadruple excitation level scales roughly as  $(2K)^4 N^4$ , while sextuple excitations scales as  $(2K)^6 N^6$ . It is apparent that the CI method increases in computational difficulty very quickly. While the full CI does scale linearly with the size of the system, the truncated CI expansions do not.

By allowing single and double excitations from a multi-reference wave function, as opposed to the single reference wave function, some triple and quadruple excitations are effectively included in the CISD expansion. References are those electronic configurations from which electrons can be excited out of in the CI expansion. This is known as multi-reference CISD (MR-CISD). Single- and multi-reference CI expansion methods are some of the few theoretical methods available for exploring atomic and molecular excited states.

One important point to note when using CI expansion methods is that the choice of orbitals can impact the accuracy of the CI expansion. There are two types of orbitals one can use when performing a CI expansion: molecular and natural orbitals. Natural orbitals are those orbitals which diagonalizes the density matrix,  $\gamma(\vec{x}_1, \vec{x}_1')$ , given by (Szabo et al, 1989: 252-257)

$$\gamma(\vec{x}_1, \vec{x}_1') = \sum_{ij} \chi_i(\vec{x}_1) \gamma_{ij} \chi_j^*(\vec{x}_1'), \quad (88)$$

where  $\gamma$  and  $\gamma_{ij}$  are defined by

$$\gamma_{ij} = \int dx_1 dx_1' \chi_i^*(\vec{x}_1) \gamma(\vec{x}_1, \vec{x}_1') \chi_j(\vec{x}_1') \quad (89)$$

The  $\chi_i$  in equation 88 are the spatial orbitals, while  $\Psi(\vec{x}_1, \vec{x}_2, \dots, \vec{x}_N)$  is the electronic wave function, which is the product of the spatial orbitals.

The molecular orbitals diagonalize the Fock matrix, but they do not diagonalize the density matrix. A CI expansion using the natural orbitals converges faster than one formed from molecular orbitals (Szabo et al, 1989: 255). Thus, a CI expansion using molecular orbitals will require more configuration state functions to achieve the accuracy

of an expansion formed from natural orbitals. In many cases, the difference in accuracy may be negligible; however, there are some cases where this accuracy difference can be substantial. One difficulty; however, is that in order to obtain the natural orbitals, one needs the CI wave function (Szabo et al, 1989: 257). Luckily, approximate natural orbitals, formed from a small number of configurations, such as an MCSCF wave function, are almost as good as natural orbitals obtained from the CI wave function (Szabo et al, 1989: 257).

One final note for electron correlation techniques is in order, especially when incorporating relativistic spin-orbit effects. Because electron correlation is determined primarily by a two-electron operator between pairs of reference configurations and between reference configurations and doubly excited configurations, it is generally more difficult to converge computationally than spin-orbit effects. Spin-orbit effects are expressed in the core potential formulation as one-electron operators between pairs of reference configurations and singly excited configurations (Yabushita et al, 1999: 5792). As a result of the two-electron operator, accurately modeling electron correlation is a more difficult problem than inclusion of relativistic spin-orbit effects, and efficiently handling the electronic correlation will, in general, lead to accurate inclusion of spin-orbit effects. And so, when incorporating spin-orbit effects into electronic structure calculations, it makes sense to include them in conjunction with electron correlation at the same time, rather than as separate steps (Yabushita et al, 1999: 5792).

While the previous methods for modeling electron correlation are all based upon approximations to the many-electron wave function (Head-Gordon, 1996: 13218), one method which is not based on wave functions, has seen tremendous growth and

application in the past decade. This technique is known as Density Functional Theory (DFT), and it is based upon the premise that the exact molecular ground state energy is a functional of the electron density (Nagy, 1998: 5). The electronic density,  $\rho$ , of an  $n$ -electron system is a function of three variables, while the  $n$ -electron wave function is a function of  $3n$  variables. This reduction in degrees of freedom results in substantial computation savings with DFT over wave function based methods. This energy is given by (Head-Gordon, 1996: 13218)

$$E(\rho) = T(\rho) + V_{en}(\rho) + J(\rho) + V_{xc}(\rho). \quad (90)$$

Here,  $T$  is the kinetic energy,  $J$  is the Coulomb repulsion,  $V_{en}$  is the electron-nuclear interaction, and  $V_{xc}$  is the electron exchange and correlation interaction. The Coulombic electron-electron and electron-nuclear terms are straightforward and can be computed classically, using a non-interacting Fermi gas model derivable from a statistical treatment of the atom has a degenerate electron gas. The kinetic energy and exchange-correlation terms cannot. Kohn and Sham showed (Kohn et al, 1996: 12974-12975; Nagy, 1998: 7-12) that this energy can be recast into a form where the kinetic energy is approximated by a system of non-interacting electrons. This results leads to the Kohn-Sham equations (Nagy, 1998: 9)

$$\left( -\frac{\nabla^2}{2} + v(\vec{r}) + v_j(\vec{r}) + v_{xc}(\vec{r}) \right) u_i = \varepsilon_i u_i, \quad (91)$$

$$v_j(\vec{r}) = \int \frac{\rho(\vec{r}')}{|\vec{r} - \vec{r}'|} d\vec{r}', \quad (92)$$

and

$$v_{xc}(\vec{r}) = \frac{\delta E_{xc}[\rho]}{\delta \rho}. \quad (93)$$

Here,  $v(\vec{r})$  is an external potential and  $u_i$  is the wave function. Thus, the electron exchange and correlation interactions, as well as the fraction of kinetic energy not accounted for in the non-interacting gas model are wrapped into the exchange-correlation functional. Various attempts at developing an exact form for this functional have been unsuccessful; however, several approximate functionals have been developed and successfully applied to electronic structure calculations (Head-Gordon, 1996: 13218). The most successful correlation functionals have been gradient-corrected approximate (GGA) correlation functionals, while successful exchange functionals are based upon parameter fits to the exchange energies of noble gases (Head-Gordon, 1996: 13218; Nagy, 1998: 41-45). Combinations of the GGA and semi-empirical functionals form hybrid functionals, which also have been very successful in treating many ground-state molecular properties. The accuracy achieved with DFT frequently rivals or beats MP2 results, with less computational effort. One drawback to DFT at present; however, is that DFT is a ground state theory only. DFT has not been successful at describing excited electronic energies. In addition, unlike wave function based theories, there is no known way to systematically improve the results obtained with DFT. Without the ability to accurately describe excited electronic states directly, or approximate excited electronic state energies via a systematic improvement process (perturbation theory), DFT, despite its successes, is simply not an option when calculation theoretical electronic spectra of uranium oxides.

## Summary

This chapter briefly covered some of the theory behind relativistic electronic structure calculations. As evidenced by results from perturbation theory, relativistic effects must be included for heavy element compounds, uranium in particular. Additionally, electron correlation effects, expected to be large in actinide molecules pose additional theoretical challenges. As a result, theoretical relativistic electronic structure calculations on actinide molecules have pushed the state-of-the-art in *ab initio* molecular calculations for many years, and they will continue to do so.

In order to accurately model excited electronic states in uranium oxides, relativistic effects must be incorporated, and some type of multi-configurational approach must be used. Because of the large number of electrons that must be treated in order to accurately describe excited electronic states, a fully-relativistic method, such as Dirac-Hartree-Fock, coupled with either many-body perturbation theory or a multi-configuration method is too computationally demanding. By using a relativistic effective core potential method, relativistic effects are incorporated to first order, and the number of electrons that must be treated explicitly in advanced correlation techniques is reduced. These compromises prove to be acceptable in the chemically active valence region of uranium, which is responsible for the optical fluorescence spectra in uranyl, as well as low energy photoelectron spectra.



### **III. Resources and Methodology**

The complexity involved in theoretical studies of heavy-element molecules requires powerful computing platforms and specialized software. While theoretical calculations on small, light-element molecules can be performed to within chemical accuracy on personal computers (PCs), comparable accuracy with actinide molecules often requires, large, massively parallel computers with large amounts of memory, disk storage capacity, and high input/output throughput. Also, software must be specifically designed, and theoretical algorithms carefully constructed, in order to make optimal use of these computing platforms.

#### **Hardware Resources**

The theoretical calculations performed in this study used parallel computing clusters at AFIT and at the Aeronautical System Center's (ASC) Major Shared Resource Center (MSRC).

The parallel computing cluster at AFIT consists of 64 PCs running Redhat Linux 7.3 operating system. Sixteen of these PCs have 1.4 GHz Athlon Advanced Micro Devices (AMD) processors with 775 megabytes (Mb) random access memory (RAM), 20 gigabyte (Gb) local disk space, and they are networked via fast Ethernet. The other 48 PCs each contain dual 1 GHz Pentium III processors, 1 Gb RAM, and 20 Gb local hard

disk storage. Thirty-two of these dual-processors PCs are networked via fast Ethernet, while the other 16 dual-processor PCs are networked via Myranet.

Three parallel clusters were used at the ASC MSRC. The first two clusters consist of Compaq ES 40 and ES 45 machines. The ES 40 cluster consists of 16 symmetric multiprocessor (SMP) nodes, with each node containing four, 833 MHz processors and 4 Gb shared memory per node. The cluster has access to a total workspace of about 800 Gb (HP/Compaq ES40/45 User's Guide, 2002: 4). The Compaq ES 45 cluster consists of 81 and 128 SMP nodes containing four, 1 GHz processors per node. Each node has 4 Gb shared memory, and the cluster has a total workspace of 8 Tb (HP/Compaq ES40/45 User's Guide, 2002: 4).

The third cluster consisted of 132 IBM SP 3 SMP nodes. Each node contains four, 375 MHz processors, 4 Gb shared memory, and 2.4 terabytes (Tb) workspace (IBM SP P3 User's Guide, 2002: 1).

### **Software Resources**

This research project used two software packages. The first package, NWChem version 4.0.1<sup>3</sup>, was developed by the Molecular Sciences Software group of the Theory, Modeling & Simulation program of the Environmental Molecular Sciences Laboratory (EMSL) at the Pacific Northwest National Laboratory (PNNL). It was designed to perform a wide range of molecular calculations on massively parallel computing platforms (NWChem, 2002; High Performance Computational Chemistry Group, 2002). NWChem was used for geometry optimizations, vibrational frequency calculations, and

---

<sup>3</sup> NWChem home page is at <http://www.emsl.pnl.gov:2080/docs/nwchem/nwchem.html>

some single point energy calculations without spin-orbit potentials on uranyl and uranate ions.

NWChem was compiled and tested on the AFIT cluster using the GNU FORTRAN 77 compiler. It was also installed and tested on the MSRC Compaq ES40/45 clusters by MSRC personnel.

The second software package used was COLUMBUS version 5.8.1.

COLUMBUS<sup>4</sup> (Lischka, 2001; Lischka, 2000; Tilson, 2000; Yabushita, 1999; Sheppard, 1988) is a suite of FORTRAN programs developed at Ohio State University and Argonne National Laboratories, and it is maintained at the University of Vienna, Austria.

COLUMBUS was used to perform SCF, MCSCF, and two-component MR-CISD calculations on both the uranyl and uranate ions. COLUMBUS was compiled and tested on the AFIT cluster using the GNU FORTRAN 77 compiler. MSRC personnel installed and tested COLUMBUS 5.8.1 on the IBM SP P3 cluster. The SCF and MCSCF calculations did not use spin-orbit potentials; however, the MR-CISD calculations included spin-orbit potentials for uranium and oxygen. Unfortunately, COLUMBUS 5.8.1 does not include a parallelized version of the spin-orbit CI (SOC) program. While this had no effect on the calculation, it limits the practical number of configuration state functions (CSFs) in the CI calculation to about 10 million. COLUMBUS 5.9 does have a parallel multi-reference SOC (MR-SOC) program.

---

<sup>4</sup> COLUMBUS home page is at <http://www.ite.univie.ac.at/~hans/Columbus/columbus.html>

## Geometry Optimizations

Geometry optimizations were performed using NWChem version 4.0.1 on both the uranyl and uranate ions to determine molecular symmetry, bond lengths, and vibrational frequencies.

All geometry optimizations used the DRIVER module of NWChem, with tight convergence tolerance. This corresponded to a root-mean-square gradient tolerance of  $10^{-5}$  and a maximum gradient of  $1.5 \cdot 10^{-5}$ . Geometry optimizations were performed without symmetry constraints, in order to determine molecular symmetry. Subsequent geometry optimizations used the molecular point-group symmetry determined by this geometry optimization. Only those geometries which yielded all positive and real vibrational frequencies at both DFT and MP2 levels of theory were considered to be valid molecular geometries.

The following basis sets and effective core potentials were used for the uranium atom during the geometry optimizations with NWChem 4.0.1:

- Christiansen, Ross, and Ermler large-core basis and ARECP (Ermler et al, 1991: 829-846)
- Küchle, Dolg, Stoll and Preuss small-core basis and RECP (Küchle et al, 1994: 7535-7542)

For the oxygen atoms, the following basis sets and core potentials were used:

- Pacios and Christiansen large-core basis and RECP (Pacios et al, 1985: 2664-2671)

- Bergner, Dolg, Küchle, Stoll, and Preuss small-core basis and RECP (Bergner et al, 1993: 1431-1441)
- Correlation-consistent, polarized, all-electron, double- $\zeta$  basis set (cc-pvdz) (Dunning, 1989: 1007-1023)
- Augmented, correlation-consistent, polarized, double- $\zeta$  (aug-cc-pvdz) (Kendall et al, 1992: 6796-6806)

Geometry optimizations were performed using Hartree-Fock SCF, MP2, and DFT levels of theory. For DFT optimizations the B3LYP (Stephans, 1994: 11623), Becke97 (Becke, 1997), and Becke98 (Becke, 1998: 9624-9631) exchange-correlation functionals were used. Optimization results are included in the next chapter.

Unconstrained uranyl optimizations resulted in a linear molecule. As a result, subsequent optimizations were constrained using  $D_{2h}$  and  $D_{4h}$  point group symmetries.

Unconstrained uranate optimizations indicated a tetrahedral and distorted tetrahedral geometries for the gas phase ion.

### **Overview of COLUMBUS Calculations**

Once an appropriate geometry was determined, COLUMBUS 5.8.1 was used to compute excited electronic state energy levels. The basic procedure for COLUMBUS calculations involved running a series of FORTRAN programs, culminating in the MR-CISD calculation. The following programs were run, in order, to compute the excited electronic state energy levels: ARGOS, CNVRT, SCFPQ, MCDRT, MCUFT, MCSCF, MOFMT, CIDRT, CIUFT, TRAN, CISRT and CIUDG.

The ARGOS program computes the one- and two-electron atomic orbital integrals used in the SCFPQ, MCSCF, and CIUDG programs. The CNVRT program converts these integrals into PK supermatrix form, to speed up SCF convergence. The SCFPQ program performs the HF self-consistent field calculations. The MCDRT and MCUFT programs set up the distinct row table for the MCSCF calculations. The MCSCF program performs the multi-configuration self-consistent field calculation, while the MOFMT program extracts molecular and natural orbital coefficients from the converged MCSCF wave function. The CIDRT and CIUFT programs set up the distinct row table for the MR-CISD calculation. The TRAN program converts the atomic orbital integrals into molecular orbital integrals, and the CISRT program sorts these integrals into groups of zero-external, one-external, and two-external integrals (Yabushita et al, 1999: 5797). The CIUDG program then diagonalizes the matrix-vector products of the Hamiltonian matrix and trial vectors in order to obtain the ground and excited electronic state energies.

### **COLUMBUS Calculations on Uranyl ( $\text{UO}_2^{2+}$ )**

Calculations on uranyl were performed using the linear  $D_{2h}$  molecular point-group symmetry, an abelian subgroup of  $D_{\infty h}$ . Refer to Appendix A for a discussion on the symmetry aspects of the linear uranyl ion and a definition of  $D_{\infty h}$  and  $D_{2h}$  terms and states arising from electronic configurations in uranyl.

Because of symmetry, the uranyl potential energy surface (PES) could be characterized by a single parameter: the U-O bond length. With symmetry, there is only one symmetry unique oxygen atom in the uranyl ion. Varying this U-O bond length was

equivalent to varying the symmetric stretch normal mode coordinate. Calculations were performed using both the large and small-core uranium RECPs. The small-core RECP was obtained from Dr. Phil Christiansen<sup>5</sup>. The small-core basis set was obtained from Dr. Russell Pitzer's group at Ohio State University (OSU). The small-core basis set is a generally contracted basis set, (7s8p7d5f4g)→[7s6p7d2f4g].

Neither the small-core RECP, nor its associated basis set have been published. The only difference between the small-core RECP and the large-core RECP was that the small-core potential included the uranium 5d shell in the valence space, while this shell was included in the core of the large-core potential. The basis set used for both the large- and small-core uranyl calculations included several diffuse p-functions and four polarization g-functions.

The large core calculations were done in order to calibrate the calculations and compare results to those obtained by OSU (Zhang et al, 1999: 6880-6886). The small core calculations were then compared to the large core uranyl results, and both results were compared to uranyl spectroscopic data (Denning, 1992: 217-275; Rabinowitch et al, 1964: 48). This comparison allowed for qualitative conclusions to be drawn on the accuracies of the large core RECP versus the small core RECP.

First, a series of SCF calculations were performed over a range of U-O bond lengths. The minimum to this potential energy surface was determined from a 4th order polynomial fit to these SCF energies. Expanding this fitting polynomial in a Taylor series about the interpolated equilibrium point, then computing the second derivative

---

<sup>5</sup> Christiansen-style RECPs and spin-orbit potentials can be downloaded from <http://www.clarkson.edu/~pac/reps.html>

yielded the symmetric stretch vibrational mode force constant, from which the symmetric stretch vibrational frequencies were computed. This fitting procedure was used to determine the potential energy surface minima and symmetric stretch force constants in all subsequent calculations on uranyl and uranate.

Following this series of SCF ground state calculations, a series of MCSCF calculations were performed, averaging the  $3\sigma_u^2$  ground-state with the  $3\sigma_u^1 1\delta_u^1$  and  $3\sigma_u^1 1\phi_u^1$  low lying excited state configurations arising from singlet and triplet  $A_g$  and triplet  $B_{1g}$ ,  $B_{2g}$ , and  $B_{3g}$  symmetries. The  $2\pi_u$  and  $3\pi_u$  orbitals were thoroughly mixed in this calculation, in a manner similar to that done in the original calculation at OSU (Zhang et al, 1999: 6883). The uranium 5d orbitals were frozen in the small-core MCSCF calculation. Thus, the uranium 5d orbitals were forced to be occupied in all references, however, the 5d electrons were included in the correlation calculations. Freezing these electrons prevented excitations from the 5d shell. Also frozen were the highest three  $A_g$  virtual orbitals and the highest  $B_{1g}$ ,  $B_{2g}$ , and  $B_{3g}$  virtual orbitals. This state-averaged MCSCF wave function over the ground- and first low-lying excited states was used in order to obtain a balanced description of the ground and low-lying excited states. Both the large-core and small-core MCSCF calculations were over a restricted active space consisting of two electrons in five orbitals, where the first orbital was restricted to have at least one electron.

Next, the converged MCSCF wave function was used as the starting point for a MR-CISD computation. Spin-orbit effects were included in the calculation during this step. The same three references used in the MCSCF calculation were also used in the



MR-CISD calculation, and the same core and virtual orbitals were frozen. The MR-CISD calculations were performed using both molecular and natural orbitals extracted from the MCSCF wave function. For the large-core calculation, the MR-CISD consisted of roughly 3.5 million CSFs. The small-core calculation had nearly 9 million CSFs.

As shown in the Appendix A, all states arising from the  $^1\Sigma_g$ ,  $^3\Delta_g$ , and  $^3\Phi_g$  states have either  $A_g$  symmetry ( $\Sigma_g$  states), degenerate  $A_g+B_{1g}$  ( $\Delta_g$  states) symmetry, or degenerate  $B_{2g}+B_{3g}$  ( $\Phi_g$ ) symmetries. In the  $\omega$ - $\omega$  spin-orbit coupling scheme<sup>6</sup>, the states with  $A_g$  correspond to  $0_g^+$  states, those states corresponding with degenerate  $A_g+B_{1g}$  correspond with  $2_g$  and  $4_g$  states, while degenerate  $B_{2g}+B_{3g}$  states correspond with  $1_g$  or  $3_g$  states.

Because of this degeneracy, the lowest six excited states could be uniquely determined by examining the first four roots with  $A_g$  symmetry and the first three roots with  $B_{2g}$  symmetry. Degeneracy of these roots was checked by computing the first four  $B_{1g}$  roots at the SCF minimum energy bond length. Using the minimum MR-CISD energies from the fourth-order polynomial fit for each state, the electronic transition energies were then computed and compared with experimental data. State assignments were made by examining the CI wave function for each root. Details for this state assignment procedure are contained in Appendix C. Results from these calculations are included in the next chapter.

---

<sup>6</sup> The spin-orbit coupling scheme where electron correlation is small with respect to spin-orbit coupling in atoms is j-j coupling. This coupling scheme is  $\omega\omega$ -coupling in linear molecules.

## **COLUMBUS Calculations on Uranate ( $\text{UO}_4^{2-}$ )**

Geometry optimizations on the uranate ion using both MP2 and DFT indicated were dependent on the geometry of the molecule. Optimizations beginning from a square planar molecule converged to a square planar molecule. Optimizations that began with a tetrahedral geometry converged to a tetrahedral geometry. Optimizing the molecular geometry using an asymmetric starting point resulted in a distorted tetrahedral molecule using both DFT and MP2. The square planar and tetrahedral geometries are likely stationary points on the potential energy surface. The tetrahedral geometry was used in subsequent calculations, because the potential energy surface could be characterized by a single parameter.

Either  $D_2$  or  $C_{2v}$  point-groups would be appropriate abelian subgroups of the  $T_d$  symmetry point-group, and the calculation on uranate was carried out using  $D_2$  point-group symmetry. See Appendix B for a discussion symmetry aspects of the tetrahedral uranate ion and a definition of terms and states arising from the  $T_d$  and  $D_2$  point-groups.

As was the case with the uranyl ion, the uranate ion potential energy surface (PES) could be characterized by a single U-O bond length in  $T_d$  and  $D_2$  point-group symmetry. Since there is only one symmetry unique oxygen atom in a tetrahedral geometry, varying this bond length simultaneously varied the bond lengths of the other oxygen atoms. This procedure is equivalent to varying the symmetric stretch normal mode coordinate in the molecule. Varying one U-O bond length varied all U-O bonds simultaneously by equal amounts. Based on the spectroscopic accuracy obtained from

the small-core uranyl calculation, the uranate calculations were performed using only the small-core uranium RECP.

The initial ARGOS input was generated automatically using the IARGOS program. This method resulted in several errors. First, the IARGOS program generated symmetry adapted linear combinations of the f- and g- functions appropriate for axially symmetric molecules. For the tetrahedral uranate molecule, a symmetry adapted linear combination using cubic f- and g- functions was appropriate. Additionally, the program created an incorrect symmetry operation generator for the molecule. These errors were subtle, and were difficult to detect. They also resulted in electronic energies that did not exhibit the appropriate symmetry appropriate for a tetrahedral molecule in  $D_2$ .

Another problem was identified with the basis set. The same basis set used for the uranyl calculations was used for the uranate calculations. SCF and MCSCF calculations resulted in exaggerated uranium 7p population, which was unexpected. Based on the uranyl results, the uranium 5f orbitals were expected to play a large role in the excited states of uranate. Subsequent analysis revealed that the large number of diffuse p-functions and g-polarization functions biased the calculation in favor of the uranium 7p orbitals. The problem was fixed by removing the diffuse p-functions and removing all but one g-polarization function. The absence of non-bonding orbitals in the tetrahedral uranate revealed the impact of the diffuse p- and polarization g- functions. Similar effects did not show up in the uranyl calculation, because of the presence of the non-bonding  $1\delta_u$  and  $1\phi_u$  orbitals. In the uranyl calculation, the basis set impacted those anti-bonding states that were much higher in energy than the low lying states of interest.

Again, a series of SCF calculations were performed over a range of symmetric stretch normal mode coordinate U-O bond lengths. Fourth-order polynomial fits were used to find the minimum energies and bond lengths for SCF, MCSCF, and MR-CISD data. Expanding this fitting polynomial in a Taylor series about the equilibrium point, then finding the second derivative yielded the symmetric stretch force constants for this normal mode, which in turn yielded the symmetric stretch vibration frequencies. From the SCF calculation, the uranate HOMO proved to be the  $5t_2$  orbital, while the LUMO was the  $6t_2$  orbital. The SCF results showed a significant HOMO-LUMO energy gap, unlike uranyl. This was due to the absence of non-bonding orbitals, unlike the uranyl molecule. The large HOMO/LUMO energy gap in the uranate molecule indicated a single-reference calculation would suffice, as opposed to uranyl, where a state-averaged, multi-reference description of the ground state was more appropriate.

Following this series of SCF ground state calculations, a series of MCSCF calculations were performed, using the ground state reference only. In this aspect, the MCSCF calculation was identical to the HF-SCF calculation. The only reason for performing this calculation was to obtain natural orbitals for use in the MR-CISD calculation. As was done in the uranyl calculations, the uranium 5d orbitals were frozen in this calculation, meaning they were occupied in all references. While excitations from the uranium 5d shell were not allowed, the electrons were allowed to participate in the correlation calculation.

Using the natural orbital coefficients from the MCSCF calculation as a starting point, a single-point MR-CISD calculation was performed on the uranate ion at the interpolated SCF minimum U-O bond length. The references used in the uranate

calculation were similar in nature to the uranyl calculation. Three references were chosen: the ground state, and those references consisting of single excitations into the low-lying, unoccupied uranium 5f orbitals ( $8a_1$ ,  $6t_2$ ), with the requirement of five electrons remaining in the HOMO. A small MR-CISD calculation with all occupied orbitals except for the  $5t_2$  HOMO frozen, and 48 virtual orbitals frozen was performed in order to characterize the low-lying excited states. This small calculation yielded the symmetry expected of a tetrahedral molecule, and gave a qualitative picture of the nature and ordering of the low-lying excited states.

It was shown in Appendix B that a large number of possible states arise from the electron configurations  $5t_2^6$ ,  $5t_2^5 6t_2^1$ , and  $5t_{21}^5 6t_2^1$ . Unlike the calculation with uranyl, the nature and ordering of the low lying excited states for uranate were unknown. Appendix C contains the details for the double-group state assignment for the uranate ion ground and excited electronic states.

## IV. Results and Discussion

In this chapter, the results of the geometry optimizations using NWChem 4.0.1, as well as the results of the COLUMBUS 5.8.1 SCF, MCSCF, and MR-CISD calculations on both the uranyl and uranate ions will be presented.

### Uranyl Geometry Optimization Results

The initial results of the geometry optimizations for the uranyl ion are presented in Table 1. Also listed is a high-fidelity theoretical, four-component, all-electron calculation incorporating electron correlation at roughly a triple and quadruple excitation level. This calculation represents the current state-of-the-art in relativistic quantum chemistry calculations on uranyl (de Jong et al, 1999: 41-52); unfortunately, excited states were not investigated in the study by de Jong et al. Table 2 and Table 3 lists the interpolated minimum bond-length and symmetric stretch vibrational frequency computed from the COLUMBUS large- and small-core potential energy surfaces for comparison with the NWChem 4.0.1 results. Several experimental results measuring the vibrational frequencies of uranyl are also listed for comparison (Toth et al, 1981: 547-549; Denning et al, 1992: 216-275). The first experimental results from Toth et al are in an aqueous HNO<sub>3</sub> environment, while the second experiment was performed on a crystal of Cs<sub>2</sub>UO<sub>2</sub>Cl<sub>4</sub>. It is known that the uranyl vibrational frequencies can be perturbed by their crystalline or aqueous environment. However, the strength of the uranyl bond minimizes the impact of crystal field perturbations on the uranyl electronic spectra. Symmetric stretch vibrational frequencies vary from 887.9 cm<sup>-1</sup> in RbUO<sub>2</sub>(NO<sub>3</sub>)<sub>3</sub> to 808 cm<sup>-1</sup> in K<sub>2</sub>UO<sub>2</sub>(CO<sub>3</sub>)<sub>2</sub>, while the uranyl fluorescent series ranges from 21199.4 cm<sup>-1</sup> in

RbUO<sub>2</sub>(NO<sub>3</sub>)<sub>3</sub> to 20096.3 cm<sup>-1</sup> in Cs<sub>2</sub>UO<sub>2</sub>Cl<sub>4</sub> (Rabinowitch et al, 1964: 48). The largest crystal field perturbation on the symmetric stretch vibrational frequency for uranyl is roughly 80 cm<sup>-1</sup>, while the maximum crystal field splitting of the electronic fluorescent spectra appears to be roughly 1103 cm<sup>-1</sup>.

Table 1. Uranyl Geometry Optimization Results

<u>Uranium RECP/basis</u>	<u>Oxygen basis</u>	<u>method</u>	<u>Constraint Symmetry</u>	<u>bond length (Å)</u>	<u>symmetric stretch (cm<sup>-1</sup>)</u>
Küchle et al, 1994	aug-cc-pvdz (Kendall et al, 1992)	DFT B3LYP	D <sub>2h</sub>	1.6997	1037
Küchle et al, 1994	aug-cc-pvdz (Kendall et al, 1992)	DFT B3LYP	D <sub>4h</sub>	1.6997	1037
Küchle et al, 1994	aug-cc-pvdz (Kendall et al, 1992)	DFT B3LYP	C <sub>1</sub>	1.6487	1219
Küchle et al, 1994	aug-cc-pvdz (Kendall et al, 1992)	DFT Becke97	D <sub>2h</sub>	1.6950	1051
Küchle et al, 1994	aug-cc-pvdz (Kendall et al, 1992)	DFT Becke98	D <sub>2h</sub>	1.6924	1059
Küchle et al, 1994	Bergner et al, 1993	MP2	C <sub>1</sub>	1.7758	906
Ermler et al, 1991	Pacios et al, 1985	DFT B3LYP	C <sub>1</sub>	1.7257	921
Ermler et al, 1991	Pacios et al, 1985	DFT B3LYP	C <sub>1</sub>	1.7040	991
Ermler et al, 1991	aug-cc-pvdz (Kendall et al, 1992)	DFT B3LYP	D <sub>4h</sub>	1.6850	1026
Ermler et al, 1991	aug-cc-pvdz (Kendall et al, 1992)	DFT Becke97	D <sub>2h</sub>	1.6834	1038
Ermler et al, 1991	aug-cc-pvdz (Kendall et al, 1992)	DFT Becke98	D <sub>2h</sub>	1.6810	1045
Ermler et al, 1991	Pacios et al, 1985	MP2	C <sub>1</sub>	1.7572	891
Ermler et al, 1991	aug-cc-pvdz (Kendall et al, 1992)	HF SCF	D <sub>2h</sub>	1.6356	1097
Ermler et al, 1991	aug-cc-pvdz (Kendall et al, 1992)	HF SCF	C <sub>1</sub>	1.6356	1099
Ermler et al, 1991	aug-cc-pvdz (Kendall et al, 1992)	HF SCF	D <sub>2h</sub>	1.6341	1097
4-component all-electron theoretical calculation <sup>7</sup>	DHF + CCSD(T)	D <sub>2h</sub> <sup>2</sup> double group		1.715	974

<sup>7</sup> de Jong et al, 1999



Table 2. COLUMBUS Large-Core Uranyl Ground-State Calculation Results

<b>Method</b>	<b><u>bond length</u></b> <b>(Å)</b>	<b><u>symmetric</u></b> <b>stretch (cm<sup>-1</sup>)</b>
HF SCF	1.6465	996
MCSCF	1.6522	1065
MR-CISD	1.6679	1038

Table 3. COLUMBUS Small-Core Uranyl Ground-State Calculation Results

<b>Method</b>	<b><u>bond length</u></b> <b>(Å)</b>	<b><u>symmetric</u></b> <b>stretch (cm<sup>-1</sup>)</b>
HF SCF	1.6625	999
MCSCF	1.6717	1087
MR-CISD	1.6869	1062

Table 4 shows the geometry optimization results for the  $\text{UO}_4^{2-}$  ion. Both DFT and MP2 geometry optimizations yielded tetrahedral ( $T_d$ ) when started in a tetrahedral geometry. Both MP2 and DFT yielded square planar molecules when started from a square planar geometry. An interesting result occurred when MP2 and DFT optimizations started with an asymmetric geometry. The DFT optimizations converged to a very flat  $D_{2d}$  geometry, almost square planar. The potential energy surface of this geometry was very flat, and the geometry optimization could not converge to the specified gradient tolerance of  $1.0 \cdot 10^{-5}$ .

Table 4. Uranate NWChem 4.0.1 Geometry Optimization Results

<u>U basis</u>	<u>O basis</u>	<u>method</u>	<u>Symmetry</u>	<u>bond length</u> (Å)	<u>symmetric stretch</u> (cm <sup>-1</sup> )
Ermler et al, 1991	aug-cc-pvdz (Kendall et al, 1992)	MP2	C <sub>1</sub>	2.0164 tetrahedral	N/A
Ermler et al, 1991	cc-pvdz (Dunning et al, 1989)	DFT B3LYP	C <sub>1</sub>	1.9764 tetrahedral	724
Ermler et al, 1991	Pacios et al, 1985	DFT B3LYP	C <sub>1</sub>	1.9918 tetrahedral	707
Ermler et al, 1991	aug-cc-pvdz (Kendall et al, 1992)	DFT B3LYP	C <sub>1</sub>	1.9851 tetrahedral	713
Küchle et al, 1994	aug-cc-pvdz (Kendall et al, 1992)	DFT B3LYP	T <sub>d</sub>	1.9676	750
Ermler et al, 1991	aug-cc-pvdz (Kendall et al, 1992)	DFT B3LYP	C <sub>1</sub>	1.933 nearly square planar	N/A

### Large-core Uranyl (UO<sub>2</sub><sup>2+</sup>) Results

COLUMBUS 5.8.1 large-core calculation results are presented next. Figure 4 shows the results of the HF SCF calculations as a function of bond length. Because of symmetry, this bond length represents the symmetric stretch normal mode coordinate of the molecule. Varying this bond length simultaneously varied both oxygen-uranium bond lengths by equal amounts.

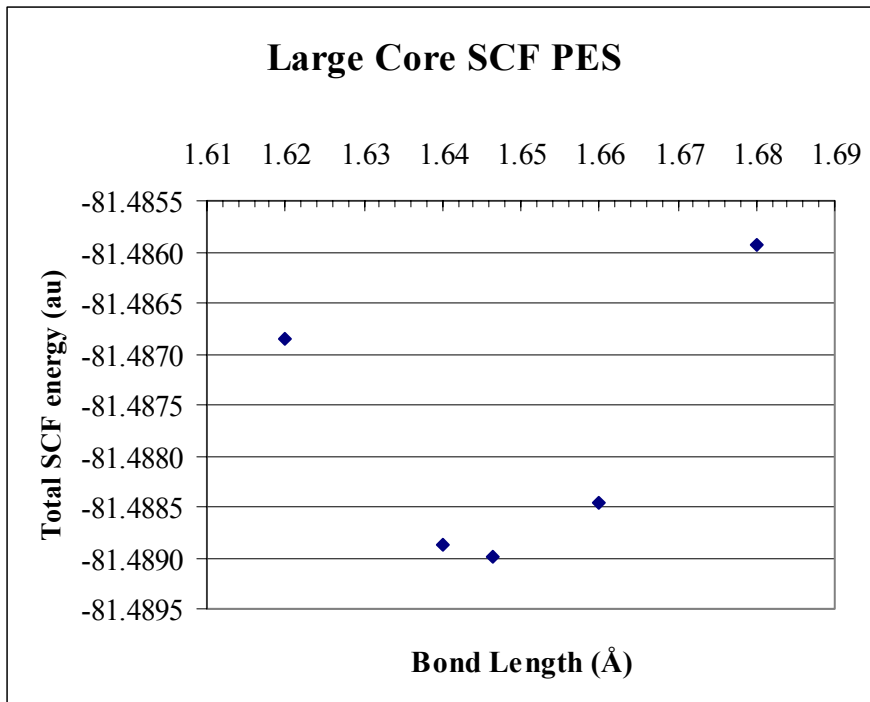


Figure 4. Large-core Uranyl SCF Potential Energy Surface

A fourth-order polynomial fit to this data yielded a minimum total electronic energy at a bond length of 1.647 Å. The second derivative of the Taylor series expansion about the equilibrium point yielded the force constant for the symmetric stretch normal mode. Table 5 contains the symmetric stretch vibrational frequency, calculated from this force constant. The frequency was scaled by 90%, as is frequently appropriate for SCF frequency calculations (Levine, 2000: 703-704).

Table 5. Large-core Uranyl SCF Symmetric Stretch Vibrational Frequencies

<u>State</u>	<u>Equilibrium Bond Length (Å)</u>	<u>Scaled Vibrational Frequency (cm<sup>-1</sup>)</u>
<sup>1</sup> Σ <sub>g</sub> <sup>+</sup>	1.6465	996

Next, the state-averaged MCSCF calculation over the  $3\sigma_u^2$ ,  $3\sigma_u^1 1\delta_u^1$ , and  $3\sigma_u^1 1\phi_u^1$  electron configuration references are shown in Figure 5.

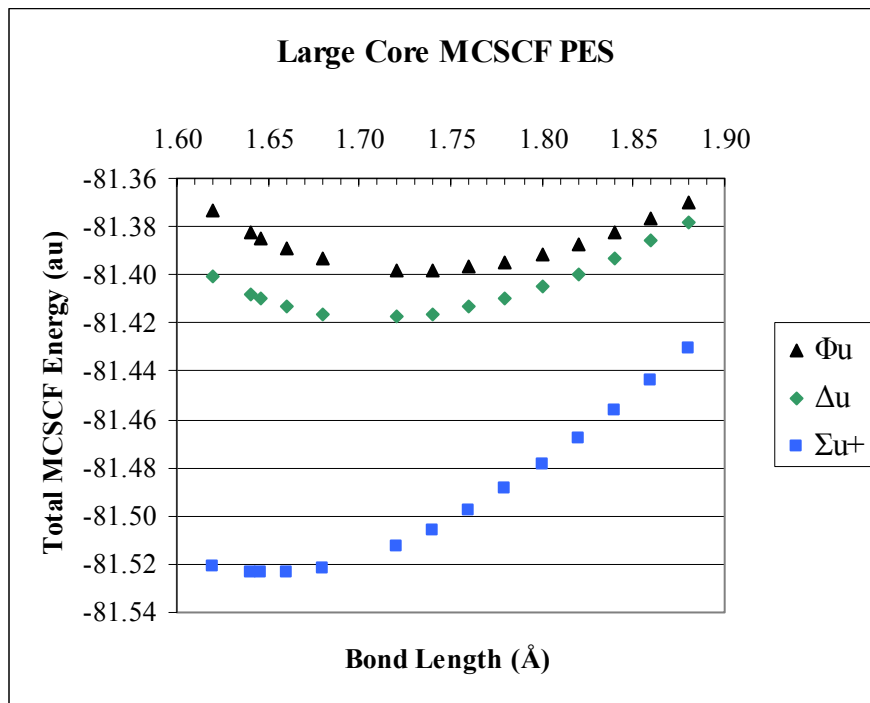


Figure 5. Large-core Uranyl MCSCF Potential Energy Surface

Again, equilibrium bond lengths were obtained from fourth-order polynomial fits to the MCSCF total electronic energy data, while the symmetric stretch vibrational frequencies were obtained from the second derivative of a Taylor series expansion about the equilibrium point. Table 6 lists the equilibrium bond lengths and symmetric stretch vibrational frequencies obtained from the MCSCF data.

Table 6. Large-core Uranyl MCSCF Symmetric Stretch Vibrational Frequencies

<b>State</b>	<b><u>Equilibrium Bond Length (Å)</u></b>	<b><u>Symmetric Stretch Vibrational Frequency (cm<sup>-1</sup>)</u></b>
$^1\Sigma_g^+$	1.6521	1065
$^3\Delta_g$	1.7082	861
$^3\Phi_g$	1.7310	815

The MR-CISD calculation was performed using the same three references used in the MCSCF calculation. Both molecular and natural orbital coefficients were extracted from the MCSCF wave function and used as the initial guess for the CISD calculation.

Figure 6 shows the MR-CISD potential energy surface obtained using the molecular orbital coefficients as the initial guess to the MR-CISD wave function.

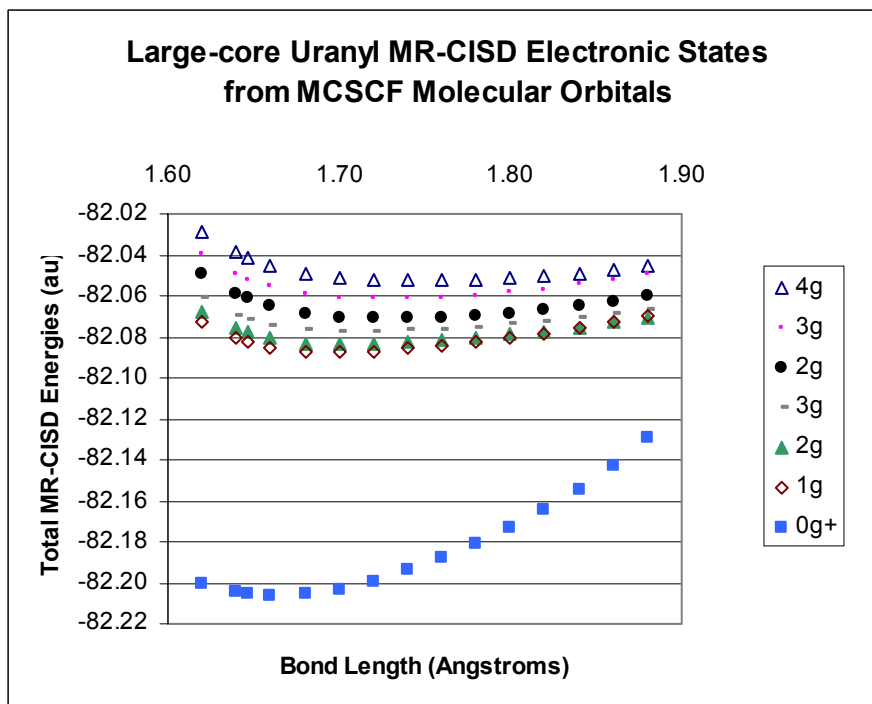


Figure 6. Large-core MR-CISD Uranyl Electronic States from Molecular Orbitals

Figure 7 shows the MR-CISD potential energy surface obtained by using the natural orbital coefficients as the initial guess to the MR-CISD wave function. As explained in the theory section, CI expansions using natural orbitals are generally more accurate than those obtained from molecular orbitals. The improved accuracy of the natural orbital CI expansion is illustrated by comparing the shapes of the MR-CISD potential energy surfaces obtained using molecular and natural orbital starting guesses. The potential energy surfaces obtained using natural orbital expansions yielded smoother potential energy surfaces, while the molecular orbital CI expansion resulted in distorted potential energy surfaces for the excited states.

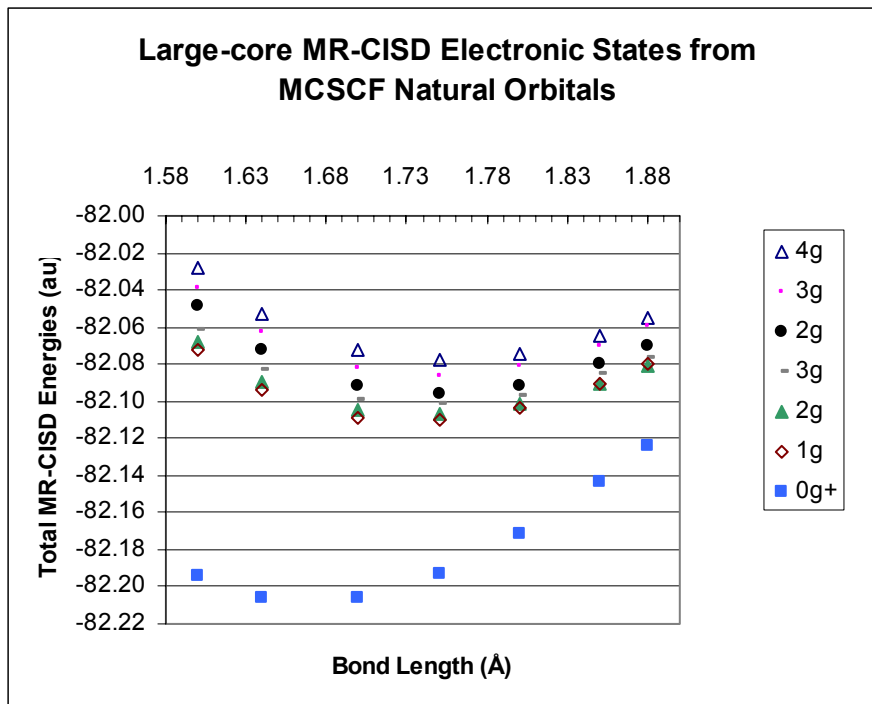


Figure 7. Large-core MR-CISD Uranyl Electronic States from Natural Orbitals

Equilibrium bond lengths and symmetric stretch vibrational frequencies for the large-core MR-CISD electronic states obtained from natural orbitals are listed in Table 7.

Table 7. Large-core Uranyl MR-CISD Symmetric Stretch Vibrational Frequencies

<u>State</u>	<u>Equilibrium Bond Length (Å)</u>	<u>Symmetric Stretch Vibrational Frequency (cm<sup>-1</sup>)</u>
0 <sub>g</sub> <sup>+</sup>	1.6630	1038
1 <sub>g</sub>	1.6967	840
2 <sub>g</sub>	1.7022	804
3 <sub>g</sub>	1.7065	802
2 <sub>g</sub>	1.7288	839
3 <sub>g</sub>	1.7252	839
4 <sub>g</sub>	1.7483	809

Finally, the composition of the MR-CISD wave function formed from natural orbitals is listed in Table 8. The effect of the spin-orbit potential in the CI calculation is apparent here. Compare the number of states arising from the MCSCF and MR-CISD calculations spin-orbit. The MR-SOCI calculation splits the MCSCF states in Figure 5, resulting in those states shown in Figure 7. Compositions do not necessary sum to 100%, due to a large number of contributions from configuration state functions with small coupling coefficients. Additionally, coupling coefficients alternated in sign. Only those states with expansion coefficients larger than 0.1 are listed in Table 8.



Table 8. Large-core Uranyl Wave Function Compositions

<u>State</u>	<u>Large-Core Wave Function Composition</u>	<u>Zhang et al (Zhang, 1999: 6884)</u>
$0_g^+$	82% $^1\Sigma_g^+$	83% $^1\Sigma_g^+$
$1_g$	84% $^3\Delta_g$	84% $^3\Delta_g$
$2_g$	58% $^3\Delta_g$ 26% $^3\Phi_g$	62% $^3\Delta_g$ 22% $^3\Phi_g$
$3_g$	52% $^3\Delta_g$ 26% $^3\Phi_g$ 6% $^1\Phi_g$	55% $^3\Delta_g$ 23% $^3\Phi_g$ 6% $^1\Phi_g$
$2_g$	25% $^3\Delta_g$ 3% $^1\Delta_g$ 56% $^3\Phi_g$	21% $^3\Delta_g$ 3% $^1\Delta_g$ 60% $^3\Phi_g$
$3_g$	32% $^3\Delta_g$ 48% $^3\Phi_g$ 4% $^1\Phi_g$	28% $^3\Delta_g$ 51% $^3\Phi_g$ 4% $^1\Phi_g$
$4_g$	84% $^3\Phi_g$	84% $^3\Phi_g$

Finally, the adiabatic electronic transition energies were computed from the large-core MR-CISD equilibrium energies. These results were compared to experimental results obtained by Denning et al on  $\text{Cs}_2\text{UO}_2\text{Cl}_4$  (Denning, 1992) and  $\text{CsUO}_2(\text{NO}_3)_3$  (Denning et al, 1979). Shown in Table 9, it is apparent that the MR-CISD method using the large-core RECP models the optical electronic spectra of uranyl rather well, to within about 3% of the experimental data, on average.

Table 9. Electronic Transition Energies from Large-core MR-CISD Results

<u>Electronic state</u>	<u>Equilibrium bond length (Å)</u>	<u>adiabatic <math>\Delta E</math> (cm<sup>-1</sup>)</u>	<u>Cs<sub>2</sub>UO<sub>2</sub>Cl<sub>4</sub></u>	<u>adiabatic % difference</u>
0 <sub>g</sub> <sup>+</sup>	1.6679			
1 <sub>g</sub>	1.7324	21430	20096	3.2%
2 <sub>g</sub>	1.7376	22151	20861	3.0%
3 <sub>g</sub>	1.7402	23378	22051	2.9%
2 <sub>g</sub>	1.7471	24637	22578	4.4%
3 <sub>g</sub>	1.7458	26872	26222	1.2%
4 <sub>g</sub>	1.7547	28736	27738	1.8%
			average	2.9%

Table 10. Large-core Uranyl Results from Zhang et al (Zhang, 1999: 6884)

<u>Electronic state</u>	<u>Equilibrium bond length (Å)</u>	<u>Symmetric Stretch Vibrational Frequency (cm<sup>-1</sup>)</u>	<u>adiabatic <math>\Delta E</math> (cm<sup>-1</sup>)</u>
0 <sub>g</sub> <sup>+</sup>	1.668	1103	
1 <sub>g</sub>	1.733	867	20719
2 <sub>g</sub>	1.739	845	21421
3 <sub>g</sub>	1.742	847	22628
2 <sub>g</sub>	1.749	900	23902
3 <sub>g</sub>	1.747	898	26118
4 <sub>g</sub>	1.755	880	27983

The comparison between this calculation and the one performed by Zhang et al (Zhang, 1999: 6884) is quite favorable. Bond lengths match closely, as do symmetric stretch vibrational frequencies. Adiabatic transition energies are slightly different; however, this difference is not unexpected because of the slightly different treatment of the ground and excited states versus the calculation performed by Zhang et al.

### Small-core Uranyl ( $\text{UO}_2^{2+}$ ) Results

The small-core HF SCF potential energy surface is displayed in Figure 8.

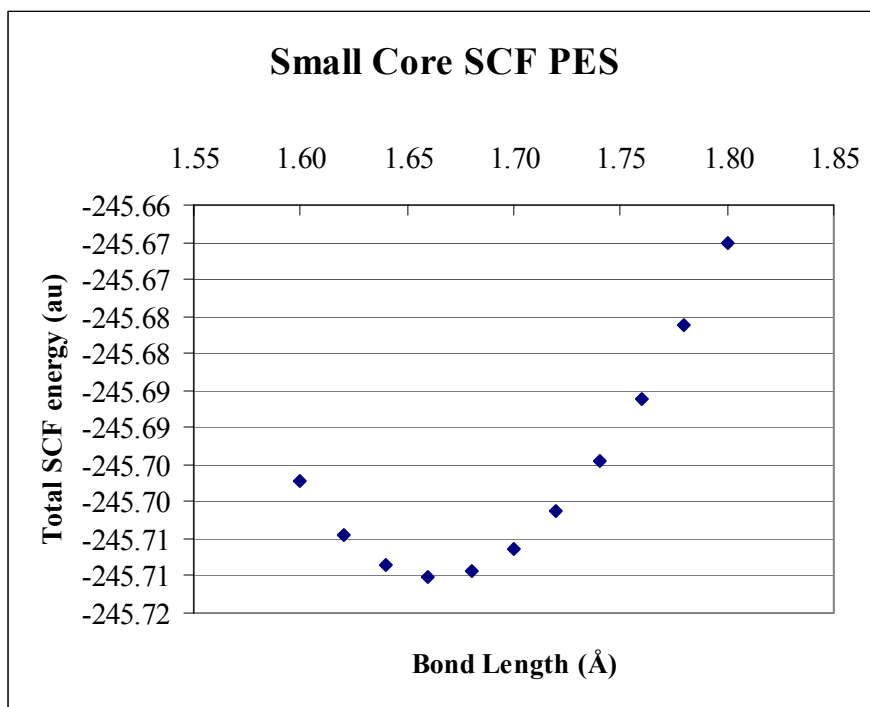


Figure 8. Small-core Uranyl SCF Potential Energy Surface

As was done in the large-core calculations, equilibrium bond lengths and minimum energies were computed from fourth-order data fits, while symmetric stretch vibrational frequencies were computed from second derivative of the Taylor series expansion about the equilibrium point. Again, the symmetric stretch vibrational

frequency from the HF SCF potential energy surface was scaled by 90%. This data is listed in Table 11.

Table 11. Small-core Uranyl SCF Equilibrium Bond Length and Symmetric Stretch Vibrational Frequency

State	Equilibrium Bond Length (Å)	Scaled Symmetric Stretch Vibrational Frequency (cm <sup>-1</sup> )
$^1\Sigma_g^+$	1.6625	999

The potential energy surfaces obtained from the small-core MCSCF calculation are shown in Figure 9.

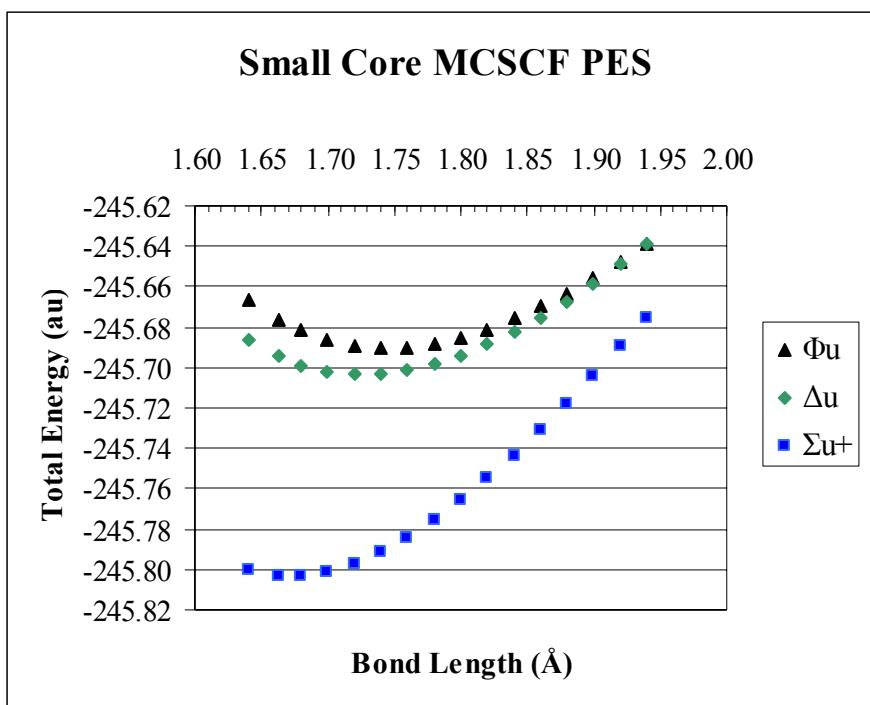


Figure 9. Small-core Uranyl MCSCF Potential Energy Surface

Table 12 lists the equilibrium bond lengths and symmetric stretch vibrational frequencies obtained from the state-averaged MCSCF results.

Table 12. Small-core Uranyl MCSCF Symmetric Stretch Vibrational Frequencies

<b>State</b>	<b>Equilibrium Bond Length (Å)</b>	<b>Symmetric Stretch Vibrational Frequency (cm<sup>-1</sup>)</b>
$^1\Sigma_g^+$	1.6717	1087
$^3\Delta_g$	1.7263	903
$^3\Phi_g$	1.7442	871

As was done with the large-core calculation, the small-core MR-CISD calculation was performed using both molecular and natural orbitals as starting points. The results of the CI expansion from the molecular orbital coefficients is shown in Figure 10. In this calculation, the molecular orbital coefficients are particularly poor, as they fail to yield bound excited states for uranyl. This situation does not represent reality.

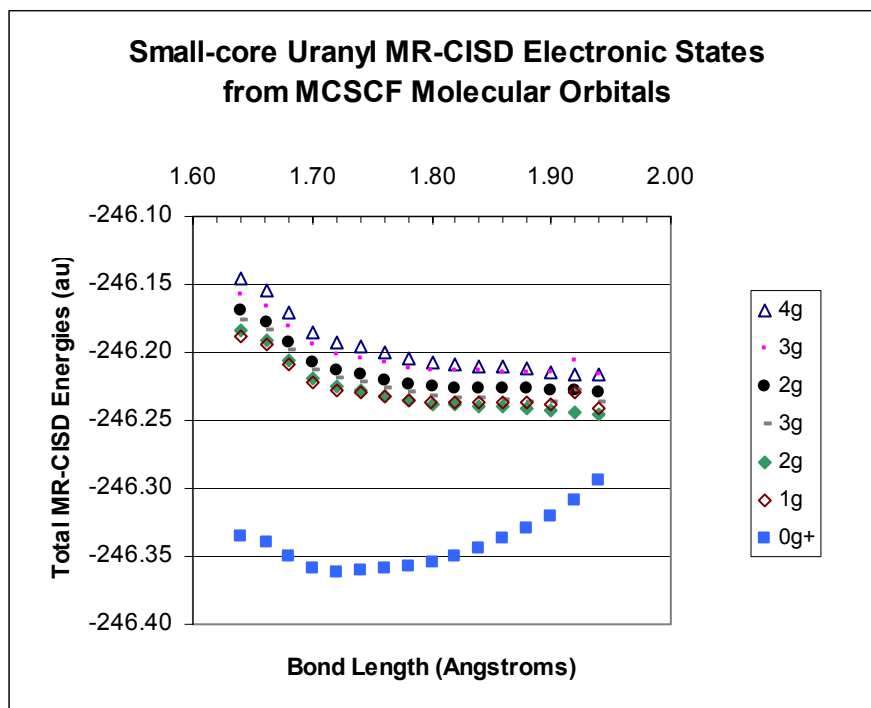


Figure 10. Small-core Uranyl MR-CISD Electronic States From Molecular Orbitals

The results CI expansion using the natural orbitals are shown in Figure 11. The difference in the accuracies between molecular and natural orbital initial guesses had a substantial impact on the final MR-CISD wave function. With the small-core calculation, the accuracy difference makes the difference between bound and unbound states.

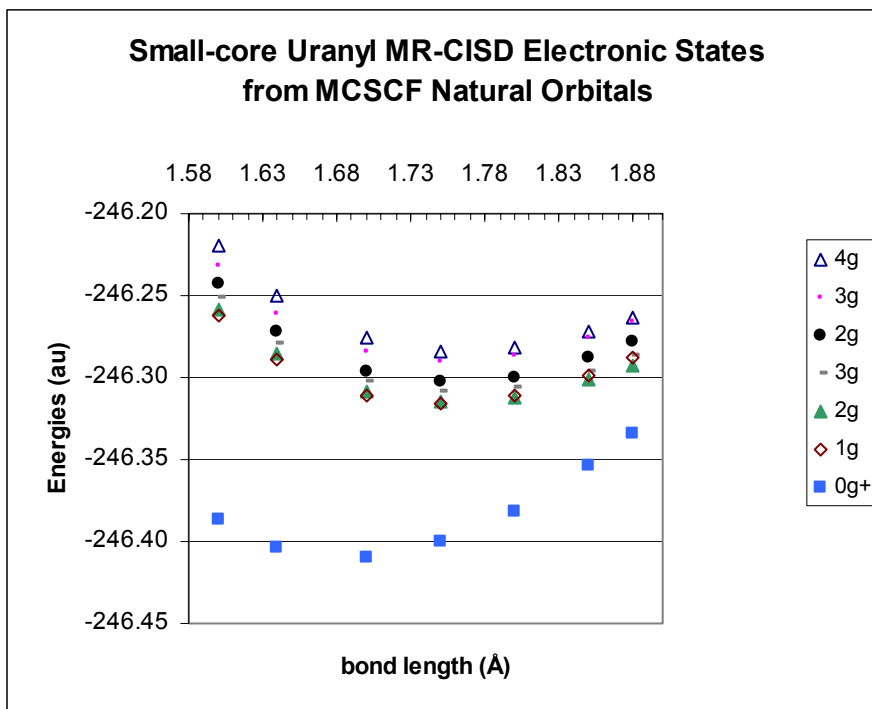


Figure 11. Small-core Uranyl MR-CISD Electronic States From Natural Orbitals

The equilibrium bond lengths and symmetric stretch frequencies for the MR-CISD electronic states are listed in Table 13.

Table 13. Small-core Uranyl MR-CISD Symmetric Stretch Vibrational Frequencies

<u>State</u>	<u>Equilibrium Bond Length (Å)</u>	<u>Symmetric Stretch Vibrational Frequency (cm<sup>-1</sup>)</u>
0 <sub>g</sub> <sup>+</sup>	1.6869	1062
1 <sub>g</sub>	1.7470	882
2 <sub>g</sub>	1.7571	845
3 <sub>g</sub>	1.7592	844
2 <sub>g</sub>	1.7553	885
3 <sub>g</sub>	1.7546	883
4 <sub>g</sub>	1.7649	856

Next, the small-core uranyl MR-CISD wave function composition is displayed in Table 14. The large-core uranyl wave function composition for the same state is also listed for comparison. The only fundamental difference between the wave functions occurs in the 2<sub>g</sub> states.

Table 14. Small- and Large-core Uranyl Wave Function Compositions

<b>State</b>	<b><u>Small-Core MR-CISD</u> <u>Wave Function</u> <u>Composition</u></b>	<b><u>Large-Core MR-CISD</u> <u>Wave Function</u> <u>Composition</u></b>
$0_g^+$	83% $^1\Sigma_g^+$	82% $^1\Sigma_g^+$
$1_g$	84% $^3\Delta_g$	84% $^3\Delta_g$
$2_g$	37% $^3\Delta_g$ 46% $^3\Phi_g$	58% $^3\Delta_g$ 26% $^3\Phi_g$
$3_g$	40% $^3\Delta_g$ 38% $^3\Phi_g$ 10% $^1\Phi_g$	52% $^3\Delta_g$ 26% $^3\Phi_g$ 6% $^1\Phi_g$
$2_g$	44% $^3\Delta_g$ 4% $^1\Delta_g$ 35% $^3\Phi_g$	25% $^3\Delta_g$ 3% $^1\Delta_g$ 56% $^3\Phi_g$
$3_g$	47% $^3\Delta_g$ 35% $^3\Phi_g$ 2% $^1\Phi_g$	32% $^3\Delta_g$ 48% $^3\Phi_g$ 4% $^1\Phi_g$
$4_g$	84% $^3\Phi_g$	84% $^3\Phi_g$

Finally, Table 15 shows the adiabatic excited state transition energies computed from the MR-CISD equilibrium energies and compared with the  $\text{Cs}_2\text{UO}_2\text{Cl}_4$  (Denning, 1992) and  $\text{CsUO}_2(\text{NO}_3)_3$  (Denning et al, 1979) experimental data.



Table 15. Electronic Transition Energies from Small-core MR-CISD Results

<b>State</b>	<b><u>Equilibrium Bond Length (Å)</u></b>	<b><u>adiabatic <math>\Delta E</math> (cm<sup>-1</sup>)</u></b>	<b><u>Cs<sub>2</sub>UO<sub>2</sub>Cl<sub>4</sub></u></b>	<b><u>adiabatic % diff</u></b>
0 <sub>g</sub> <sup>+</sup>	1.6869			
1 <sub>g</sub>	1.7470	20813	20096	1.8%
2 <sub>g</sub>	1.7571	20951	20861	0.2%
3 <sub>g</sub>	1.7592	22189	22051	0.3%
2 <sub>g</sub>	1.7553	23549	22578	2.1%
3 <sub>g</sub>	1.7546	26251	26222	0.1%
4 <sub>g</sub>	1.7649	27729	27738	0.0%
			average $\Delta E$	0.7%

Table 16. Comparison Between Theoretical and Experimental Uranyl Fluorescent Electronic Spectra and Symmetric Stretch Vibrational Frequencies (Rabinowitch et al, 1964: 48)

<u>Compound</u>	<u>Fluorescent Series (cm<sup>-1</sup>)</u>	<u>Symmetric stretch vibrational frequency (cm<sup>-1</sup>)</u>
Rb <sub>2</sub> UO <sub>2</sub> Cl <sub>4</sub> 2H <sub>2</sub> O	19961	831.8
K <sub>2</sub> UO <sub>2</sub> Cl <sub>4</sub> 2H <sub>2</sub> O	19970	831.6
Cs <sub>2</sub> UO <sub>2</sub> Cl <sub>4</sub>	20096	836.1
K <sub>2</sub> UO <sub>2</sub> (SO <sub>4</sub> ) <sub>2</sub>	20389	827
Rb <sub>2</sub> UO <sub>2</sub> (SO <sub>4</sub> ) <sub>2</sub>	20390	838.2
UO <sub>2</sub> (NO <sub>3</sub> ) <sub>2</sub> 6H <sub>2</sub> O	20578	863.9
Cs <sub>2</sub> UO <sub>2</sub> (SO <sub>4</sub> ) <sub>2</sub> 3H <sub>2</sub> O	20594	860.5
<b>Large core (OSU)</b>	<b>20719</b>	<b>867</b>
UO <sub>2</sub> (NO <sub>3</sub> ) <sub>2</sub> 3H <sub>2</sub> O	20779	874.0
Rb <sub>2</sub> UO <sub>2</sub> (NO <sub>3</sub> ) <sub>4</sub>	20808	887.9
<b>Small core (this work)</b>	<b>20813</b>	<b>882</b>
K <sub>2</sub> UO <sub>2</sub> (NO <sub>3</sub> ) <sub>4</sub>	20818	870.3
K <sub>2</sub> UO <sub>2</sub> (CO <sub>3</sub> ) <sub>2</sub>	20943	808.0
PbUO <sub>2</sub> (CH <sub>3</sub> COO) <sub>4</sub>	20958	853.0
CsUO <sub>2</sub> (CH <sub>3</sub> COO) <sub>3</sub>	20992	842.2
RbUO <sub>2</sub> (CH <sub>3</sub> COO) <sub>3</sub>	21049	852.1
NH <sub>4</sub> UO <sub>2</sub> (CH <sub>3</sub> COO) <sub>3</sub>	21056	847.0
CsUO <sub>2</sub> (NO <sub>3</sub> ) <sub>3</sub>	21090	884.0
NH <sub>4</sub> UO <sub>2</sub> (NO <sub>3</sub> ) <sub>4</sub>	21098	885.7
NaUO <sub>2</sub> (CH <sub>3</sub> COO) <sub>3</sub>	21135	855.2
KUO <sub>2</sub> (NO <sub>3</sub> ) <sub>3</sub>	21183	875.5
RbUO <sub>2</sub> (NO <sub>3</sub> ) <sub>3</sub>	21199	887.9
<b>Large core (this work)</b>	<b>21430</b>	<b>840</b>
(NH <sub>4</sub> ) <sub>2</sub> UO <sub>2</sub> (SO <sub>4</sub> ) <sub>2</sub>	23358	840
<b>Experiment average</b>	<b>20884</b>	<b>854.9</b>

The small-core uranyl MR-CISD energies agrees more closely with the Cs<sub>2</sub>UO<sub>2</sub>Cl<sub>4</sub> experimental data than the large-core results, coming within less than 1% of the experimental values on average. Additionally, the experimental transition energies

are component averaged, due to the crystal field splitting observed in the experimental spectroscopy.

Based on the orbital coefficients obtained from the SCF wave function, the  $3\sigma_u^2$  LUMO consists of primarily uranium 5d, and 7s orbitals bonding with oxygen 1s orbitals. There is also a small oxygen 2p component. The first excited states, arising from the  $3\sigma_u^1 1\delta_u^1$  electron configuration, consist almost entirely of uranium 5f orbitals, indicating a charge transfer process between the axial oxygen atoms and the uranium atom. The last three excited states, arising from the  $3\sigma_u^1 1\phi_u^1$  electron configuration also are substantially of uranium 5f character. Thus, the lowest lying excited states of uranyl all involve charge transfer from oxygen 1s and 2p orbitals to uranium 5f orbitals.

### **Small-core Uranate ( $\text{UO}_4^{2-}$ ) Results**

Based on the accuracy of the small-core uranyl results comparison with the precise  $\text{Cs}_2\text{UO}_2\text{Cl}_4$  experimental data, all uranate ion calculations were performed using only the small-core RECP. The SCF equilibrium bond length was computed from fourth-order polynomial fits to the raw data, while the symmetric stretch (breathing-mode) vibrational frequencies were obtained from the second derivative of the Taylor series expansion about the equilibrium point. The resulting HF SCF minimum bond length was used for the single-point MR-CISD energy calculation. Figure 12 shows the HF SCF potential energy surface computed.

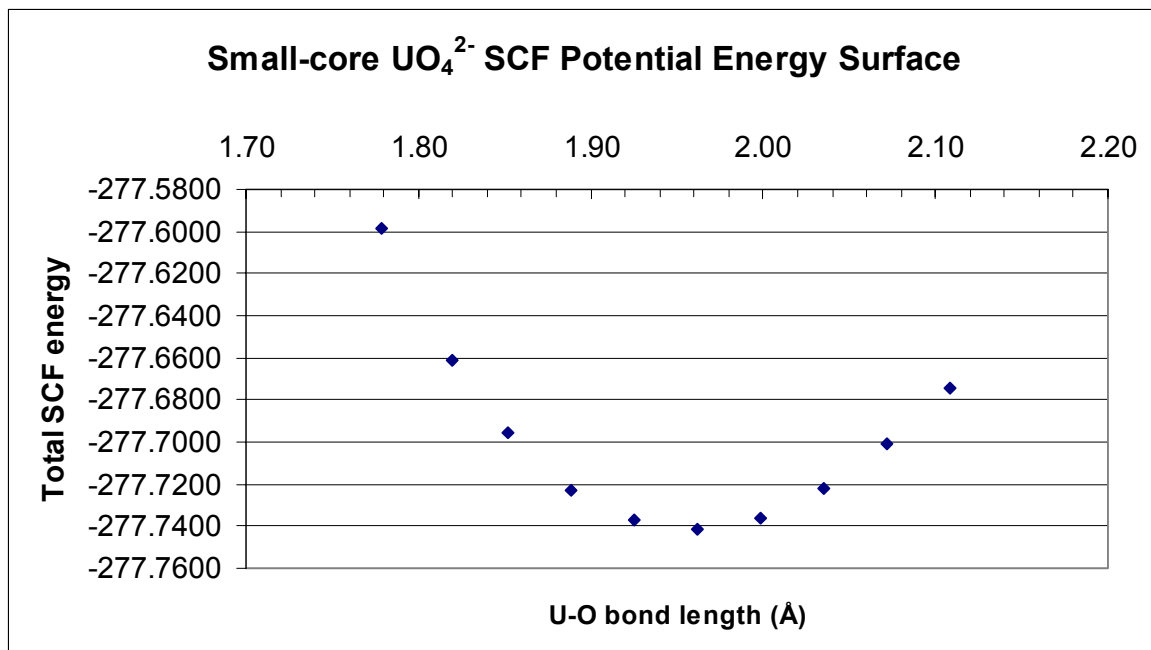


Figure 12. Uranate SCF Potential Energy Surface

The uranate ground state, since it is a closed shell molecule, is the completely symmetric singlet state, or  $^1A_1$  in  $T_d$  symmetry. The SCF breathing frequency was scaled by 90%. SCF results for the equilibrium bond length and breathing frequency are shown in Table 17.

Table 17. Small-core Uranate SCF Symmetric Stretch Vibrational Frequencies

<b>State</b>	<b><u>Equilibrium Bond Length (Å)</u></b>	<b><u>Symmetric Stretch Scaled Vibrational Frequency (cm<sup>-1</sup>)</u></b>
<sup>1</sup> A <sub>1</sub>	1.9575	780

The small-core uranate MCSCF computation used only the ground state as a reference. The decision to use only a single reference was based upon the relatively large HOMO-LUMO energy gap found in the SCF calculation.

Because the MCSCF calculation only used the ground state as a reference, its results should mirror the HF SCF calculation. In contrast, the uranyl MCSCF calculation was state-averaged over the ground state and first excited states. This was due to the relatively small separation in energy between the uranyl HOMO and LUMO. The only benefits from the uranate MCSCF calculation were improved virtual orbital energies as opposed to the HF SCF virtual orbital energies, and the ability to extract natural orbitals from the MCSCF wave function for use as a starting wave function in the MR-CISD calculation.

Using the natural orbitals extracted from the single-reference MCSCF wave function as a starting point, a small MR-CISD calculation was performed using over several references. The references used in the MR-CISD calculation included single excitations from the  $5t_2^6$  HOMO, which was mainly an oxygen 2p orbital, into the low-lying uranium 5f orbitals, a situation analogous to the uranyl calculation. These low-lying orbitals were the  $8a_1$  and  $6t_2$  orbitals. The lowest 48 virtual orbitals were frozen in this small CI calculation. In Appendix B, it was determined that there are a possible 13

states of A symmetry, including the ground state, and a total of 12 possible states of B<sub>1</sub>, B<sub>2</sub>, and B<sub>3</sub> symmetry arising from the three references used. The number of CSFs of A symmetry in D<sub>2</sub> was 380,521, while there were 380,088 CSFs of B<sub>1</sub>, B<sub>2</sub>, and B<sub>3</sub> symmetry. Compared with the small-core uranyl MR-CISD calculation with nearly 9 million CSFs, the uranate CI calculation is quite small. While this is not enough CSFs to give a quantitative picture of the excited states of uranate, it should suffice to give a qualitative picture of the nature and a rough ordering of excited states. Table 18 lists the double group state assignments and contributing  $\Gamma$ S terms for the states of A symmetry in D<sub>2</sub>, while Table 19 lists the double group state assignments and contributing terms for the states of B<sub>1</sub> symmetry in D<sub>2</sub>. Table 20 lists the lowest seven double-group states, their contributing  $\Gamma$ S terms, and the vertical electronic transition energies to the ground-state.

Table 18. Small-core Uranate MR-CISD Double Group Terms Of A Symmetry in D<sub>2</sub>  
and Their GS Compositions

<b>Double Group Term</b>	<b>Small-Core Wave Function GS Composition</b>
1A <sub>1</sub>	96% <sup>1</sup> A <sub>1</sub> from (5t <sub>2</sub> ) <sup>6</sup>
1E	85% <sup>3</sup> T <sub>2</sub> from (5t <sub>2</sub> ) <sup>5</sup> (4a <sub>1</sub> ) <sup>1</sup>
1A <sub>2</sub>	91% <sup>3</sup> T <sub>2</sub> from (5t <sub>2</sub> ) <sup>5</sup> (6t <sub>2</sub> ) <sup>1</sup>
2A <sub>2</sub>	55% <sup>1</sup> A <sub>1</sub> from (5t <sub>2</sub> ) <sup>5</sup> (6t <sub>2</sub> ) <sup>1</sup> 33% <sup>3</sup> T <sub>1</sub> from (5t <sub>2</sub> ) <sup>5</sup> (6t <sub>2</sub> ) <sup>1</sup>
2E	66% <sup>3</sup> T <sub>1</sub> from (5t <sub>2</sub> ) <sup>5</sup> (6t <sub>2</sub> ) <sup>1</sup> 21% <sup>1</sup> E from (5t <sub>2</sub> ) <sup>5</sup> (6t <sub>2</sub> ) <sup>1</sup>

Table 19. Small-core Uranate MR-CISD Double Group Terms Of B<sub>1</sub> Symmetry in D<sub>2</sub>  
and Their GS Compositions

<b>Double Group Term</b>	<b>Small-Core Wave Function GS Composition</b>
1T <sub>1</sub>	37% <sup>3</sup> E from (5t <sub>2</sub> ) <sup>5</sup> (6t <sub>2</sub> ) <sup>1</sup> 26% <sup>3</sup> T <sub>2</sub> from (5t <sub>2</sub> ) <sup>5</sup> (4a <sub>1</sub> ) <sup>1</sup> 13% <sup>3</sup> T <sub>1</sub> from (5t <sub>2</sub> ) <sup>5</sup> (6t <sub>2</sub> ) <sup>1</sup> 13% <sup>3</sup> T <sub>2</sub> from (5t <sub>2</sub> ) <sup>5</sup> (6t <sub>2</sub> ) <sup>1</sup>
1T <sub>2</sub>	30% <sup>3</sup> E from (5t <sub>2</sub> ) <sup>5</sup> (6t <sub>2</sub> ) <sup>1</sup> 28% <sup>3</sup> T <sub>1</sub> from (5t <sub>2</sub> ) <sup>5</sup> (6t <sub>2</sub> ) <sup>1</sup> 21% <sup>3</sup> T <sub>2</sub> from (5t <sub>2</sub> ) <sup>5</sup> (6t <sub>2</sub> ) <sup>1</sup>
2T <sub>1</sub>	45% <sup>3</sup> E from (5t <sub>2</sub> ) <sup>5</sup> (6t <sub>2</sub> ) <sup>1</sup> 36% <sup>1</sup> T <sub>1</sub> from (5t <sub>2</sub> ) <sup>5</sup> (6t <sub>2</sub> ) <sup>1</sup>
3T <sub>1</sub>	56% <sup>3</sup> T <sub>1</sub> from (5t <sub>2</sub> ) <sup>5</sup> (4a <sub>1</sub> ) <sup>1</sup> 22% <sup>3</sup> A <sub>1</sub> from (5t <sub>2</sub> ) <sup>5</sup> (6t <sub>2</sub> ) <sup>1</sup>
2T <sub>2</sub>	39% <sup>3</sup> T <sub>2</sub> from (5t <sub>2</sub> ) <sup>5</sup> (6t <sub>2</sub> ) <sup>1</sup> 29% <sup>3</sup> T <sub>1</sub> from (5t <sub>2</sub> ) <sup>5</sup> (6t <sub>2</sub> ) <sup>1</sup> 19% <sup>1</sup> T <sub>2</sub> from (5t <sub>2</sub> ) <sup>5</sup> (6t <sub>2</sub> ) <sup>1</sup>
3T <sub>2</sub>	40% <sup>1</sup> T <sub>2</sub> from (5t <sub>2</sub> ) <sup>5</sup> (4a <sub>1</sub> ) <sup>1</sup> 31% <sup>3</sup> T <sub>2</sub> from (5t <sub>2</sub> ) <sup>5</sup> (4a <sub>1</sub> ) <sup>1</sup>

Table 20. Small-core Uranate MR-CISD Low-Lying Vertical Electronic Transition

Energies at 1.9253 Å

<b>Double Group Term</b>	<b>Contributing ΓS States</b>	<b>Vertical ΔE (cm<sup>-1</sup>)</b>
2E	66% <sup>3</sup> T <sub>1</sub> 21% <sup>1</sup> E	34043
2A <sub>1</sub>	96% <sup>1</sup> A <sub>1</sub>	33959
1A <sub>2</sub>	91% <sup>3</sup> T <sub>2</sub>	33815
1E	85% <sup>3</sup> T <sub>2</sub>	33571
2T <sub>1</sub>	45% <sup>3</sup> E 36% <sup>1</sup> T <sub>1</sub>	33480
1T <sub>2</sub>	30% <sup>3</sup> E 28% <sup>3</sup> T <sub>1</sub> 21% <sup>3</sup> T <sub>2</sub>	33305
1T <sub>1</sub>	37% <sup>3</sup> E 26% <sup>3</sup> T <sub>2</sub> 13% <sup>3</sup> T <sub>1</sub> 13% <sup>3</sup> T <sub>2</sub>	32633
1A <sub>1</sub>	96% <sup>1</sup> A <sub>1</sub>	0



## V. Conclusions and Recommendations

This thesis has outlined the theory behind several theoretical methods used in calculating molecular properties of actinide compounds. Excited state spectra of the uranyl ion was calculated using both large- and small-core RECPs, and the results of these calculations were compared with previous theoretical work and experimental measurements of fluorescent series spectra.

The large-core uranyl calculations performed in this research faithfully reproduced the calculations performed at OSU (Zhang, 1999), with some small variations. These variations are explained by the slight difference in the treatment of the ground and excited states in this calculation as compared with the OSU calculation.

When compared with the precise spectroscopy obtained for  $\text{Cs}_2\text{UO}_2\text{Cl}_4$  by Denning et al (Denning et al, 1976; Denning, 1992), the small-core RECP and basis set yield a better match with experiment on average than the large-core results, although both RECPs and basis sets compare favorably with experiment. Because of this, the small-core RECP outperforms the large-core RECP when examining fluorescent spectra of the uranyl ion.

The match between experimental and theoretical electronic spectra for both the large- and small-core calculations for uranyl validates the assumed valence-core separability inherent in the relativistic effective core potential approximation. The large-core uranyl calculation compared reasonably well with experimental measurements of excited electronic spectra, and the calculations involved a relatively modest computational effort. The small-core calculation removed the uranium 5d shell electrons from the core potential, and allowed them to participate in the MR-CISD calculation.

Assuming the crystal field perturbations to the uranyl electronic energies over the range of uranyl-containing crystals measured average to zero, the small core theoretical result is in good agreement with the fluorescent series measurements averaged over all the experiments. The implication is then that the average experimental fluorescent spectra represents an unperturbed uranyl ion, at least to first order. Thus, the main trade-off between the large- and small-core calculation is the availability of more electrons to be correlated, and that this extra electron correlation gives improved results when compared with experiment. Thus, in the uranyl ion, electron correlation is more important than relativistic effects, and the 5d electron shell in uranium plays a small role in the chemical bonding in uranium oxides.

The next reasonable step is to examine the excited state spectra of the uranate ( $\text{UO}_4^{2-}$ ) ion using this small-core RECP. This ion is also a closed-shell molecule, and geometry optimizations using DFT and MP2 indicate the ion can be stable in a tetrahedral geometry, but the flattened tetrahedral geometry had a slightly lower energy in the DFT optimization. Using tetrahedral geometry, the potential energy surfaces could be parameterized by a single parameter, the U-O bond length, greatly simplifying the study of the potential energy surfaces. This single bond-length represents the symmetric stretch normal mode coordinate of the molecule. Varying this coordinate simultaneously varies all four oxygen-uranium bond lengths by an equal amount. Comparison between the low-lying excited states of uranyl and uranate illustrates the effect the oxygen coordination has on the electronic spectra of uranium oxides.

In the uranyl ion, there are non-bonding uranium 5f orbitals, which are relatively unaffected by the oxygen ligands. In the tetrahedral uranate ion, this is not the case. Here, there orbitals are either bonding or anti-bonding: no non-bonding uranium 5f orbitals are present. The preliminary result of this is that low-lying uranate electronic transitions occur in the ultraviolet spectrum, while the similar transitions in the uranyl ion

are in the optical spectrum. This is the reason for the characteristic green-yellow fluorescence in many uranium oxides. The presence or absence of the stable uranyl unit, and thus the non-bonding uranium 5f orbitals, dictates the nature of the electronic spectra.

The results of this research reveal the methods and challenges behind the theoretical study of actinide molecules. The study of simple, heavy-element molecules such as the uranyl ion has been quite successful; however, application of these theoretical techniques to more complicated, and more relevant uranium oxide compounds is difficult, both computationally, and theoretically. Advances in parallel computing and software resources has begun to allow the accurate study of increasingly complicated actinide molecules. This capability will have enormous impact on such fields as nuclear reactor fuel design, nuclear stockpile stewardship, and nuclear forensics.

## Appendix A: Symmetry Considerations for the Linear Uranyl Ion

All uranyl geometry optimization calculations performed using NWChem 4.0.1 resulted in a linear molecule. The most appropriate symmetry point group for a linear molecule is the  $D_{\infty h}$  point group. COLUMBUS calculations using the graphical unitary group approach (GUGA) CI program must be performed using an abelian point group. The abelian sub group of  $D_{\infty h}$  used in this research was the  $D_{2h}$  point-group. The correlation table between the  $D_{\infty h}$  and  $D_{2h}$  symmetry point groups is given in Table 21.

Next, the symmetries of the uranium atomic orbitals in  $D_{\infty h}$  and  $D_{2h}$ , as well as the symmetries of linear combinations of the two oxygen atomic orbitals in both the were found  $D_{\infty h}$  and  $D_{2h}$  point-groups were found in order to create the ARGOS input file. Table 22 and Table 23 show these orbital symmetries.

Table 21. Correlation Between  $D_{\infty h}$  and  $D_{2h}$  Symmetry Point-Groups (Cotton, 1971: 359-362).

$D_{\infty h}$	$D_{2h}$
$\Sigma_g^+$	$A_g$
$\Delta_g$	$A_g+B_{1g}$
$\Phi_g$	$B_{2g}+B_{3g}$

Table 22. Uranium Atomic Orbitals in  $D_{\infty h}$  and  $D_{2h}$  Symmetry Point Groups

<u>Orbital</u>	<u><math>D_{\infty h}</math></u>	<u><math>D_{2h}</math></u>
s	$\sigma_g^+$	$a_g$
$p_z$	$\sigma_u^+$	$a_u$
$p_x, p_y$	$\pi_u$	$b_{2u}+b_{3u}$
$d_{z^2}$	$\sigma_g^+$	$a_g$
$d_{xz}, d_{yz}$	$\pi_g$	$b_{2g}+b_{3g}$
$d_{xy}, d_{x^2-y^2}$	$\delta_g$	$a_g+b_{1g}$
$f_{z^3}$	$\sigma_u^+$	$a_u$
$f_{xz^2}, f_{yz^2}$	$\pi_u$	$b_{2u}+b_{3u}$
$f_{xyz}, f_{z(x^2-y^2)}$	$\delta_u$	$a_u+b_{1u}$
$f_{x(x^2-3y^2)}, f_{y(3x^2-y^2)}$	$\phi_u$	$b_{2u}+b_{3u}$

Table 23. Two Oxygen Atomic Orbitals Along z-axis in  $D_{\infty h}$  and  $D_{2h}$

<u>Orbital</u>	<u><math>D_{\infty h}</math></u>	<u><math>D_{2h}</math></u>
$s + s$	$\sigma_g^+$	$a_g$
$s - s$	$\sigma_u^+$	$b_{1u}$
$p_z + p_z$	$\sigma_u^+$	$b_{1u}$
$p_z - p_z$	$\sigma_g^+$	$a_g$
$p_y + p_y$ $p_x + p_x$	$\pi_u$	$b_{2u} + b_{3u}$
$p_y - p_y$ $p_x - p_x$	$\pi_g$	$b_{2g} + b_{3g}$

Because the references used in the MR-CISD calculation are all products of ungerade<sup>8</sup> orbitals, all the possible states arising from these references will be gerade. The references used in the MR-CISD calculations were the  $3\sigma_u^2$ ,  $3\sigma_u^1 1\delta_u^1$ , and  $3\sigma_u^1 1\varphi_u^1$  electron configurations. Table 24 shows the possible states arising from these electron configurations in both  $\Lambda S$ <sup>9</sup> and  $\omega\omega$ <sup>10</sup> coupling schemes.

<sup>8</sup> ungerade = odd parity

<sup>9</sup> Russell-Sanders coupling is called LS coupling in atoms,  $\Lambda S$  coupling in linear molecules

<sup>10</sup> j-j coupling in atoms,  $\omega\omega$  coupling in linear atoms

Table 24. Uranyl Possible States from CISD References in both  $\Lambda S$  and  $\omega\omega$  Coupling

Schemes

<u>Reference configuration</u> <u>n</u>	<u>Possible States</u> <u>(<math>\Lambda S</math> coupling)</u>	<u>Possible States</u> <u>(<math>\omega\omega</math> coupling)</u>
$3\sigma_u^2$	$^1\Sigma_{0g}^+$	$0_g^+$
$3\sigma_u^1 1\delta_u^1$	$^3\Delta_{3g}$ $^3\Delta_{2g}, ^1\Delta_{2g}$ $^3\Delta_{1g}$	$1_g$ $2_g$ $3_g$
$3\sigma_u^1 1\varphi_u^1$	$^3\Phi_{4g}$ $^3\Phi_{3g}, ^1\Phi_{3g}$ $^3\Phi_{2g}$	$2_g$ $3_g$ $4_g$

Table 25 shows the spatial, spin, and total wave function symmetries arising from each uranyl reference configuration.

Table 25. Total Wave Function Symmetry in  $D_{2h}$  From Reference Electronic Configurations

<u>Electron configuration</u>	<u><math>\Delta S</math> Term</u>	<u><math>D_{2h}</math> Spatial Symmetry</u>	<u><math>D_{2h}</math> Spin-Symmetry</u>	<u><math>D_{2h}</math> Double-Group Symmetry</u>
$3\sigma_u^2$	$^1\Sigma_g^+$	$A_g$	$A_g$	$A_g$
$3\sigma_u^1 1\delta_u^1$	$^3\Delta_g$	$A_g+B_{1g}$	$B_{1g}+B_{2g}+B_{3g}$	$A_g$ $B_{1g}$ $2 B_{2g}$ $2 B_{3g}$
$3\sigma_u^1 1\phi_u^1$	$^3\Phi_g$	$B_{2g}+B_{3g}$	$B_{1g}+B_{2g}+B_{3g}$	$2 A_g$ $2 B_{1g}$ $B_{2g}$ $B_{3g}$



## Appendix B: Symmetry Considerations of the Tetrahedral Uranate Ion

The optimum uranate ion geometry found using NWChem 4.0.1 was dependent on the starting geometry. If the geometry optimization was started in a tetrahedral configuration, the final geometry was tetrahedral. The geometry obtained from an asymmetric starting point was a flattened tetrahedral, or a  $D_{2d}$  molecule. The  $D_{2d}$  geometry had a slightly lower energy than the tetrahedral geometry using DFT. Analysis of the potential energy surfaces of a  $D_{2d}$  molecule is complicated by the fact that there are two independent bond lengths. For this reason, the tetrahedral molecular geometry was examined. Using a tetrahedral symmetry, the potential energy surfaces could be characterized by a single parameter, as was the case in the uranyl ion.

A tetrahedral geometry is best described using a  $T_d$  symmetry point group. However, as was the case with the uranyl calculation, the COLUMBUS calculations using the GUGA CI program must be performed using an abelian point group. The uranate calculations were performed using the  $D_2$  symmetry point-group. The correlation table between the  $T_d$  and  $D_2$  symmetry point groups is given in Table 26.

Table 26. Correlation Table Between  $T_d$  and  $D_2$  Symmetry Point-Groups (Cotton, 1971: 356-363).

$T_d$	$D_2$
$A_1$	A
$A_2$	A
E	A+A
$T_1$	$B_1+B_2+B_3$
$T_2$	$B_1+B_2+B_3$

In a similar fashion to the uranyl calculations, the  $T_d$  and  $D_2$  symmetries of the uranium and four oxygen atomic orbitals was found, and the appropriate ARGOS input file was generated. The symmetries of the uranium orbitals in  $T_d$  and  $D_2$  symmetry point-groups are shown in Table 27, while the symmetries of the linear combinations of four oxygen atoms are shown in Table 28.

Table 27. Linear Combination of Uranium Atomic Orbitals in  $T_d$  and  $D_2$  Symmetry Point

Groups

<u>Orbital</u>	<u><math>T_d</math></u>	<u><math>D_2</math></u>
s	$A_1$	A
$p_z$ $p_y$ $p_x$	$T_2$	$B_1$ $B_2$ $B_3$
$d_{z^2}$ $d_{x^2-y^2}$	E	A
$d_{xy}$ $d_{xz}$ $d_{yz}$	$T_2$	$B_1$ $B_2$ $B_3$
$f_{z^3}$ $f_{y^3}$ $f_{x^3}$	$T_2$	$B_1$ $B_2$ $B_3$
$f_{xyz}$	$A_1$	A
$f_{y(z^2-x^2)}$ $f_{y(z^2-x^2)}$ $f_{x(z^2-y^2)}$	$T_1$	$B_1$ $B_2$ $B_3$

Table 28. Combination of Four Tetrahedral Oxygen Atomic s-Orbitals in  $T_d$  and  $D_2$

<u>Oxygen orbital</u>	<u><math>T_d</math></u>	<u><math>D_2</math></u>
s	$A_1+T_2+T_1$	$A+B_1+B_2+B_3$
$p_z$	$A_1+T_2+T_1$	$A+B_1+B_2+B_3$
$p_y$	$A_1+T_2+T_1$	$A+B_1+B_2+B_3$
$p_x$	$A_1+T_2+T_1$	$A+B_1+B_2+B_3$

Three electronic configurations were used as references in the MR-CISD calculation: the  $5t_2^6$  ground state, as well as  $5t_2^5 8a_1^1$  and  $5t_2^5 6t_2^1$ , which represent excitations in the uranium 5f orbitals. The possible double group states in  $T_d$  and  $D_2$  symmetry point groups arising from these three references are listed in Table 29 (Herzberg, 1966: 570).

Table 29. Uranate Total Wave Function Symmetry in D<sub>2</sub> From Reference Electronic Configurations

<u>Electron configuration</u>	<u>T<sub>d</sub> ΓS<sup>11</sup> Terms</u>	<u>T<sub>d</sub> Spatial Symmetry</u>	<u>T<sub>d</sub> Spin-Symmetry</u>	<u>T<sub>d</sub> Double Group Terms</u>	<u>D<sub>2</sub> Double Group Terms</u>
$5t_2^6$	$^1A_1$	A <sub>1</sub>	A <sub>1</sub>	A <sub>1</sub>	A
$5t_2^5 8a_1^1$	$^1T_2$	T <sub>2</sub>	A <sub>1</sub>	T <sub>2</sub>	B <sub>1</sub> +B <sub>2</sub> +B <sub>3</sub>
$5t_2^5 8a_1^1$	$^3T_2$	T <sub>2</sub>	T <sub>1</sub>	A <sub>2</sub> E T <sub>1</sub> T <sub>2</sub>	A 2A B <sub>1</sub> +B <sub>2</sub> +B <sub>3</sub> B <sub>1</sub> +B <sub>2</sub> +B <sub>3</sub>
$5t_2^5 6t_2^1$	$^1A_1$ $^1E$ $^1T_1$ $^1T_2$	A <sub>1</sub> E T <sub>1</sub> T <sub>2</sub>	A <sub>1</sub>	A <sub>1</sub> E T <sub>1</sub> T <sub>2</sub>	A A+A B <sub>1</sub> +B <sub>2</sub> +B <sub>3</sub> B <sub>1</sub> +B <sub>2</sub> +B <sub>3</sub>
$5t_2^5 6t_2^1$	$^3A_1$ $^3E$ $^3T_1$ $^3T_2$	A <sub>1</sub> E T <sub>1</sub> T <sub>2</sub>	T <sub>1</sub>	T <sub>1</sub> T <sub>1</sub> +T <sub>2</sub> A <sub>1</sub> +E+T <sub>1</sub> +T <sub>2</sub> A <sub>2</sub> +E+T <sub>1</sub> +T <sub>2</sub>	B <sub>1</sub> +B <sub>2</sub> +B <sub>3</sub> 2B <sub>1</sub> +2B <sub>2</sub> +2B <sub>3</sub> 3A+2B <sub>1</sub> +2B <sub>2</sub> +2B <sub>3</sub> 3A+2B <sub>1</sub> +2B <sub>2</sub> +2B <sub>3</sub>
<b>Total</b>				3A <sub>1</sub> +2A <sub>2</sub> +4E+ 6T <sub>1</sub> +6T <sub>2</sub>	13A+12(B <sub>1</sub> +B <sub>2</sub> +B <sub>3</sub> )

It is evident from Table 29 that the total number of possible states arising from the three electron configuration references is much larger in the tetrahedral uranate ion than in the linear uranyl ion.

<sup>11</sup> Russell-Sanders coupling in non-linear poly atomic atoms is called ΓS coupling

## Appendix C: State Assignments Using MR-CISD Wave Functions

For both the uranyl and uranate ions, the MR-CISD calculation was performed using an abelian point-group that was a sub-group of the actual symmetry group corresponding to the molecular symmetry. The SCF, MCSCF and MR-CISD wave functions obtained in the calculations all reflect the symmetry of the calculation, which in turn, echoed the overall molecular symmetry.

In the MR-CISD calculations, symmetry considerations and degeneracy reduced the total number of calculations necessary to characterized all the possible states arising from the electron references. For the uranyl calculation, calculating four MR-CISD roots of  $A_g$  symmetry and three roots of  $B_{2g}$  symmetry completely characterized the ground state and six excited electronic states possible from reference electron configurations (see Table 24 and Table 25). Once these MR-CISD wave functions are obtained, all that remains is identification of each state corresponding to the particular MR-CISD root.

### Uranyl MR-CISD State Assignment

In the case of the uranyl ion, the MR-CISD state assignment was relatively straightforward, using the information in Table 24 and the process of elimination.

The output of the MR-CISD calculation lists electron configurations in the CI expansion with a CI coefficient above a certain threshold. Also listed is the spin multiplicity of the configuration. Listed below is an excerpt from the first MR-CISD root of  $A_g$  symmetry in the small-core uranyl calculation.

--- list of ci coefficients ( ctol = 1.00E-02 ) total energy( 1) = -246.4005545447

internal orbitals

level	1	2	3	4	5	6	7	8	9	10	11	12	13	14	15	16
orbital	3	4	5	47	61	77	78	93	94	106	107	79	74	80	95	108
symmetry	ag	ag	ag	b2g	b3g	b1u	b1u	b2u	b2u	b3u	b3u	b1u	au	b1u	b2u	b3u

path	s	ms	csf#	c(i)	ext. orb.(sym)
z*	1	1	1	0.908837	+ - + - + - + - + - + - + -
z	1	1	6	-0.035430	+ - + - + - + - + - + - + - + -
z	1	1	10	-0.035430	+ - + - + - + - + - + - + - + -
z	1	1	13	-0.011775	+ - + - + - + - + - + - + - + -

The orbital number lists the unfrozen, occupied core orbitals and reference orbitals. The next line lists the symmetry of each orbital. The pluses and minuses represent electron spin-up or spin-down. On the left side, the c(i) represents the CI coefficient, and the s represents the spin-multiplicity. For this example, the 79 b<sub>3u</sub> is the 3σ<sub>u</sub><sup>2</sup> HOMO and is a singlet. This corresponds to the HF SCF ground state, and is the 0<sub>g</sub><sup>+</sup> state. Identification of the other states proceeds in a similar fashion. States are most easily identified through their Ω values and spin-multiplicity. For example, roots of A<sub>g</sub> symmetry can only correspond to even Ω values. Thus, A<sub>g</sub> roots can only be 0<sub>g</sub><sup>+</sup>, 2<sub>g</sub>, or 4<sub>g</sub> states, while B<sub>2g</sub> roots can only be 1<sub>g</sub> or 3<sub>g</sub> states. The 4<sub>g</sub> state can be identified by the fact that there can be no contributions from the 3σ<sub>u</sub><sup>1</sup>1δ<sub>u</sub><sup>1</sup> configuration. It can only arise from the 3σ<sub>u</sub><sup>1</sup>1φ<sub>u</sub><sup>1</sup> reference or from excitations from π<sub>u</sub> orbitals. The 2<sub>g</sub> and 3<sub>g</sub> states can be differentiated by the singlet states. For example, the 2<sub>g</sub> states contains a small contribution from the singlet 3σ<sub>u</sub><sup>1</sup>1δ<sub>u</sub><sup>1</sup> configuration. This uniquely identifies the

$2_g$  states. The  $3_g$  states are identified by the presence of the singlet  $3\sigma_u^1 1\phi_u^1$  configuration. The  $1_g$  states are identified by the absence of any singlet configurations from the  $3\sigma_u^1 1\delta_u^1$  or  $3\sigma_u^1 1\phi_u^1$  reference configurations. Thus, all seven states arising from the three references are uniquely identified and ordered in energy.

### **Uranate MR-CISD State Assignment**

State identification in the tetrahedral uranate ion proceeds in a similar fashion. The E states are identified by their degeneracy. Two consecutive, degenerate roots of A symmetry correspond to an E state. The  $A_1$  state can be identified by noting that the first root of A symmetry corresponds to the ground state, a  $^1A_1$  state. Identification of  $A_2$  states is slightly more complicated, and it relies on the CI coefficients of the ground state. The  $A_1$  and  $A_2$  states, while both of A symmetry in  $D_2$ , are differentiable by the relative signs of the CI coefficients of various electron configurations in each wave function. The key to identification of an  $A_2$  state is to find electron configurations in the ground state that are identical in the  $A_2$  state, and examine the CI coefficients. The CI coefficients of the electron configurations in the  $A_1$  state should come into the  $A_2$  state with different signs, while they will have the same sign in another  $A_1$  state. Thus,  $A_1$  and  $A_2$  states can be differentiated by the phases of their wave functions, relative to the CI coefficients in the ground state, once a series of identical electron configurations are located between the ground state ( $A_1$ ) and the state to be identified.

Differentiation between  $T_1$  and  $T_2$  states proceeds along a similar fashion. However, the complication here is to first identify either a  $T_1$  or  $T_2$  state, then use the



relative phases of the CI coefficients in identical electron configurations to distinguish between the two. Here, the spin multiplicity can help.  $T_1$  or  $T_2$  states can be identified by locating a singlet state from a  $t_2^1 a_1^1$  or  $t_1^1 a_1^1$  electron configuration. Therefore,  $T_1$  and  $T_2$  states can be identified from either singlet states arising from excitations into  $a_1$  from  $t_1$  or  $t_2$  orbitals, or into  $t_1$  or  $t_2$  orbitals from  $a_1$  orbitals. Once one such state is found, other  $T_1$  or  $T_2$  states can be differentiated by examining the relative phases of the CI coefficients.

## List of Abbreviations

AFIT	Air Force Institute of Technology
AMD	Advanced Micro Devices
ARECP	Averaged Relativistic Effective Core Potential
ASC	Aeronautical System Center
aug-cc-pvdz	Augmented, Correlation-Consistent Polarized Valence Double Zeta
B3LYP	Becke Three Parameter Lee-Yang-Parr hybrid exchange-correlation functional
CAS	Complete Active Space
CCSD(T)	Coupled-Cluster Singles and Doubles (Triples)
CISD	Configuration Interaction, Single and Double excitations
CSF	Configuration State Function
DFT	Density Functional Theory
DHF	Dirac-Hartree-Fock
EMSL	Environmental Molecular Sciences Laboratory
eV	electron volt ( $1.602176 \times 10^{-19}$ J)
Gb	Gigabyte
GCA	Gradient-Corrected Approximation
GHz	Gigahertz
HF	Hartree-Fock
HOMO	Highest Occupied Molecular Orbital
kcal	kilocalories (4184 J)
LUMO	Lowest Unoccupied Molecular Orbital
Mb	Megabyte

MCSCF	Multi-Configuration Self-Consistent Field
MHz	Megahertz
MP2	Møller-Plesset second-order perturbation theory
MR-CISD	Multi-Reference Configuration Interaction with Single and Double excitations
MSRC	Major Shared Resource Center
O	Oxygen
OSU	Ohio State University
PES	Potential Energy Surface
PC	Personal Computer
PNNL	Pacific Northwest National Laboratory
RAM	Random Access Memory
RECP	Relativistic Effective Core Potential
SCF	Self-Consistent Field method
SO	Spin-Orbit
SOCI	Spin-Orbit Configuration Interaction
Tb	Terabyte
U	Uranium

## Bibliography

- Aoyama, T., Yamakawa, H., and Matsuoka, O. "Relativistic self-consistent field methods for molecules. II. A single-determinant Dirac-Fock self-consistent-field method for closed-shell polyatomic molecules." *Journal of Chemical Physics*, 73, 3: 1329-1332 (22 Apr 80).
- "ASC MSRC Hardware Resources." n. pag. <http://www.asc.hpc.mil/hardware/index.php> (2002).
- Balasubramanian, K.. Relativistic Effects in Chemistry, Part A: Theory and Techniques. John Wiley and Sons, Inc. (1997).
- Becke, A., D. "Density-functional thermochemistry. V. Systematic optimization of exchange-correlation functionals." *Journal of Chemical Physics*, 107, 20: 8554-8560 (22 November 1997).
- Becke, A., D. "Density-functional thermochemistry. IV. A new dynamical correlation functional and implications for exact-exchange mixing." *Journal of Chemical Physics*, 104, 3: 1040-1046 (15 January 1996).
- Becke, A. D. "Density-functional thermochemistry. III. The role of exact exchange." *Journal of Chemical Physics*. 98: 5648-5652 (1993).
- Becke, A. D. "Density-functional thermochemistry. II. The effect of the Perdew-Wang generalized-gradient correlation correction." *Journal of Chemical Physics*. 97, 12: 9173-9177 (15 December 1992).
- Becke, A. D. "Density-functional thermochemistry. I. The effect of the exchange-only gradient correction." *Journal of Chemical Physics*. 96, 3: 2155-2160 (1 February 1992).
- Bergner, A., Dolg, M., Küchle, W., Stoll, H., and Preuss, H. "Ab initio energy-adjusted pseudopotentials for elements of groups 13-17." *Molecular Physics*, 80, 6: 1431-1441 (1993).
- Bethe, H. A. and Salpeter, E. E. Quantum Mechanics of One- and Two-Electron Atoms. Springer-Verlag (1957).

- Bjorken, J. D., and Drell, S. D. Relativistic Quantum Mechanics. McGraw-Hill Book Company (1964).
- Blaudeau, J.-P., Brozell, S. R., Matsika, S., and Pitzer, R. M. "Atomic Orbital Basis Sets for Use with Effective Core Potentials." *International Journal of Quantum Chemistry*, 77: 516-520 (2000).
- Bleijenberg, K. C., "Charge transfer transitions within the octahedral uranate group." *Journal of Chemical Physics*, 73, 2: 617-621 (21 Mar 80).
- Breit, G. "Dirac's Equation and the Spin-Spin Interactions of Two Electrons." *Physical Review*, 39: 616-624 (6 Jan 32).
- Breit, G. "The Fine Structure of He as a Test of the Spin Interactions of Two Electrons." *Physical Review*, 36, 3: 383-397 (1 Aug 30).
- Breit, G. "Possible Effects of Nuclear Spin on X-ray Terms." *Physical Review*, 35, 12: 1447-1451 (15 Jun 30).
- Breit, G. "The Effect of Retardation on the Interaction of Two Electrons." *Physical Review*, 34, 4: 553-573 (15 Aug 29).
- Cotton, F. A. Chemical Applications of Group Theory, 2nd Edition. Wiley-Interscience (1971).
- Darwin, C. G., "The Wave Equations of the Electron." *Proceedings of the Royal Society of London A*, 118: 654-680 (1928).
- Davidson, E. R. and Feller, D. "Basis Set Selection for Molecular Calculations." *Chemical Reviews*, 86: 681-696 (April 1986).
- de Jong, W. A., Visscher, L., and Nieuwpoort, W. C. "On the bonding and the electric field gradient of the uranyl ion." *Journal of Molecular Structure (Theochem)*, 458: 41-52 (1999).
- Dekock, R. L., Baerends, E., Jan, B., Paul, M., and Snijders, J. G. "On the Nature of the First Excited States of the Uranyl Ion." *Chemical Physics Letters*, 105, 3: 308-316 (16 March 1984).
- Denning, R. G., Snellgrove, T. R., and Woodward, D. R. "The electronic structure of the uranyl ion Part I. The electronic spectrum of  $\text{Cs}_2\text{UO}_2\text{Cl}_4$ ." *Molecular Physics*, 32, 2, 419-442 (1976).

- Denning, R. G., Snellgrove, T. R., and Woodwark, D. R. "The electronic structure of the uranyl ion II. The electronic spectrum of  $\text{Cs}_2\text{UO}_2(\text{NO}_3)_3$  and  $\text{NaUO}_2(\text{CH}_3\text{COO})_3$ ." *Molecular Physics*, 37, 4, 1089-1107 (1979).
- Denning, R. G., Snellgrove, T. R., and Woodwark, D. R. "The electronic structure of the uranyl ion III. Theory." *Molecular Physics*, 37, 4: 1109-1143 (1979).
- Denning, R. G. "Electronic Structure and Bonding in Actinyl Ions." Structure and Bonding, Volume 79, Springer-Verlag, Berlin-Heidelberg (1992).
- Denning, R. G., Green, J. C., Hutchings, T. E., Dallera, C., Tagliaferri, A., Giarda, K. Brookes, N. B., Braicovich, L. "Covalency in the uranyl ion: A polarized x-ray spectroscopic study." *Journal of Chemical Physics*, 117, 17: 8008-8020 (1 November 2002).
- Dirac, P. A. M. Quantum Mechanics. 4th Edition, Oxford University Press (1958).
- Dirac, P.A.M., "The Quantum Theory of the Electron. Part II." *Proceedings of the Royal Society London, Series A*, 117: 351-361 (1928).
- Dirac, P.A.M., "The Quantum Theory of the Electron." *Proceedings of the Royal Society London, Series A*, 118: 610-624 (1928).
- Dunning, T. H. Jr. "Gaussian basis sets for use in correlated molecular calculations. I. The atoms boron through neon and hydrogen." *Journal of Chemical Physics*, 90, 2: 1007-1023 (15 January 1989).
- Dirac, P.A.M., "The Quantum Theory of the Electron. Part II." *Proceedings of the Royal Society London, Series A*, pp. 351-361 (1928).
- Docrat, T. I., Mosselmans, J. F. W., Charnock, J. M., Whiteley, M. W., Collision, D., Livens, F. R., Jones, C., and Edmiston, M. J. "X-ray Absorption Spectroscopy of Tricarbonatodioxouranate(V),  $[\text{UO}_2(\text{CO}_3)_3]^{5-}$ , in Aqueous Solution." *Inorganic Chemistry*, 38: 1879-1882 (1999).
- Dyall, K. G., Taylor, P. R., Faegri, K., Partridge, H. "All-electron molecular Dirac-Hartree-Fock calculations: The group IV tetrahydrides  $\text{CH}_4$ ,  $\text{SiH}_4$ ,  $\text{GeH}_4$ ,  $\text{SnH}_4$ , and  $\text{PbH}_4$ ." *Journal of Chemical Physics*, 95, 4: 2583-2594 (30 Apr 1991).
- Ermiler, W. C., Ross, R. B., and Christiansen, P. A. "Spin-Orbit Coupling and Other Relativistic Effects in Atoms and Molecules." *Advances in Quantum Chemistry*, 19: 139-179 (1988).

- Ermler, W. C., Ross, R. B., and Christiansen, P. A. "Ab Initio Relativistic Effective Potentials with Spin-Orbit Operators. VI. Fr Through Pu." *International Journal of Quantum Chemistry*, 40: 829-846 (1991).
- Foldy, L. L., Wouthuysen, S. A., "On the Dirac Theory of Spin 1/2 Particles and Its Non-Relativistic Limit." *Physical Review*, 78, 1: 29-36 (25 Nov 49).
- Gagliardi, L., and Roos, B. O. "Uranium triatomic compounds XUY (X, Y = C, N, O): a combined multiconfigurational second-order perturbation and density functional study." *Chemical Physics Letters*, 331: 229-234 (1 December 2000).
- Garcia-Hernandez, M., Lauterbach, C., Krüger, S., Matveev, A., and Rösch, N. "Comparitive Study of Relativistic Density Functional Methods Applied to Actinide Species  $\text{AcO}_2^{2+}$  and  $\text{AcF}_6$  for  $\text{Ac} = \text{U}, \text{Np}$ ." *Journal of Computational Chemistry*, 23, 8: 831-846 (2002).
- Gerloch, Malcolm. Orbitals, Terms, and States. John Wiley and Sons. (1986).
- Griffiths, Trevor, R., Volkovich, Vladimir, A. "A review of the high temperature oxidation of uranium oxides in molten salts and in the solid state to form alkali metal uranates, and their composition and properties." *Journal of Nuclear Materials*, 274: 229-251 (1999).
- Görller-Walrand C, and De Jaegere, S., "Correlation between the vibronic spectra of the uranyl ion and the geometry of its coordination." *Spectrochimica Acta*, 28A: 257-268 (7 May 1971).
- Han, Y. and Hirao, K. "Density functional studies of  $\text{UO}_2^{2+}$  and  $\text{AnF}_6$  ( $\text{An} = \text{U}, \text{Np}$ , and  $\text{Pu}$ ) using scalar-relativistic effective core potentials." *Journal of Chemical Physics*, 113,17: 7345-7350 (1 November 2000).
- Harris, D. C., Bertolucci, M. D. Symmetry and Spectroscopy: An Introduction to Vibrational and Electronic Spectroscopy. Dover Publications, Inc. (1989).
- Harrison, R. J. "Computational Chemistry for Nuclear Waste Characterization and Processing: Relativistic Quantum Chemistry of Actinides." n. pag. [http://www.emsl.pnl.gov:2080/proj/tms/hpcc\\_actinides/](http://www.emsl.pnl.gov:2080/proj/tms/hpcc_actinides/). June 1997.
- Hay, P. J. *Journal of Chemical Physics*, 79: 5469 (1983).
- Head-Gordon, M. "Quantum Chemistry and Molecular Processes." *Journal of Physical Chemistry*, 100: 13213-13225 (1996).

- Herzberg, G. Molecular Spectra and Molecular Structure III. Electronic Spectra and Electronic Structure of Polyatomic Molecules. D. Van Nostrand Company, Inc. (1966).
- High Performance Computational Chemistry Group. "NWChem, A Computational Chemistry Package for Parallel Computers, Version 4.0.1." Pacific Northwest National Laboratory, Richland, WA, (2002).
- "HP/Compaq ES40/45 User's Guide." Aeronautical Systems Center Major Shared Resource Center, Release 1.2 (4 September 2002).
- Hunt, R. D., and Andrews, L. "Reactions of pulsed-laser evaporated uranium atoms with molecular oxygen: Infrared spectra of UO, UO<sub>2</sub>, UO<sub>3</sub>, UO<sub>2</sub><sup>2+</sup>, UO<sub>3</sub>-O<sub>2</sub> in solid argon." *Journal of Chemical Physics*, 98, 5: 3690-3696 (1 March 1993).
- "IBM SP P3 User's Guide." Aeronautical Systems Center Major Shared Resource Center, Release 2.0 (28 September 2000).
- Ismail, N., Heully, J-L., Saue, T., Daudey, J-P, Marsden, C. "Theoretical studies of the actinides: method calibration for the UO<sub>2</sub><sup>2+</sup> and PuO<sub>2</sub><sup>2+</sup> ions." *Chemical Physics Letters*, 300: 296-302, (1999).
- Jackson, J. D. Classical Electrodynamics, 2nd Edition. John Wiley and Sons. (1975).
- Kaltsoyannis, N. "Computational Study of Analogues of the Uranyl Ion Containing the -N=U=N- Unit: Density Function Theory Calculations on UO<sub>2</sub><sup>2+</sup>, UON<sup>+</sup>, UN<sub>2</sub>, UO(NPH<sub>3</sub>)<sup>3+</sup>, U(NPH<sub>3</sub>)<sub>2</sub><sup>4+</sup>, [UCl<sub>4</sub>{NPR<sub>3</sub>}<sub>2</sub>] (R = H, Me), and [UOCl<sub>4</sub>{NP(C<sub>6</sub>H<sub>5</sub>)<sub>3</sub>}]." *Inorganic Chemistry*, 39: 6009-6017, (2000).
- Kaltsoyannis, N. "Relativistic effects inorganic and organometallic chemistry." *Journal of the Chemical Society, Dalton Transactions*, pp. 1-11, 1997.
- Katz, J. J., Seaborg, G. T., and Morss, L. R. The Chemistry of the Actinide Elements, 2nd Edition, Volumes I and II. Chapman and Hall Ltd. 1986.
- Kellogg, C. B., "An Introduction to Relativistic Electronic Structure Theory in Quantum Chemistry." unpublished report (12 Sep 97).
- Kendall, R. A., Dunning, T. H., Harrison, R. J. "Electron affinities of the first-row atoms revisited. Systematic basis sets and wave functions." *Journal of Chemical Physics*, 96, 9: 6796-6806 (1 May 1992).
- Kim, Y. "Relativistic Self-Consistent-Field Theory for Closed-Shell Atoms." *Physical Review*, 154, 1: 17-39 (9 Jun 66).



- Koelling, D. D., Ellis, D. E., Bartlett, R. J., "Relativistic energy levels and bonding in actinide hexafluorides." *Journal of Chemical Physics*, 64, 3: 3331-3340 (1 Jun 76).
- Kohn, W., Becke, A., Parr, R. G. "Density Functional Theory of Electronic Structure." *Journal of Chemical Physics*, 100, 12974-12980, (1996).
- Krol, D. M. "Analysis of the Luminescence Spectra of some Uranates." *Journal of the Chemical Society, Dalton Transactions*, 6, 8: 687-693 (1981).
- Krol, D. M., and Blasse, G., "Luminescence and energy migration in Ba<sub>2</sub>CaUO<sub>6</sub>." *Journal of Chemical Physics*, 69, 7: 3124-3127 (17 Apr 78).
- Küchle, W., Dolg, M., Stoll, H., and Preuss, H. "Energy-adjusted pseudopotentials for the actinides. Parameter sets and test calculations for thorium and thorium monoxide." *Journal of Chemical Physics*, 100, 10: 7535-7542 (15 May 1994).
- Landau, L. D., and Lifshitz, E. M. Quantum Mechanics (Non-relativistic Theory). Course of Theoretical Physics, Volume 3, 3rd Edition. Pergamon Press (1977).
- Levine, I. N. Quantum Chemistry, 5th Edition. Prentice-Hall, Inc. Upper Saddle River, New Jersey (2000).
- Lee, Y. S., Ermiler, W. C., Pitzer, K. S. "Ab Initio effective core potentials including relativistic effects. I. Formalism and applications to the Xe and Au atoms." *Journal of Chemical Physics*, 67, 12: 5861-5876 (15 Dec 77).
- Lewis, W. B., Asprey, L. B., Jones, L. H., McDoweel, R. S., Rabideau, S. W., Paine, R. T., "Electronic and vibronic states of uranium hexafluoride in the gas and in the solid phase at very low temperatures." *Journal of Chemical Physics*, 65, 7: 2707-1061 (1 Oct 76).
- Lischka, H., "The Columbus Quantum Chemistry Programs Home Page." n. pag. <http://www.itc.univie.ac.at/~hans/Columbus/columbus.html>. (1 December 2001).
- Lischka H., Shepard, R., Pitzer, R. M., Shavitt I., Dallos M., Müller Th., Szalay P. G., Seth M., Kedziora G. S., Yabushita S., and Zhang Z. "High-level Multireference Methods in the Quantum-Chemistry Program System COLUMBUS: Analytic MR-CISD and MR-AQCC Gradients and MR-AQCC-LRT for Excited States, GUGA Spin-orbit CI and Parallel CI Density." *Physical Chemistry. Chemical Physics* 3: 664-673 (18 December 2000).
- Lischka H., Shepard R., Shavitt I., Pitzer R. M., Dallos M., Müller Th., Szalay P. G., Brown F. B., Ahlrichs R., Böhm H. J., Chang A., Comeau D. C., Gdanitz R., Dachsel H., Ehrhardt C., Ernzerhof M., Höchtel P., Irlé S., Kedziora G., Kovar T.,

- Parasuk V., Pepper M. J. M., Scharf P., Schiffer H., Schindler M., Schüler M., Seth M., Stahlberg E. A., Zhao J.-G, Yabushita S., and Zhang Z. "COLUMBUS, an *ab initio* electronic structure program", release 5.8.1(2001).
- Liu, W., Kuchle, W., and Dolg, M. "Ab Initio pseudopotential and density-functional all-electron study of ionization and excitation energies of actinide atoms." *Physical Review A*, 58, 2: 1103-1109, (1998).
- Loewenschuss, A., and Marcus, Yizhak. "The Entropies of Polyatomic Gaseous Ions." *Chemical Reviews*, 84, 2: 89-115 (April 1984).
- Majumdar, D., Balasubramanian, K., Nitsche, H. "A comparative theoretical study of bonding in  $\text{UO}_2^{++}$ ,  $\text{UO}_2^+$ ,  $\text{UO}_2$ ,  $\text{UO}_2^-$ ,  $\text{OUCO}$ ,  $\text{O}_2\text{U}(\text{CO})_2$ , and  $\text{UO}_2\text{CO}_3$ ." *Chemical Physics Letters*, 361: 143-151 (24 July 2002).
- Malli, G., and Oreg, J. "Relativistic self-consistent-field theory for molecules." *Journal of Chemical Physics*, 63, 2: 830-841 (15 Jul 75).
- Matsika, S., and Pitzer, R. M. "Actinyl Ions in  $\text{Cs}_2\text{UO}_2\text{Cl}_4$ ." *Journal of Physical Chemistry A*, 105: 637-645 (2001).
- Matsika, S., Zhang, Z., Brozell, S. R., Blaudeau, J.-P., Wang, Q., and Pitzer, R. M. "Electronic Structure and Spectra of Actinyl Ions." *Journal of Physical Chemistry A*, 105: 3825-3828 (2001).
- Matsuoka, O., Suzuki, N., Aoyama, T., and Malli, G.. "Relativistic self-consistent field methods for molecules. I. Dirac-Fock multiconfiguration self-consistent field theory for molecules and a single-determinant Dirac-Fock self-consistent-field method for closed-shell linear molecules." *Journal of Chemical Physics*, 73, 3: 1320-1328 (22 Apr 80).
- McQuarrie, D. A., Simon, J. D., Physical Chemistry: A Molecular Approach. Unveristy Science Books (1997).
- Meinrath, G. "Uranium(VI) speciation by spectroscopy." *Journal of Radioanalytical and Nuclear Chemistry*, 224, 1-2: 119-126, (1997).
- Morozov, A. M., Morozova, L. G., Feofilov, P. P. "Luminescence of Uranium in Single Crystals with Scheelite Structure." *Optics and Spectroscopy*, 32: 50-54 (14 Apr 71).
- Nagy, A. "Density Functional Theory and Applications to Atoms and Molecules." *Physics Reports*, 298, 1-79 (1998).

- Nakajima, T., Yanai, T., and Hirao, K.. "Relativistic Electronic Structure Theory." *Journal of Computational Chemistry*, 23: 847-860 (2002).
- "NWChem: High Performance Computational Chemistry Software." n. pag. <http://www.emsl.pnl.gov:2080/docs/nwchem/nwchem.html> (2002).
- Pacios, L. F., and Christiansen, P. A. "Ab initio relativistic effective potentials with spin-orbit operators. I. Li through Ar." *Journal of Chemical Physics*, 82, 6: 2664-2671 (15 March 1985).
- Pepper, M., and Bursten, B. E. "The Electronic Structure of Actinide-Containing Molecules: A Challenge to Applied Quantum Chemistry." *Chemical Reviews*, 91: 719-741 (1991).
- Perdew, J. P., and Wang, Y. "Accurate and simple analytic representation of the electron-gas correlation energy." *Physical Review B*, 45, 23: 13244-13249 (15 June 1992).
- Perdew, J. P., Chevary, J. A., Vosko, S. H., Jackson, K. A., Pederson, M. R., Singh, D. J., and Fiolhais, C. "Atoms, molecules, solids, and surfaces: Applications of the generalized gradient approximation for exchange and correlation." *Physical Review B*, 46: 6671-6687 (1992).
- Perdew, J. P. "Density-functional approximation for the correlation energy of the inhomogeneous electron gas." *Physical Review B*, 33, 12: 8822-8824 (15 June 1986).
- Pyykkö, P. n. pag. Database "RTAM" (Relativistic Quantum Chemistry Database, 1915-2002, <http://www.csc.fi/rtam/>) (2002).
- Pyykkö, P. "Could uranium(XII) hexoxide, UO<sub>6</sub> (O<sub>h</sub>) exist?" *Chemical Physics Letters*, 328: 415-419, (2000).
- Pyykkö, P. "Quasirelativistic Pseudopotential Study of Species Isoelectronic to Uranyl and the Equatorial Coordination of Uranyl." *Journal of Physical Chemistry*, 98: 4809-4813 (1994).
- Pyykkö, P. "The Large Range of Uranyl Bond Lengths: Ab Initio Calculations on Simple Uranium-Oxygen Clusters." *Inorganic Chemistry*, 30: 3787-3788 (1991).
- Pyykkö, P. "Relativistic Effects in Structural Chemistry." *Chemical Reviews*, 88: 563-594 (March 1988).
- Raghavachari, K., Anderson, J. B. "Electron Correlation Effects in Molecules." *Journal of Physical Chemistry*, 100: 12960-12973 (1996).

- Ratner, M. A., and Schatz, G. C. Introduction to Quantum Mechanics in Chemistry. Prentice Hall, Upper-Saddle River, NJ (2001).
- Reiher, M., and Heß B. "Relativistic Electronic-Structure Calculations for Atoms and Molecules." *Modern Methods and Algorithms of Quantum Chemistry, Proceedings, 2nd Edition*. John von Neumann Institute for Computing, Jülich, pp. 479-505 (2000).
- Rianda, R., Frueholz, R. P., Kuppermann, A., "Electronic Spectroscopy of UF<sub>6</sub> and WF<sub>6</sub> by electron impact." *Journal of Chemical Physics*, 70, 2: 1056-1061 (15 Jan 79).
- Saue, T., Faegri, K., Helgaker, T., Gropen, O. "Principles of direct 4-component relativistic SCF: application to cesium auride." *Molecular Physics*, 91, 5: 937-950 (20 Feb 1997).
- Schmider, H. L., and Becke, A. D. "Optimized density functionals from the extended G2 test set." *Journal of Chemical Physics*, 108, 23, 9624-9631 (1998).
- Schreckenback, G., Hay, P. J., Martin, R. L. "Theoretical Study of Stable Trans and Cis Isomers in [UO<sub>2</sub>(OH)<sub>4</sub>]<sup>2-</sup> Using Relativistic Density Functional Theory." *Inorganic Chemistry*, 37: 4442-4451 (1998).
- Shepard R., Shavitt I., Pitzer R. M., Comeau D. C., Pepper M., Lischka H., Szalay P. G., Ahlrichs R., Brown F. B., and Zhao J. "A Progress Report on the Status of the COLUMBUS MRCI Program System." *International Journal of Quantum Chemistry, Quantum Chemistry Symposium*, 22: 149 (1988).
- Starostin, N. V. "Theory of Spectra of Uranate Compounds." *Optics and Spectroscopy* 32: 820-822 (12 May 71).
- Stephans, S. G., Devlin, J. F., Chaboalowski, C. F., and Frisch, M. J. "Ab Initio Calculations of Vibrational Absorption and Circular Dichroism Spectra Using SCF, MP2, and Density Functional Theory Force Fields." *Journal of Chemical Physics*, 98: 11623 (1994).
- Szabo, A., and Ostlund, N. S. Modern Quantum Chemistry: Introduction to Advanced Electronic Structure Theory. Dover Publications, Inc. Mineola, NY (1996).
- Toth, L. M., and Begun, G. M. "Raman Spectra of Uranyl Ion and Its Hydrolysis Products in Aqueous HNO<sub>3</sub>." *Journal of Physical Chemistry*, 85: 547-549 (1981).

- Tsushima, S., Suzuki, A. "Ab initio effective core potential study of equatorially coordinated uranyl species: effect of hydration to the calculated properties." *Journal of Molecular Structure (Theochem)*, 487: 33-38 (1999).
- Tsushima, S., and Reich, T. "A theoretical study of uranyl hydroxide monomeric and dimeric complexes." *Chemical Physics Letters*, 347: 127-132, (2001).
- Wanner, H., and Forest, I (editors). Chemical Thermodynamics of Uranium. Chemical Thermodynamics, Volume 1, pp 30-31, 85-98. North-Holland Elsevier Science Publishers (1992).
- Van den Berge, S., Miserque, F., Gouder, T., Gaudreau, B., and Verwerft, M. "X-ray photoelectron spectroscopy on uranium oxides: a comparison between bulk and thin layers." *Journal of Nuclear Materials*, 294: 168-174, (2001).
- Veal, B. W., Lam, D. J., Diamond, H., and Hoekstra, H. R. "X-ray photoelectron-spectroscopy study of oxides of the transuranium elements Np, Pu, Am, Cm, Bk, and Cf." *Physical Review B*, 15, 6: 2929-2941 (15 March 1977).
- Veal, B. W., Lam, D. J., Carnall, W. T., Hoekstra, H. R. "X-ray photoemission spectroscopy study of hexavalent uranium compounds." *Physical Review B*, 12, 12: 5651-5663 (15 December 1975).
- Yabushita, S., Zhang, Z., and Pitzer, R. M. "Spin-Orbit Configuration Interaction Using the Graphical Unitary Group Approach and Relativistic Core Potential and Spin-Orbit Operators." *Journal of Physical Chemistry*, 103: 5791-5800 (1999).
- Zhang, Z., and Pitzer, R. M. "Application of Relativistic Quantum Chemistry to the Electronic Energy Levels of the Uranyl Ion." *Journal of Physical Chemistry A*, 103: 6880-6886 (1999).

## Vita

Captain Eric V. Beck graduated from Carson City High School in Carson City, Nevada in 1989. He completed a Bachelor of Science degree with a dual major in physics and mathematics at the University of Nevada, Reno in May 1993.

Captain Beck joined the United States Air Force in May of 1995, and was commissioned in August 1995 at Officer Training School, Maxwell Air Force Base (AFB), Alabama. His first assignment was at the Air Force Research Laboratory, Space Vehicles Directorate in the Astrodynamics branch, Kirtland AFB, lasting from October 1995 through April 1998. While stationed at Kirtland AFB, Captain Beck co-authored the Orbit Analysis Software Survey. He also assisted data acquisition and analysis for high-accuracy orbit determination using angles-only data obtained from the low-cost RAVEN telescope. In addition, he functioned as the laboratory's representative to NASA Lewis Research Center's Breakthrough Propulsion Physics Steering Group.

Following his assignment at Kirtland AFB, Capt Beck was assigned to the Air Force Information Warfare Center (AFIWC) at Lackland AFB, Texas. While stationed at AFIWC, Capt Beck served as a project engineer in Radio Frequency Measurements branch of the Systems and Analysis directorate. Here, he worked on test and measurement of local San Antonio radio and television signals, the MC-130H AN/APQ-170 multimode radar, and the C-130J AN/APN-241 multimode radar. Following this duty, Capt Beck moved to the Radar and Communications Analysis Flight of the 453rd

Electronic Warfare Squadron (still at AFIWC), where he contributed to the Air War Over Serbia (AWOS) Radar Warning Receiver (RWR) effectiveness after-action report and C-17 collision avoidance system upgrade vulnerability analysis.

In August 2002, he entered the Graduate School of Engineering and Management, Air Force Institute of Technology in order to pursue a M.S. degree in nuclear physics.

Upon graduation, he will begin a Ph.D. program in applied physics.

REPORT DOCUMENTATION PAGE			Form Approved OMB No. 074-0188		
The public reporting burden for this collection of information is estimated to average 1 hour per response, including the time for reviewing instructions, searching existing data sources, gathering and maintaining the data needed, and completing and reviewing the collection of information. Send comments regarding this burden estimate or any other aspect of the collection of information, including suggestions for reducing this burden to Department of Defense, Washington Headquarters Services, Directorate for Information Operations and Reports (0704-0188), 1215 Jefferson Davis Highway, Suite 1204, Arlington, VA 22202-4302. Respondents should be aware that notwithstanding any other provision of law, no person shall be subject to a penalty for failing to comply with a collection of information if it does not display a currently valid OMB control number. <b>PLEASE DO NOT RETURN YOUR FORM TO THE ABOVE ADDRESS.</b>					
1. REPORT DATE (DD-MM-YYYY) 03-10-2003		2. REPORT TYPE Master's Thesis		3. DATES COVERED (From - To) Aug 2002 - Mar 2003	
4. TITLE AND SUBTITLE  THEORETICAL COMPARISON OF THE EXCITED ELECTRONIC STATES OF THE URANYL AND URANATE IONS			5a. CONTRACT NUMBER		
			5b. GRANT NUMBER DE-A107-021D14328		
			5c. PROGRAM ELEMENT NUMBER		
6. AUTHOR(S)  Beck, Eric V., Captain, USAF			5d. PROJECT NUMBER		
			5e. TASK NUMBER		
			5f. WORK UNIT NUMBER		
7. PERFORMING ORGANIZATION NAMES(S) AND ADDRESS(S) Air Force Institute of Technology Graduate School of Engineering and Management (AFIT/EN) 2950 Hobson Way, Building 640 WPAFB OH 45433-7765			8. PERFORMING ORGANIZATION REPORT NUMBER  AFIT/GNE/ENP/03-01		
9. SPONSORING/MONITORING AGENCY NAME(S) AND ADDRESS(ES) Dr. Charles Brennan AFTAC/TMNE 1030 South Highway A1A Patrick AFB, FL 32925-3002 Dr. Kathy McCarthy INEEL PO Box 1625 Idaho Falls, ID 83415-2208			10. SPONSOR/MONITOR'S ACRONYM(S)		
			11. SPONSOR/MONITOR'S REPORT NUMBER(S)		
12. DISTRIBUTION/AVAILABILITY STATEMENT  APPROVED FOR PUBLIC RELEASE; DISTRIBUTION UNLIMITED.					
13. SUPPLEMENTARY NOTES					
14. ABSTRACT This thesis examines the ground and excited electronic states of the uranyl ( $\text{UO}_2^{2+}$ ) and uranate ( $\text{UO}_4^{2-}$ ) ions using Hartree-Fock self-consistent field (HF SCF), multi-configuration self-consistent field (MCSCF), and multi-reference single and double excitation configuration interaction (MR-CISD) methods. The MR-CISD calculation included spin-orbit operators. Molecular geometries were obtained from self-consistent field (SCF), second-order perturbation theory (MP2), and density functional theory (DFT) geometry optimizations using the NWChem 4.01 massively parallel <i>ab initio</i> software package. COLUMBUS version 5.8 was used to perform in-depth analysis on the HF SCF, MCSCF, and MR-CISD potential energy surfaces. Excited state calculations for the uranyl ion were performed using both a large- and small-core relativistic effective core potential (RECP) in order to calibrate the method. This calibration included comparison to previous theoretical and experimental work on the uranyl ion. Uranate excited states were performed using the small-core RECP as well as the methodology developed using the uranyl ion.					
15. SUBJECT TERMS Relativistic Quantum Mechanics, Actinides, Uranium Oxide, Electronic Spectroscopy, Uranyl, Quantum Chemistry					
16. SECURITY CLASSIFICATION OF:		17. LIMITATION OF ABSTRACT	18. NUMBER OF PAGES	19a. NAME OF RESPONSIBLE PERSON	
a. REPORT	b. ABSTRACT			c. THIS PAGE	Eric V. Beck, Capt, USAF (ENP)
U	U	UU	129	19b. TELEPHONE NUMBER (Include area code) (937) 255-3636, ext 6347; e-mail: eric.beck@afit.edu	